Laser Fabrication of Lead Selenide Thin Films for Infrared Focal Plane Array Applications

---

A Ph.D. thesis

presented to the faculty advisory committee at the School

of Engineering and Applied Science of the

University of Virginia

In partial fulfillment

of the requirements for the degree of

Doctor of Philosophy

Charles L. Brown Department of Electrical and Computer Engineering

---

By **Joel T. Harrison**

under the advisement of

Dr. Mool C. Gupta

Spring 2022

APPROVAL SHEET

This Ph.D. dissertation is submitted in partial fulfillment of the requirements

for the degree of

Doctor of Philosophy (Electrical and Computer Engineering)

_____

Joel T. Harrison

This Ph.D. dissertation has been read and approved by the Examining Committee:

_____

Professor Mool C. Gupta, Advisor (ECE)

_____

Professor Andreas Beling, Committee Chair (ECE)

_____

Professor Joshua J. Choi (ChE)

_____

Professor Jon F. Ihlefeld (ECE & MSE)

_____

Professor Kyusang Lee (ECE & MSE)

Accepted for the School of Engineering and Applied Science:

_____

Professor Jennifer L. West, Dean, School of Engineering and Applied Science

April 2022

ABSTRACT

The demand for integrating infrared (IR) detectors and imaging systems in consumer products and defense applications is rapidly growing. The requirement for IR uncooled, highly responsive, and spectrally tailored devices are driving a resurgence of interest in lead selenide (PbSe) thin films for detectors and focal plane array (FPA). PbSe has been used for MWIR (3 – 5 μm) detectors for over 70 years, however, the photoconductivity mechanism is still not well understood, and higher device performance is desired. The large Bohr exciton radius of PbSe (~46 nm) facilitates strong quantum confinement properties and spectral tailoring as far down as 690 nm. New thin-film deposition methods and processing approaches are needed to better control and expand PbSe thin film properties and to understand the photoconductivity mechanism.

The primary goals of this thesis work are (1) to demonstrate a new method for PbSe thin film fabrication using laser sintering deposition (LSD) of micro/nano particles of PbSe (2) to improve the understanding of the photoconductive mechanism in PbSe thin films through optical, electrical, morphological, and structural characterization (3) to fabricate a photodetector sensor and focal plane array device using the LSD method combined with laser patterning, avoiding some of the difficulties of using photolithography liftoff.

The new method introduced in this work is a 3-step process called Laser Sinter Deposition (LSD). The first step produces colloidal nanocrystals (NC) by *planetary ball milling* high-purity PbSe in a methanol solution. The second step is the rapid *centrifugal deposition* of the PbSe NCs on silicon substrates. Finally, *laser sintering* is accomplished by rastering a pulsed or continuous-wave laser (UV, visible, or IR) to sinter and form a continuous polycrystalline thin film with superior substrate adhesion and highly tailorable properties. Laser processing has the advantage of allowing spatially defined sintering, ultra-rapid sintering (millisecond to nanosecond) to activate doping, selectively ablation of material with depth control, reorganizing crystalline structures including defect reduction, and the potential for trapping of non-equilibrium structures. Another advantage of LSD is the ability for selective depth sintering (SDS) by exploiting the absorption depth of different laser wavelengths.

This work shows that LSD can be tailored to produce a thin film of PbSe with nearly identical properties to films prepared by Chemical Bath Deposition (CBD), in terms of electrical, compositional, and physical properties. In contrast to CBD, LSD produces superior substrate adhesion, unique morphological control (columnar versus equiaxed grains), and provides spatially tailorable grain modification (lateral and transverse)., In contrast to all other deposition methods, the LSD process also allows in-situ doping of the nanocrystals prior to laser sintering which allows precise concentration of dopant potassium iodide, resulting in a more dense film, an inter-grain coating of PbI_2, and a 300% increase in photoresponse compared to films without KI. PbSe thin films were oxidized and iodized (sensitization process) to enhance the photoresponse. We report a process agnostic model of the complex interactions between oxidation and iodization to identify the narrow process window that exists in the sensitization process. In doing this, we identify a previously unreported compound ($Pb_3Se_2O_6I_2$) that exists in the transition layer between the base layer of PbSe and the top layer of PbI_2. This compound is only observed in highly photoresponsive films. The inter-grain $PbSeO_3$ coating is confirmed through Transmission Electron Microscopy (TEM) and helps in regulating the diffusion of iodine

along grain boundaries which assists to densify the film and enhancing the photoresponse. The presence of iodine decreases dark current, while simultaneously assisting in recrystallizing PbSe during sensitization.

One interesting discovery is that p-type PbSe film with a carrier concentration of 4.8 x 10^{18} cm^{-3} can be converted to n-type with a carrier concentration of 9.2 x 10^{18} cm^{-3} with a simple laser treatment using a 355 nm (UV) wavelength laser by selectively reducing the selenium concentration. The UV treatment also improved carrier mobility by nearly 500%, from 6.5 to 37.5 $cm^2/V{\cdot}s$. Laser processing also simplifies device fabrication by allowing *selective in-situ patterning* of PbSe, the metal conductor (Au), and substrate, in one system to eliminate the need for photolithography. Unlike other forms of rastered patterning, such as e-beam lithography, laser patterning is accomplished at raster speeds of 10 meters per second in one step without photoresist or chemicals.

This work successfully demonstrates the complete laser fabrication of both discrete 3.5 cm^2 photodetectors with a Detectivity of 1.01 x 10^9 $cm{\cdot}Hz^{-1/2}/W$ and the capability of laser patterning focal plane array (FPA) with *vertical contact* pixels as small as 60 x 70 µm at a 100 µm pitch to fabricate a 37 x 68 pixel FPA on a 1 cm x 2 cm substrate in < 30 seconds. This work demonstrates the functional operation of a laser patterned 120 pixel FPA prototype of *lateral contact* pixels (240 µm x 260 µm). This work successfully demonstrates lasers can be used successfully to fabricate both thin films of a few microns in thickness as well as complex integrated devices such as focal plane arrays (FPAs).

In summary, we have successfully demonstrated a new method of thin-film deposition using laser sintering of nanoparticles, provided an enhanced understanding of the photoconductive mechanism in PbSe, and IR devices like photodetectors and focal plane arrays can be fabricated by direct laser patterning.

TABLE OF CONTENTS

LIST OF FIGURES

ACKNOWLEDGEMENTS

I would like to express my sincerest gratitude and appreciation to all who have supported me during my time in the doctoral program at the University of Virginia. I could not have accomplished this without your support. To my wife, Mary, and my two daughters, Kate and Meg, I want to thank you from the bottom of my heart for your patience and support. I love you with all my heart.

I am extremely grateful to my advisor and mentor, Professor Mool Gupta, for taking a chance on an older, stubborn, and set-in-his-ways student back in 2017, and for helping me take off my engineering blinders and open my eyes to the scientific approach.

I would also like to thank my committee: Professor Andreas Beling, for serving as my committee chair; Professor Joshua Choi, Professor Jon Ihlefeld, and Professor Kyusang Lee for agreeing to be on my committee.

I acknowledge the tremendous support of The Naval Surface Warfare Center, Dahlgren Division (NSWCDD) for supporting my studies and encouraging me to press on. I could not have accomplished this without the support of the Chief Technology Officer, the NSWCDD Academic Fellowship Program (AFP), and the mentoring and support of Dr. Pearl Rayms-Keller. I would like to thank the Naval Surface Warfare Center, Dahlgren Division (NSWCDD) for the support of this graduate research under the Office of Naval Research, grant number N00014-21-WX-0-0334.

Additionally, I would like to thank James (Sid) Ketchum, Karen Long, Dr. Joseph Hunt, Dr. Michael Lowry, and William (Bill) Roberts for their support. I would also like to thank Dr. Moon Hyung Jang, Elisa Pantoja Rodriguez, George Wilkes, Arpan Sinha, and Justin Bickford.

CHAPTER 1: Introduction

1.1 History and Evolution of Lead Selenide Thin Films

For 70+ years, lead chalcogenides (PbS, PbSe, and PbTe) have been researched for their unique room-temperature photosensitivity to infrared radiation. The most common application utilizes their semiconductive properties in the form of a polycrystalline thin film used as a photodetector of mid-wave infrared (MWIR) wavelengths (3 - 5 μm). Rapid advances in material science, fabrication process controls, and solid-state physics have resulted in more sensitive detectors; however, unfortunately, they lead to high complexity and manufacturing costs, and/or thermal management requirements using external cooling have limited their insertion into many commercial and military applications. A resurgence of interest in lead chalcogenides, primarily lead selenide (PbSe), has occurred for three main reasons. These are lead selenide has (1) a high-photoresponse at room temperature and (2) simple fabrication, and (3) a large Bohr exciton radius of 46 nm, allowing bandgap tuning of photosensitivity to shorter wavelengths with quantum dots (QD). Table 1 summarizes the specific properties relating to bandgap tuning for lead chalcogenides.

Table 1: Table of properties related to bandgap for common lead chalcogenides

Lead Chalcogenide	Bohr Radius (nm)	Bulk Bandgap E_g (eV)	Wavelength (μm)	QD Eg range (eV)
PbS	18	0.41	3	0.41 - 1.6
PbSe	46	0.28	4.4	0.28 - 1.7
PbTe	150	0.31	4	0.31 - 1.1

In recent years other improvements have been made as research into these unique materials increases, however, the methods for thin film deposition remain fairly unchanged. With the exception of quantum dot synthesis, most thin films (0.5 – 2 μm) for MWIR applications are deposited using one of two methods, (1) physical vapor deposition (PVD) or (2) chemical bath deposition (CBD). Both deposition methods have their own set of benefits and limitations. While significant efforts have resulted in improvements for PVD, CBD deposition is much more common, and (currently) produces the highest photosensitivity at the lowest cost. CBD does, however, suffer from cross-sample uniformity (thickness, morphology, stoichiometry, etc), poor substrate adhesion, poor process control leading to sample-to-sample variation, and requires a wet chemical deposition process incompatible for easy integration with Si CMOS technology[1,2]. The addition of potassium iodide is known to improve the photoresponse; however, precise doping CBD films with KI is inherently difficult due to the poor control of the CBD process. All depositions methods require thermal sensitization, which is highly dependent on adequate process control during film deposition. Variations in film thickness, morphology, stoichiometry, and substrate adhesion are just a few of the issues that result in low yield for all conventional PbSe-based detector fabrication methods. As for the PbSe device, which requires patterning, such as focal plane array (FPA), the added complexity and chemical exposure of the PbSe to photoresist, the subsequent chemical photoresist strip, and PbSe etchants further degrades the films photoresponse due to the sensitivity of the PbSe and PbI_2 to chemical contamination.

1.2 Intrinsic Properties of Lead Selenide and Photoconductivity

This work focuses on PbSe; however, much of what is covered applies to PbTe and PbS as well. There are many properties of PbSe that attract researchers; its narrow and direct bandgap (0.27 eV) and large nominal Bohr exciton radius (~46 nm) offer superior versatility for tuning the spectral photoresponse. [3] The narrow *intrinsic* (bulk) bandgap of PbSe makes it sensitive to the MWIR regime of the electromagnetic (EM) spectrum (3 – 5 μm). The relatively large Bohr exciton radius enables its strong

quantum confinement characteristics. Each of these properties is interesting alone but combined, allows for an exceptional ability to shift the bandgap and spectral range of optical photoresponsivity with relative ease. Furthermore, the large Bohr radius allows relatively reproducible and straightforward polycrystalline thin film processing to obtain nanocrystals with unique properties. This allows investigations of quantum size effects with particle dimensions that are more stable, having a smaller surface-to-volume ratio.[3 4]

Table 2: Material properties of intrinsic crystalline PbSe

Crystal Properties		Physical Properties	
Crystal type	Cubic	Density (g/cm^3)	8.15
Structure	Halite	Lattice Constant (Å)	6.12
Space Group	Fm3m	Molecular Weight (g/mol)	286.2
Electronic Properties (293 K)		**Thermal Properties**	
Bandgap (eV)	0.28	Thermal Conductivity (W/m·k)	1.7
Electron mobility (cm^2/V·s)	1000	Melting Point (°C)	1067.00
Hole Mobility (cm^2/V·s)	900	Heat of Formation (kJ/Mol)	393

One of the most exciting aspects of PbSe is how its properties contrast with other semiconductors. The bandgap of most semiconductors widens with pressure and decreases with temperature, while the bandgap of PbSe narrows with pressure and increases with temperature.[5] This is discussed in detail by Wei et al.[6] and Svane et al.[7] and is related to spin-orbit phenomena as a consequence of band ordering at the L point.[8] Ekuma et al. calculated a 1% compression of the lattice parameter for PbSe, resulting in a 0.11 eV bandgap decrease.[8] Streltsov et al. showed that with sufficient pressure (13-25 GPa), PbSe transitions from a cubic (NaCl) semiconductor to an orthorhombic (CsCl) metal and superconductor.[9]

Due to the high absorption coefficient (Figure 1) at IR wavelengths (3 - 5 μm) at photon energies (0.4 – 0.25 eV), and to maximize the photoresponse, polycrystalline thin films of 500 nm - 2.0 μm thickness are generally targeted. Polycrystalline grain size can be modulated during film deposition in many ways with substrate temperature and substrate surface conditions but typically ranges from 100 nm to 400 nm. Grain size is a major factor in the sensitization process and influences the diffusion of oxygen and iodine along grain boundaries. It should be noted that crystallite size can be the same or smaller than gain size. Grain size should not be confused with crystallite size as individual grains are often polycrystalline[4].

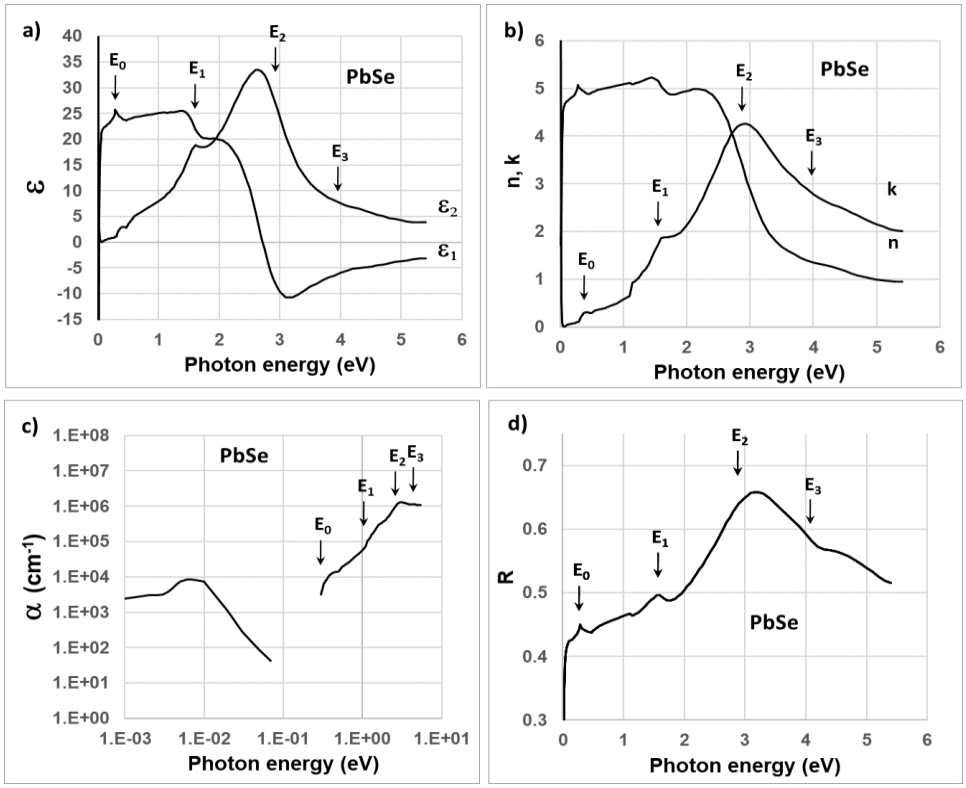

Figure 1: Photon energy-dependent optical and electrical properties of PbSe [dielectric constant ($e^* = e_1 + ie_2$), complex refractive index (n*=n+ik), absorption coefficient (a), and normal-incidence reflectivity (R) at RT].[62] These values can vary due to temperature, material synthesis, and stoichiometry.

1.3 Current Methods for Deposition of PbSe Thin Films

This literature review is focused on polycrystalline PbSe thin films for MWIR photodetectors with the primary goal in mind to introduce *laser sinter deposition* (LSD). Secondly, it is the intent to contrast the controls of other deposition methods with the many laser parameters (continuous versus pulsed, pulse length, repetition rate, scan speed, etc.) to (1) improve understanding of the photo-mechanism that makes PbSe work and (2) improve the photoresponse with added process control for experimentation. This literature review will briefly cover all deposition processes but will focus on CBD deposited PbSe films since this is the most common deposition method. While single-crystalline or monolayers of epitaxial layers of PbSe can be readily produced with MBE or ALD, they are not ideal for thicker polycrystalline forms of PbSe, therefore we will not further review these ultra-thin film deposition methods. A comprehensive literature review covering all aspects of PbSe properties, deposition methods, and device applications is published by our research group.[4]

1.3.1 Chemical Bath Deposition (CBD)

Chemical bath deposition is the most common and currently produces the lowest cost and highest IR responsivity of all the deposition methods,[10–13] PbSe films of thicknesses ranging from 0.5 – 2 μm for MWIR applications are generally deposited on silicon, glass, or GaAs substrates. The typical randomly oriented polycrystalline morphology and inherent grain sizes (100 – 400 nm) produced by CBD lend well to the subsequent sensitization processing, which requires diffusion and incorporation of both oxygen and iodine in and around the PbSe grain boundaries. Of all the deposition methods for PbSe-based MWIR applications, CBD is the most mature for photodetector applications due to it being a simple and low-cost option with high photoresponse. CBD process is performed with a combination of Pb-based and Se-based pre-cursor chemistries in a reaction bath with tight dependencies on bath temperature and pH. Table 3 summarizes the many different recipes used by researchers and industry.[4]

Table 3: Table of reported recipes for CBD deposited PbSe.

Source	Year	Substrate	Recipe
Gorer[14]	1995	glass	60 mM $Pb(CH_3COO)_2$ + 160 - 320 mM TSC + 50 mM Na_2SeSO_3 + KOH. pH = 10. **Selenosulfate:** 0.5 M Na_2SO_3 + 0.2 M Se (70 °C, several hrs)
			60 mM $Pb(CH_3COO)_2$ + 0.6 - 4.3 M KOH + 50 mM Na_2SeSO_3. pH > 13. **Selenosulfate:** 0.5 M Na_2SO_3 + 0.2 M Se (70 °C, several hrs)
Grozdanov[15]	1998	glass, polyester	10 - 12 mL 0.5 M $Pb(NO_3)_2$ + 2 M NaOH + 10 mL 1 M Na_2SeSO_3. T = 70 °C; pH = 10. **Selenosulfate:** 1 M Na_2SO_3 + 1 M Se followed by sintering.
Hankare[16]	2003	glass	10 mL 0.25 M $Pb(NO_3)_2$ + 1 M tartaric acid + 1 M KOH + 10 mL 0.25 M Na_2SeSO_3. T = 4.85 – 25 °C.
Sarkar[17]	2006	glass	60 mM $Pb(CH_3COO)_2$ + 50 mM Na_2SeSO_3 + 0.6 M KOH. pH = 13. **Selenosulfate:** 0.5 M Na_2SO_3 + 0.2 M Se
	2006		60 mM $Pb(CH_3COO)_2$ + 50 mM Na_2SeSO_3 + 160 mM TSC. pH = 10.5. **Selenosulfate:** 0.5 M Na_2SO_3 + 0.2 M Se
Kassim[18]	2010	glass	20 mL 0.15 M $Pb(NO_3)_2$ + 10 mL triethanolamine + 20 mL 0.15 M Na_2SeO_4. T = 25 – 80 °C; pH = 6
Templeman[19]	2014	GaAs	60 mM $Pb(CH_3COO)_2$ + 50 mM Na_2SeSO_3 + KOH. pH > 13. **Selenosulfate:** 0.5 M Na_2SO_3 + Se
Jang[20–22]	2019	SiO2/Si	1 M $Pb(CH_3COO)_2$ + 1 M CH_4N_2Se + KOH. T = 80 °C; t = 1 hr; pH = 10 . Oxidation at 460 °C for 6.25 mins. Iodization at 300 °C for

The incorporation of alternative sources of iodine and the use of iodine-based dopant in the CBD process for PbSe MWIR photodetectors is promising. Smirnova et al. reported the addition of ammonium iodide (NH_4I) in the CBD bath, influencing the grain size and morphology. It did not impact the ~1:1 stoichiometry of the PbSe. In contrast, the concentration of NH_4I in the bath linearly affects the Pb:I atomic ratio and increases the PbSe lattice parameter suggesting iodine is being incorporated into the PbSe crystals during deposition.[23] This work does not report any influence on the oxidation step of the sensitization process nor impact on IR photoconductivity or responsivity. Subsequent work reported by Yurk et al. and Maskaeva builds on this by evaluating the influence of adding antioxidants and NH_4I to the CBD bath during PbSe deposition.[24] [4]

Several antioxidants were evaluated by Yurk and were found to heavily impact the stability of the selenurea precursor chemistry for up to five days. Higher alkalinity was found to increase the decomposition of selenurea, but Na_2SO_3 and $C_6H_8C_6$ were found to have a stabilizing effect. A small amount of reduction in the PbSe lattice constant and an increase in the share of nanocrystals and optical bandgap were also reported (0.78 – 1.0 eV).[24] Maskeave et al. combined the NH_4I and antioxidants and reported a PbSe crystallite size ranging from 60 nm to 2 nm; however, the bandgaps reported, post anneal, were found to range from 0.27 to 0.35 eV.[25] It is unclear what caused the discrepancy between their reported optical bandgap. Maskaeva also introduced both NH_4I and performed a thermal anneal. The anneal may have merged the crystallites to a scale above the Bohr radius of PbSe to achieve an optical bandgap of bulk PbSe. The presence of elevated iodine levels (NH_4I) may have influenced PbSe crystal growth and oxygen incorporation into the PbSe grain, making the film's optical bandgap correlate to larger crystallite geometry associated with MWIR wavelengths.[4]

PbSe deposition via CBD is reported as being highly sensitive to substrate type and surface conditions concerning morphology, crystalline preference, and adhesion. Shandalov et al. reported that their CBD process resulted in superior wetting and adhesion to GaAs substrate as opposed to SiO_2 and glass.[26] They reported poor adhesion and lack of a continuous film for SiO_2. Others successfully deposited a high-quality continuous PbSe film on thermally oxidized silicon substrates by roughening the surface for better adhesion and grain nucleation.[10,11,27,28]

Kumar et al. deposited a PbSe film on a glass substrate and fully sensitized it to achieve an impressive D* of 2.8 x 10^{10} cm $Hz^{1/2}$ W^{-1}.[29,30] Kumar provides extensive TEM and SAED analysis and thoroughly documents the key finding of this high D* film. A schematic depicting the TEM and SAED results in the layout of a comprehensive picture of the chemical and morphological properties for fabricating high IR responsive PbSe film. [4]

Qiu et al. reported a thin film fabrication method to better tune a PbSe-based thin film to a specific optical bandgap/wavelength.[31] They used a two-step CBD process to deposit PbSe NC on top of CdS NCs to form a heterojunction. Instead of growing a film with specific wavelength sensitivity, Qiu formed a PbSe-based film with significant quantum confinement characteristics (blue-shift) followed by thermal annealing to both repair crystalline order, reduce interface defects and grow the PbSe grains (red-shift). Annealing potentially offers a linear and cumulative solution for tuning the film bandgap and band alignment. With increasing temperature, both crystalline defects are reduced, and the dark photocurrent is suppressed. They achieved a sensitivity R_{peak} of 0.36 A W^{-1} and a D* of 4.2 x 10^8 cm $Hz^{1/2}$ W^{-1} with a cutoff wavelength of 4.2 µm.[31]

Templeton et al. reported a unique morphology controlled by substrate temperature during their CBD deposition process.[32] By varying the substrate temperature between 15 – 40 °C, they were able to obtain distinct PL signals ranging from 1.9 – 4.4 µm in wavelength, respectively.[32] The deposition rate was slow; however, the columnar morphology could be beneficial for maximizing absorption by light scattering. There was no mention of sensitization.

Rapid progress in using different complexing agents, precursors chemistries, and QD precipitation methods proves CBD has the flexibility to cover the IR spectrum while remaining relatively simple and inexpensive. Although many other deposition processes can be used to grow thin films, CBD is a very

mature process, and this assures CBD will remain in heavy use. Other deposition methods are increasing in use and offer advanced process control such as PVD but still need development and process maturation. Again, a comprehensive list of published CBD recipes is shown in Table 3.

While CBD currently produces some of the best PbSe thin films for MWIR photodetectors, there are many limitations and drawbacks. Some of the most challenging are listed below.

- Limited process control due to the strong dependency on substrate temperature and bath pH
- Poor substrate adhesion requires surface treatment for substrate
- Slow deposition rates with radial dependent properties (center to edge)
- Large amounts of hazardous chemical waste following deposition

1.3.2 Other deposition methods for PbSe

There are many methods for depositing polycrystalline thin films of PbSe using various forms of physical or chemical vapor deposition (PVD and CVD). There are additional methods such as pulsed laser deposition (PLD), molecular beam epitaxy (MBE), and atomic layer deposition (ALD), however, they are less common or specific to extremely low deposition rates and pristine epitaxial single crystal layers. CVD includes low pressure (LPCVD) and plasma-enhanced (PECVD), and both offer a higher level of process control for growing precision films, including polycrystalline thin films but the equipment and processing costs are also higher. PVD is grouped with thermal evaporation and sputtering from high purity, physical targets in a very controlled chamber environment under high vacuum, temperature-controlled platens, and a choice between inert and reactive carrier gasses.

Still, CBD is the most common and practical because it offers a simple and low-cost process, providing many options for thin films for IR-sensitive Photodetectors.[4] While many groups choose to continue to perform research on the more mature CBD deposition method; however, physical vapor deposition will undoubtedly continue to mature, enabling much more advanced photodetectors as well as other device types. It is expected that novel deposition methods such as laser sinter deposition (LSD) will become more common, as seen in this thesis.[33]

1.3.3 Laser Processing and thin films by sintering micro/nanoparticles

Laser Sinter Deposition (LSD) is a new and very promising alternative for all other deposition methods.[4] Leading up to this work, a joint provisional patent was filed by the University of Virginia and the Department of Navy. The work in this thesis focuses on expanding the potential of laser processing, both as a method for depositing thin films as well as laser treatment and laser patterning of thin films for detectors and focal plane array (FPA). Lasers are widely used for surface treatments; however, no reports have been made of successfully laser sintering PbSe using the method described in this thesis *and* integrating laser treatment to rapidly form customizable FPA, eliminating the need for photolithography.

There is an increase in the use of laser processing to anneal thin films to modify and enhance properties. Jang et al. used the 1070 nm laser (1 J/cm^2) to perform a rapid anneal on a fully sensitized thin film of PbSe deposited by CBD. Jang reported a dark resistance increase of > 32% following IR annealing which translated to a significant increase in D* from 0.55 x 10^{10} cm·Hz$^{1/2}$W^{-1} to 1.23 x 10^{10} cm·Hz$^{1/2}$W^{-1}. Jang reported that the anneal increased the iodine incorporation in Se sites on the surface of PbSe grains. The iodine provides more donor electrons to recombine with holes in the p-type film and increases the dark resistance.[34]

While not for MWIR detection, a group in China published an article using a CO_2 (10.6 μm) laser to sinter an inorganic oxide film of $Mg_xZn_{1-x}O$. The film is photoresponsive to the 290 - 340 nm (UV) regime. The groups reported an impressive D* of 5.46 x 10^{13} cm·Hz$^{1/2}$W^{-1}.[35] The $Mg_xZn_{1-x}O$ material was synthesized chemically and deposited via spin coater. The laser processing was limited to sintering a blanket film; however, the thickness was not reported.[35] Wang et al. coincidentally published in the same month and Journal of Alloys and Compounds, Elsevier as the first publication for this LSD process for PbSe.

The same group from Changchun University of Science and Technology published an article in the same journal on $Al_{0.3}Zn_{0.7}O$-based UV detectors using laser sintering of nanocrystals. The group reported photoresponse to 250 - 400 nm (UV) wavelength and a D* of 3.6 x 10^9 cm·$Hz^{1/2}W^{-1}$. The group spin-coated a thin film on quartz slides and laser sintering was done to form a film of $Al_{0.3}Zn_{0.7}O$.[36]

1.4 PbSe Thin Film Devices

Thin film IR devices are split into three types, photoconductive, phototransistor, and photodiodes. There are a variety of compatible substrates that are IR transparent and heat tolerable such as glass, silicon, quartz, sapphire, GaAs, and even transparent conductive oxides. The choice between insulative and conductive substrate is dependent on the device type. Figure 2 shows the two most common device configurations and is highly dependent on the application. Lateral photo devices are easier to fabricate and interface with (wire-bonding) and are ideal for simple larger area devices. Vertical photodetector cells offer higher density patterning, ideal for the two-dimensional focal plane array but require a photo-transparent substrate conductor and are more costly and challenging to integrate into multichip imaging systems. The choice of metal contact material is also dependent on the IR device to ensure work function alignment to provide ohmic contacts. Gold is the most common contact type.

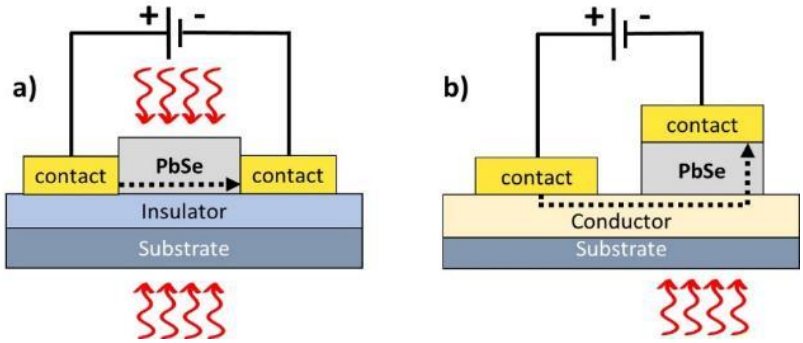

Figure 2: The two primary device layout types for PbSe photodetectors a) lateral device allowing illumination from above or below, through the substrate and b) vertical device usually limited to through the substate illumination due to contact shadowing, ideal for densely patterned focal plane array (FPA).

For this work, the focus will be applied to the photoconductor type as that is the most common type for PbSe. Photoconductors are usually made of a thin film of polycrystalline semiconductors such as PbSe. The films are thermally sensitized to dope the film and create a carrier trap barrier between grains that act as one type of carrier trap. For example, under IR illumination, e-h pairs are produced and under bias conditions, electron traps located at grain boundaries allow an increase in hole lifetime, allowing a considerable increase in conductivity (Figure 3). Photoconductive films such as PbSe generally have linear current-voltage characteristics and act as a photoresistor. Photodiodes are formed with a p-n junction of IR-sensitive material. The materials are chosen or doped for band alignment to become highly conductive under IR illumination. And phototransistors are formed as a three-terminal device to turn on conduction through an insulative gate under IR illumination. The PbSe films demonstrated in this work are all of the photoconductive IR device types.

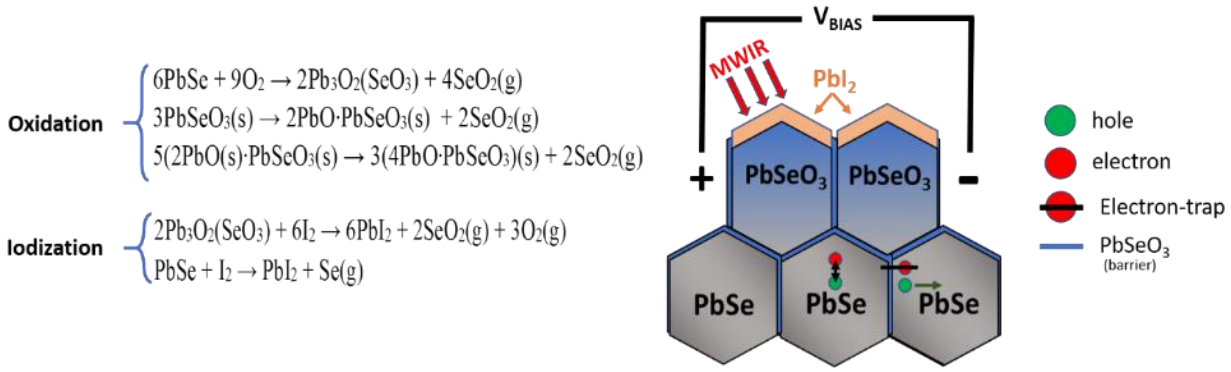

Figure 3: Reactions of PbSe during oxidation (No-KI) and Iodization. (right) Image of PbSe grains after sensitization. $PbSeO_3$ barrier between grains acts as an electron trap during MWIR illumination, resulting in photoconduction. Photoexcited electron-hole pairs recombine rapidly without the presence of e-traps. This diagram is an ideal condition for MWIR photoconduction. The influence of KI assists in setting up this conduction, although some believe KI also acts as a source of holes under MWIR.[12]

The contacts for all devices must be ohmic to maximize the ratio between the illuminated and dark resistance thus, the resistance of the PbSe to contact materials must not form a Schottky barrier. The device only operates under voltage bias conditions, and the illumination of the photo-active layer (PbSe) generates carriers (temporary changes in carrier density).

The photodetector sensitivity is limited by the noise. There are four types of noise mechanisms (1) Thermal noise due to carrier agitation (Johnson-Nyquist), (2) shot noise due to a finite number of carriers passing through the detector film, (3) flicker, also referred to as 1/f noise due to the averaging effects of stochastic paths taken by the carriers, and (4) generation-recombination noise due to stochasticity of the generation-recombination of the carriers in the detector.[4] The following equations describe the respective noise types.

$$i_j = \sqrt{\frac{4kT\Delta f}{R_d}} \quad \textbf{(1)}$$

$$i_s = \sqrt{2q|I|\Delta f} \quad \textbf{(2)}$$

$$i_f = I\sqrt{\frac{1}{f}\frac{\alpha_H \Delta f}{\rho l A}} \quad \textbf{(3)}$$

$$i_{gr} = 2qG\sqrt{\eta E_q A\Delta f + g_{th} l A \Delta f} \quad \textbf{(4)}$$

$\boldsymbol{k}$ is the Boltzmann constant, $\boldsymbol{T}$ is the absolute temperature in kelvin, $\Delta\boldsymbol{f}$ is the noise spectral bandwidth, $\boldsymbol{R_d}$ is the detectors electrical resistance, $\boldsymbol{q}$ is the unit charge, $|\boldsymbol{I}|$ is the mean direct current flow, $\boldsymbol{f}$ is the operating frequency, $\boldsymbol{\alpha_H}$ is the material-dependent Hooge's constant, $\boldsymbol{\rho}$ is the carrier concentration, $\boldsymbol{l}$ is the detector thickness, $\boldsymbol{A}$ is the device area, $\boldsymbol{G}$ is the photoconductive gain, η is the quantum efficiency, $\boldsymbol{E_q}$ is the photon irradiance, and $\boldsymbol{g_{th}}$ is due to thermally generated carriers.[4]

The applications for infrared photoconductive-based devices are primarily for imaging sensors and motion detection.[4] The application of imaging sensor generally involve a two-dimensional array of cells (pixels). The interface or connectivity of the cells in a 2D array necessitates an IR transparent film with conductive trace integrated with a read-out integrated circuit (ROIC) or integration and alignment of an ROIC flip-chip. The integration and fabrication of such ROIC chips is another complexity outside of the scope of this thesis. This work will focus on laser film deposition and laser patterning of the 2D pixel array.

1.5 PbSe Photoconductivity and its Mechanism

The high electron and hole mobility of intrinsic (bulk) PbSe (Table 2) allows for highly electrically conductive polycrystalline thin films at room temperature (RT). This, as well as good optical absorption properties, enables high photoresponsivity under photon excitation. The blue shift in the band absorption edge is the result of the strong confinement characteristics of PbSe. This shift is so easily achieved, that many groups have shifted the bandgap from the intrinsic gap of 0.28 eV to as much as 1.8 eV, corresponding to wavelengths of 4.6 μm to 690 nm, respectively.

While PbSe has been used as an infrared responsive material for over 70 years, the photoconductive mechanisms are still under debate. The models depend heavily on the grain morphology, sensitization, and deposition/synthesis method. PbSe films are often near stoichiometrically balanced (1:1); however, this is highly dependent on the deposition method and conditions during material deposition. It is well understood that intrinsic PbSe (p-type or n-type) is not IR responsive without additional processing, referred to as sensitization.

Some groups refer to sensitization as oxidation or thermal annealing in the air; however, while the process is simple and many groups can achieve IR responsivity with relative ease, the conditions and interactions of oxygen and iodine have significant implications for maximizing photon absorption, achieving linear current-voltage conditions (Figure 4). There are a variety of accepted models for how thermal oxidation enables an IR response in PbSe. The general understanding is that oxidation between PbSe grain boundaries (core-shell p-n junction model) or layered film interfaces (vertical p-n junction model) forms a potential barrier that acts as an electron trap. The incident photon generates an e-h pair, and the barrier traps the electron, resulting in an enhanced hole carrier lifetime. This influences the conductivity and, under an external electric field, translates to a change in conductance. Optimization of sensitization for applications such as FPA usually utilizes halogen doping, often iodine. This is called iodization and is necessary to increase the IR photoconductivity signal. Hechster et al. observed that annealing in a chlorine environment, as opposed to oxygen, improved the signal-to-noise ratio in thin films of PbSe.[37]

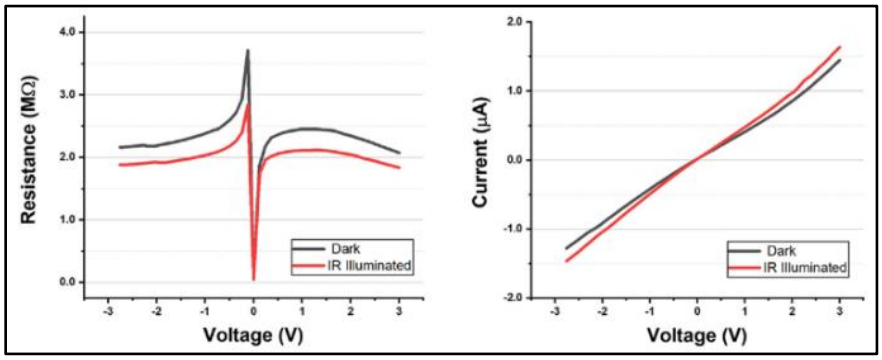

Figure 4: Photocurrent response curves of a sensitized PbSe polycrystalline thin film (1 - 2 μm), dark and illuminated, with a 4-5 μm light source (18 mW/cm²).[33]

(The preceding sections 1.1 – 1.5 were written by the author of this thesis and reproduced from Ref. [4] *with permission from the Royal Society of Chemistry).*[4]

1.6 Research Problems and Thesis Outline

At the inception of this thesis, the understanding of the mechanism behind the high MWIR photoresponse of PbSe thin films was poorly understood. While PbSe has been used as a room temperature mid-wave infrared (MWIR) photodetector for over seven decades, many researchers have reported results reproducing a high MWIR photoresponse at room temperature, yet none have provided a thorough and comprehensive analysis of the interactions which occur between the oxygen and iodine

incorporation. Many have observed that during the sensitization process, iodine influences the PbSe polycrystalline morphology, and oxygen diffuses to grain boundaries which likely act as electron traps but none provided a comprehensive breakdown of the interaction of oxygen and iodine to define a process window. This work reports a comprehensive model, through the design of experiment (DOE) methodology, describing the inter-layer and inter-grain interactions from all perspectives (chemical, morphological and electrical). Through this methodology, the process window for the sensitization is defined, which is agnostic to the deposition method of polycrystalline thin films of PbSe.

It is this researcher's opinion that the root cause of the poor understanding of how PbSe works, is the archaic method used to produce these films until recently, which has been limited to primarily chemical bath deposition (CBD). CBD is very simple in concept; however, fabricators of commercially available PbSe detectors are forced to overcome the many process challenges of CBD and thus hold their fabrication secrets closely. Among others, CBD suffers from poor process control, including, but not limited to poor substrate adhesion (film delamination), sample to sample variation (poor yield), and across-wafer thickness/stoichiometry variations. Other deposition methods offer greater process control but have historically fallen short in achieving a high photoresponse.

There are two primary methods for producing polycrystalline PbSe thin films (0.5 – 2.0 μm), chemical bath deposition (CBD) and chemical or physical vapor deposition (CVD/PVD). Vapor deposition methods offer superior process control at an expense, both in fabrication cost and complexity. The equipment is significantly more costly to acquire and maintain and large amounts of hazardous material are produced.

The primary goals of this work are to introduce a novel alternative method to (1) produce polycrystalline PbSe thin films, (2) provide a means to manipulate and tailor thin films properties (morphology, chemistry, texture, and composition) regardless of the deposition method, and (3) identify and integrate various laser treatments to produce MWIR device with comparable or improved performance. In this work, we introduce a novel thin film deposition method called *laser sinter deposition* (LSD). LSD is a simple, low-cost alternative method for producing *polycrystalline* PbSe thin films while solving the many known issues of traditional methods. It is the intent to use the many benefits of laser processing to provide a new deposition method with tailorable process controls that enable (1) improved understanding behind the photo-mechanism that makes PbSe work and (2) improve the photoresponse with tailorable process control for experimentation. Figure 5 outlines the approach and process flow within this work. This is broken into three stages. The first stage involves an iterative approach to develop and define the laser sinter deposition process to produce an equivalent polycrystalline thin film of PbSe to that of CBD. The second stage involves exhaustive physical, optical, electrical, and photoresponsive characterization to form a process window and model to further understand the mechanism and maximize the MWIR photoresponse. The final stage is the evaluate, document, and integrate various laser treatments to streamline the rapid and customizable fabrication of photodetectors (including focal plane array) with the ability to tailor film properties following thin film deposition. Tailoring thin films with laser processing is not limited to LSD deposited PbSe. Laser processing can be used to improve the PbSe film to substrate adhesion of CBD.

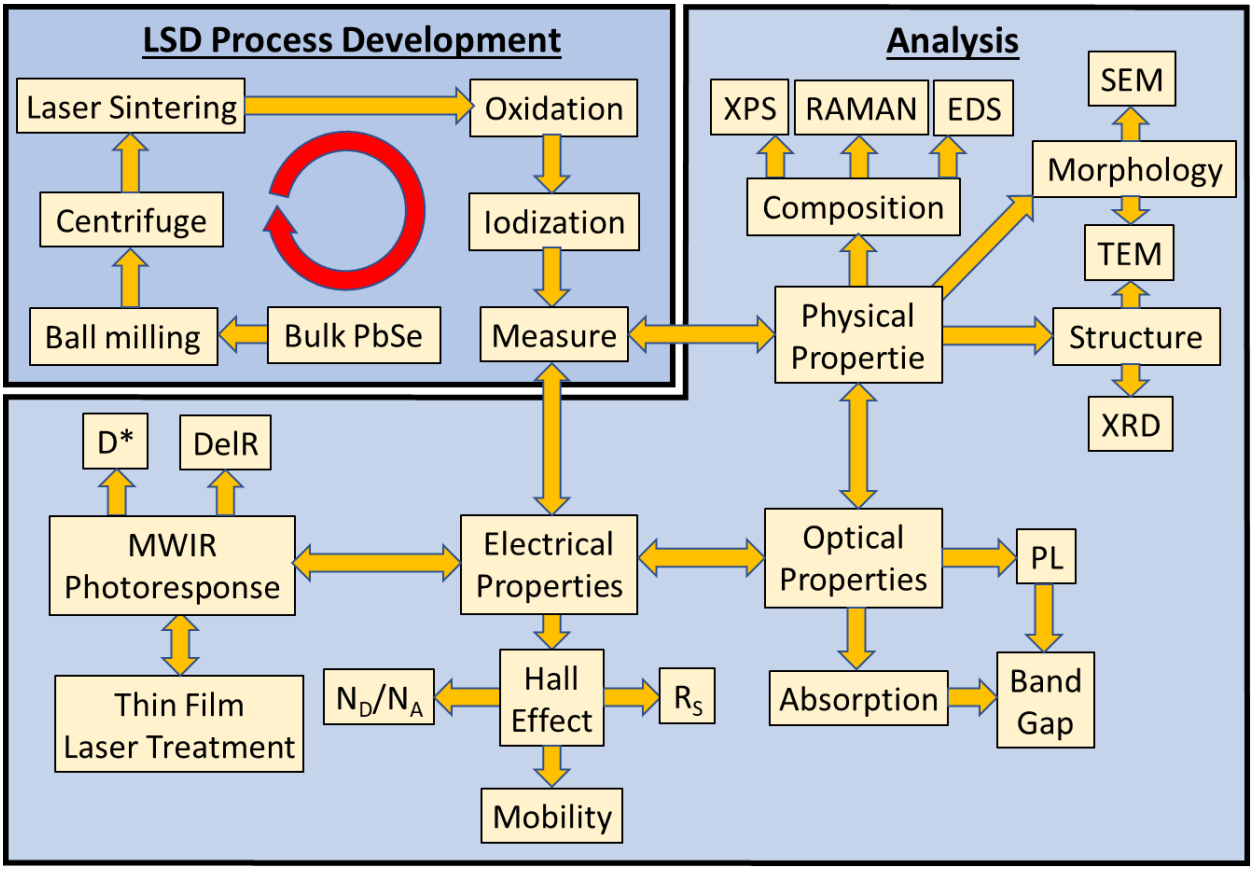

Figure 5: Process flow and methodology used in this work to introduce a new deposition method, characterize the tailorable aspects, and produce high photoresponse thin film equivalent to CBD deposited thin films. During this process, all opportunities for improvement will be documented and shared. Definition of terms: (Detectivity (D*), Photoluminescence (PL), Shee Resistance (Rs), Percent change in resistance (DelR), X-ray Photoelectron Spectroscopy (XPS), Energy Dispersive Spectroscopy (EDS), Laser Sinter Deposition (LSD), Carrier Concentration (N_D/N_A), Scanning Electron Microscopy (SEM), Transmission Electron Microscopy (TEM).

CHAPTER 2: Laser Sinter Fabrication of PbSe Thin Films

2.1 Introduction

This work aims to develop and introduce a novel method for depositing polycrystalline thin films to provide an alternative deposition method and advance both the understanding of the mechanism behind PbSe photoconduction and controlling the material properties of polycrystalline PbSe thin films. The new thin film deposition process is called Laser Sinter Deposition (LSD). The LSD process consists of three simple steps to produce nanoparticles, uniformly deposit them on substrates, and selectively laser sinter the particles into a dense polycrystalline thin film. Additionally, the LSD process solves many of the challenges with other methods by providing rapid processing reducing selenium loss, and superior film-to-substrate adhesion suffered by CBD. For electrical isolation between conductive thin films and the silicon substrate, the PbSe film was deposited on silicon substrates with a 2.0 μm thick thermally grown silicon dioxide (SiO_2) layer.

The laser sinter deposition method is in its infancy; however, it is maturing rapidly and offers many advantages including simplicity, low cost, and a reduction of hazardous waste compared to other methods. In addition to being a new method for depositing PbSe, LSD can also be used to address the problem of traditional deposition methods such as improved substrate adhesion, ultra-rapid thermal annealing, and in-situ doping. Surface *treatments* using lasers have a long history[65], however, none have reported expanding the laser processing to sinter nanocrystal powders of PbSe for thin film applications. LSD offers the advantage of allowing spatially defined sintering, rapid sintering to promote doping with depth control, reorganizing of crystalline structures including defect reduction, and the trapping of non-equilibrium structures[38]. This work will utilize LSD and these potentials to demonstrate the advantage laser processing has over other deposition methods. Another advantage of LSD is the ability for selective depth sintering (SDS) by exploiting the absorption depth of different laser wavelengths in the PbSe material.[33]

2.2 Experimental Setup of Laser Sinter Deposition (LSD)

The laser sinter deposition (LSD) process consists of three steps, shown in Figure 6 below. The steps consist of the formation of fine nanocrystals (NC), followed by uniform deposition of NCs on a suitable substrate, followed by laser sintering to densify and form a continuous thin film with superior adhesion to the substrate.

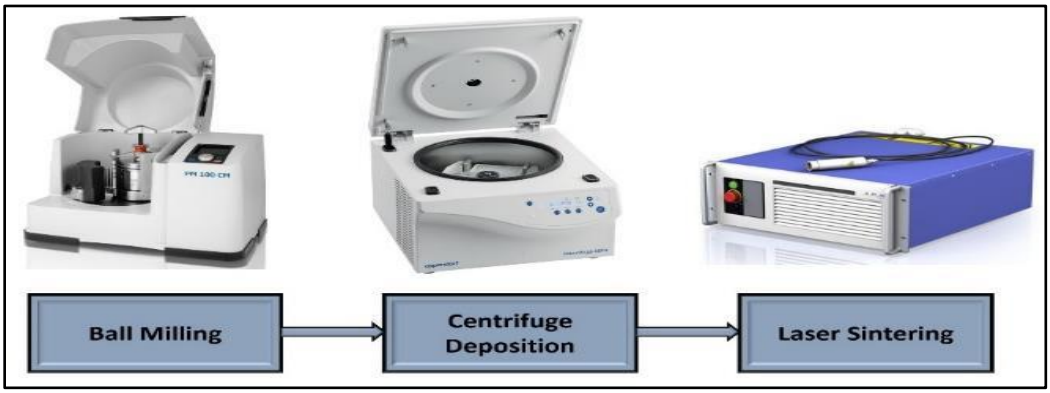

Figure 6: Laser Sinter Deposition (LSD) equipment (left to right: Planetary ball mill, centrifuge, pulsed laser (1070 nm)[34]

The first step uses a *planetary ball mill* to form high purity (99.99%) and stoichiometrically balanced (50:50) PbSe nanocrystals (NCs) from PbSe ingot. A wet ball milling process is necessary to obtain fine

nanocrystals, reduce frictional heat buildup during the milling process [40], and safely contain the particles in colloidal form. Several solvents were evaluated and methanol was found to be ideal for forming and suspending the PbSe in colloidal form. Another reason for using methanol in the ball milling process is to maintain a known concentration of PbSe NCs in a colloidal solution for ultra-small and accurate dosing during the subsequent centrifuge deposition process.

The second step uses a tabletop centrifuge system to *drop out* the suspended colloidal PbSe NCs from the PbSe-methanol solution and form a compact, thin film of micro/nanocrystals on a substrate. This is achieved by ultrasonication to uniformly disperse a known concentration of PbSe NCs in methanol and using an adjustable micro-pipette to consistently draw a precise and predetermined amount of PbSe solution. A targeted substrate is then placed at the bottom of a vial and partially filled with fresh methanol. The micro-pipette is used to draw a set amount of PbSe NC for transfer to the vials of methanol containing the substrates. Uniform dispersion is maintained in the vial by further ultrasonication in a bath. The centrifuge is then used to *drop out* the colloidal PbSe NCs and pack them on the substrate. The methanol, now clear, is removed, and the substrate dried. The substrate now has a uniform amount of compact PbSe NCs distributed across the surface, as shown in Figure 7 (left). The samples are ready for laser sintering (right).

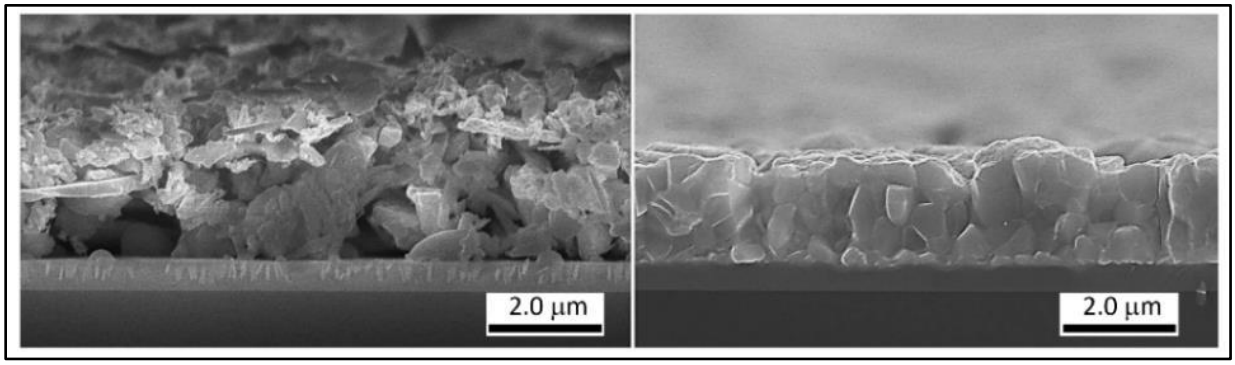

Figure 7: Scanning electron microscope images of cross-sectioned as-deposited PbSe nanocrystals (left) and post-laser-sintered (right) on an oxide-coated silicon substrate

The final step of the LSD process uses a 1070 nm laser to sinter and densify the PbSe powder within the argon purged 3D printed chamber. The 1070 nm laser is ideal for adequate absorption and sintering of a 500 – 1,500 nm thin film of PbSe NCs. The PbSe NCs *absorb* the 1070 nm wavelength for sintering and recrystallizing the NCs, but also allow sufficient *transmission* to heat the silicon substrate to achieve superior adhesion while simultaneously forming a polycrystalline thin film. CBD deposited thin films of PbSe require substrate treatment and roughening for adhesion of the film but still suffer from flaking and delamination. Figure 7 (right) shows a scanning electron microscope (SEM) cross-section of an LSD processed PbSe thin film. Notice the densification and equiaxial polycrystalline grain formation, as well as the lack of separation with the substrate.

2.2.1 Determination of Crystalline Strain from Laser Sintering Process

To determine if film stress is induced by the laser sintering process, a thermal anneal study was performed. The standard sensitization process for most lead-based IR sensitive films (PbSe and PbS) requires oxidation at elevated temperatures. Oxidation usually occurs at temperatures exceeding 385^{o} C. This may be sufficient to alleviate film stress; therefore, a thermal anneal may not be necessary. However, this experiment aimed to identify if stress occurs in the ball milling or the laser sintering process and attempted to identify and delineate between the two.

Stress-induced into the crystalline lattice during the ball milling and laser sintering process is a possibility and could be determined by measuring the level of strain in the film. This is difficult to measure directly in polycrystalline thin films. In this case, we used x-ray diffraction (XRD) to measure

the two different forms of strain in a polycrystalline material (uniform and non-uniform strain). Uniform strain is indicated by a shift in the characteristic XRD peaks for material, while non-uniform strain translates to a broadening of the relative XRD peak with a diminished intensity[20] (Figure 8). In the case where a thermal anneal is performed to relieve stress, XRD peak narrowing can be due to a combination of nonuniform strain relief as well as grain growth or grain merging.

$$D = \frac{k\lambda}{\beta_D \cos\theta} \qquad \textbf{(5)}$$

Grain size can also be extracted from the XRD spectrum using Scherrer's equation (5) and can be compared to actual grain size measurements taken with SEM. In this case, D is the particle size, k is a constant of 0.94, λ is the wavelength of x-ray radiation (1.5406 angstroms), β_D is the peak full width at half maximum (FWHM), and θ is the peak position.

Some changes in the XRD spectrum can be convoluted by grain growth, so moderate anneal temperatures (475^o C) and durations were used to limit grain growth. Localized site-specific measurements were made with SEM to correlate XRD data to the top-down physical dimension. Any discrepancy between SEM and XRD concerning grain size is an indication that the PbSe grains may be composed of polycrystalline agglomerates.

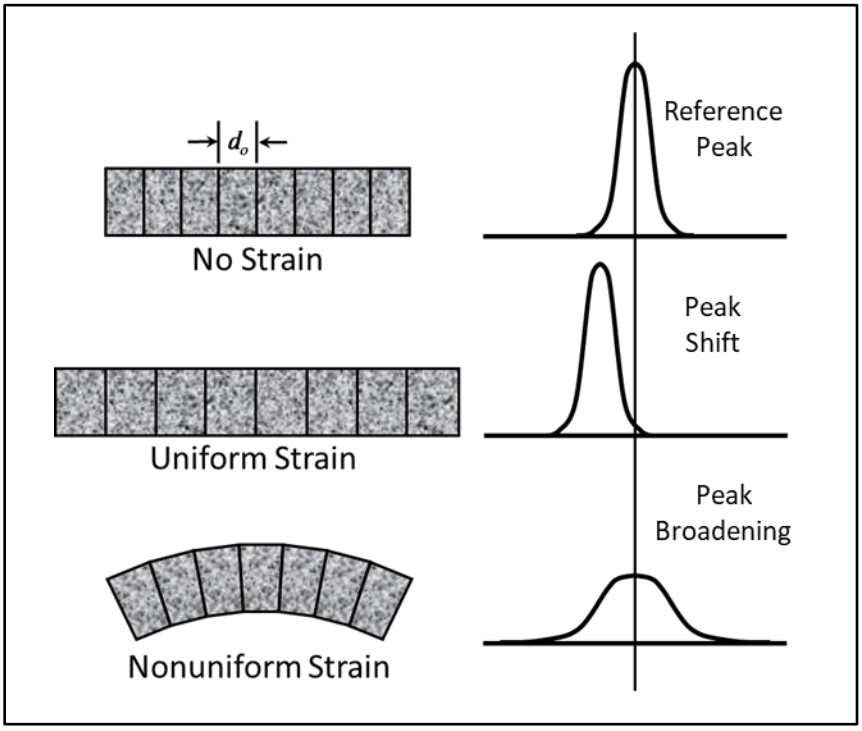

Figure 8: XRD characteristics of strained crystalline material. No strain and reference XRD peak (Top), Uniform film strain with a relative shift of the (no strain) reference characteristic XRD peak (middle), and Nonuniform strain with wider peak (bottom).[41]

2.3 The Laser Sinter Deposition (LSD) Process

2.3.1 Ball Milling Optimization

Producing the ideal form and distribution of PbSe nanocrystals (NC) begins with 0.5 g of lead (II) selenide ingot purchased from Sigma Aldrich. The PbSe is then *wet ball milled* in a Retch Planetary Ball Mill (model PM100) to form PbSe nanocrystals suspended in methanol solution (Figure 9). The ideal

coarseness of the NC powder for the LSD process is a particle size distribution between 50 nm – 2.0 μm per SEM inspection. High-energy wet-milling with a planetary ball mill is a safe and effective way to form fine NC powders finer than 100 nm suspended in a solvent.[33] Selenium loss in PbSe is known to occur under elevated temperatures, so careful consideration was given during the ball milling process to minimize heating from friction[42].

To reduce contamination of the NC media during ball milling, a zirconium oxide (ZrO_2) ball milling cup (50 mL) and ball material (3 mm) were used. ZrO_2 is chosen specifically for its hardness (~7.9 Mohs) and purchased directly from Retsch Inc. Both *agate* and *stainless steel* ball milling (cup and ball material) were evaluated as well but caused considerable contamination due to erosion of the ball and cup material during the ball milling process. For this reason, ZrO_2 or harder is necessary for the LSD process.

Following ball milling, the concentrated solution of PbSe NCs now suspended in methanol is transferred to a container and diluted to a predetermined concentration for the subsequent deposition process.

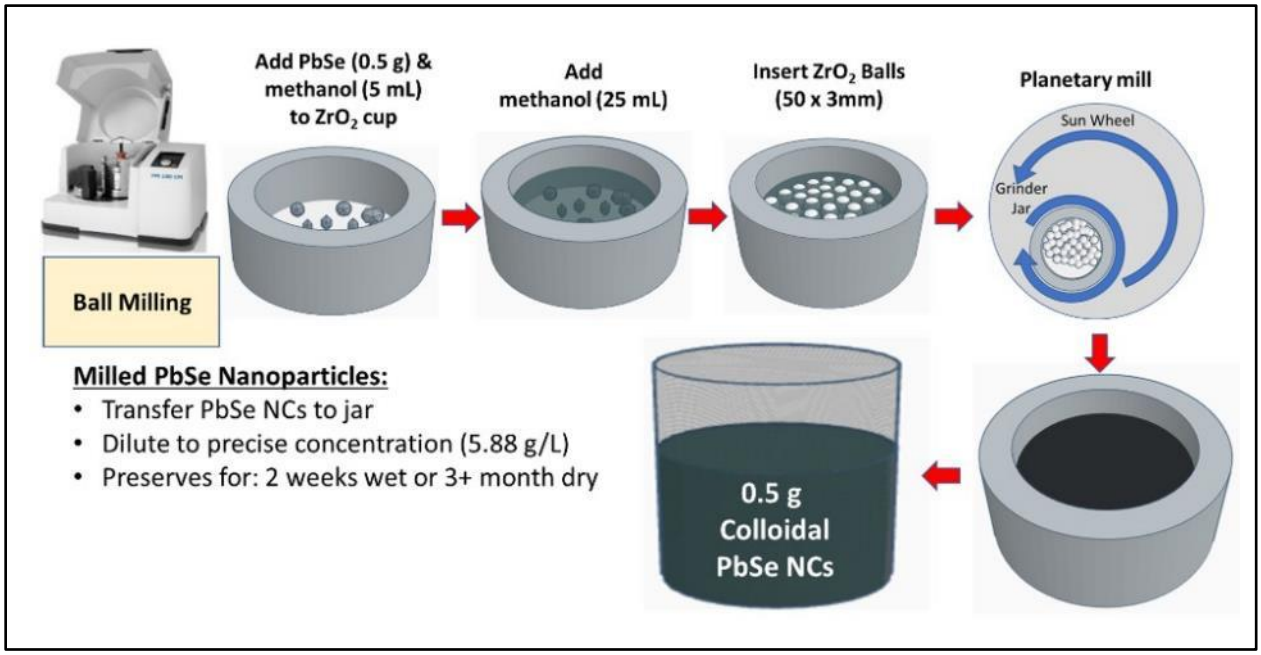

Figure 9: Schematic of Planetary Ball Milling to produce colloidal PbSe nanocrystals (NC).

2.3.2 Centrifuge Deposition of Colloidal PbSe Nanocrystals

(100) silicon substrates with 2,000 nm thick thermally grown SiO_2 were used in this study for electrical isolation from the substrate. Two sizes of substrates are used, small 10 mm x 20 mm wafer pieces and 50 mm diameter (circular) wafers. The wafer pieces are placed in vials with lids (20 ml vial or 200 mL, respectively) partially filled with pure methanol (Figure 10). Concentrated colloidal PbSe NCs suspended in methanol are ultrasonicated and pipetted out in precise amounts for a predetermined thickness (Table 4). The vials are then spun in the centrifuge at ~4,000 rpm (~3,200 G's) for 15 minutes to separate the PbSe NCs and densify the powder. Once complete, the solution is now completely transparent, leaving a uniformly deposited and densely compact film of PbSe NCs across the substrate. The methanol is removed and the samples are dried on a hot plate at 75° C for 5 minutes.[33]

Table 4 Concentration of PbSe and solvent per milling batch and per sample via centrifuge deposition

PbSe NC Concentrate (post milling)			Methanol Dilution (for centrifuge)			
Silicon substrate	PbSe milled (g)	Methanol (mL)	Volume of Soln. (mL)	PbSe NC (mg/vial)	Vial Size (mL)	Methanol (mL/vial)
10 mm x 20 mm	0.5	55	0.4	3.6	20	10
50 mm wafer	0.5	55	2.2	19.2	200	100

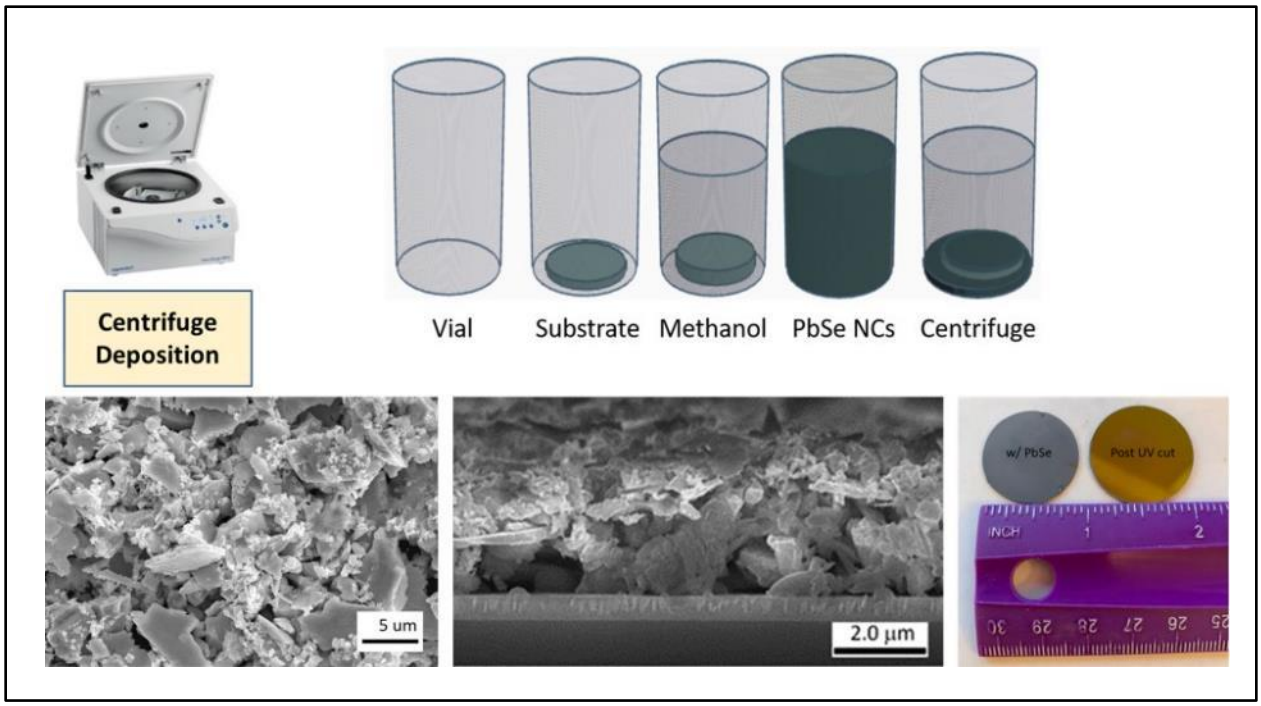

Figure 10: Schematic of Centrifuge deposition process for suspended colloidal PbSe nanocrystals into a uniform thin film of powder. Topdown SEM image showing the size distribution of PbSe micro/nanocrystals following centrifuge deposition (bottom left), cross-sectional SEM image of micro/nanocrystals (bottom middle), and example of laser cut substrates (bottom right), before (amber) and after (matte gray)

2.3.3 Laser Sintering Chamber Design

Due to the inherent toxicity of PbSe, laser sintering was done in a vented chamber and purged with argon to eliminate exposure and minimize oxidation of the PbSe film. SolidWorks was used to design a custom chamber and printed in a *Formlabs 2* resin-based 3D printer (Figure 11). With the sample inside the chamber and purged with inert gas, the laser is rastered with a galvo (Sino sg7210) into the chamber through a BK7 window purchased from Edmunds Optics (Figure 11). A constant substrate temperature is maintained, and improved temperature uniformity is achieved during extended laser rastering with a liquid-cooled heat exchanger and sample chuck inside the chamber. The substrate temperature is reported to play a critical role in film morphology.[32,33]

Various laser types were used to evaluate the impact of different wavelengths in the sintering of PbSe NCs and the interactions with the substrate. The laser types evaluated include, long pulse (100 µs) IPG fiber YAG of 1070 nm wavelength, nanosecond short-pulse (50 ns) IPG fiber laser of 1064 nm wavelength, and a diode-pumped solid-state (DPSS) short-pulse (25 ns) laser (Coherent MATRIX) of 355 nm wavelength. The YAG laser (IPG Photonics, YLR-150/1500) with a 1070 nm wavelength was most promising as it allowed both pulsed and continuous-wave options, and this wavelength had the potential to improve film adhesion by simultaneously heating the silicon substrate. Spot size, raster scan speed, line-scan pitch, and power were the primary laser parameters evaluated.[33]

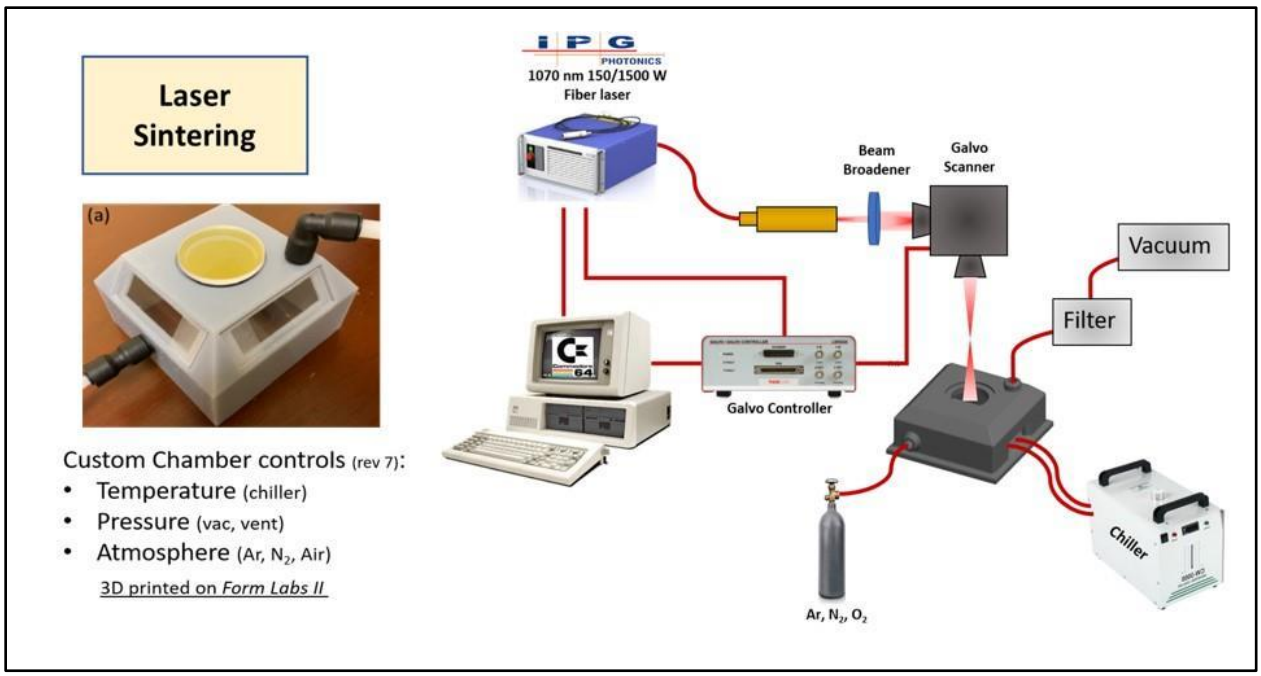

Figure 11: Schematic of Laser Sintering of the PbSe nanocrystals to form a dense conductive thin film of polycrystalline PbSe.

2.3.4 Laser Sintering using 1070 nm wavelength laser

The 1070 nm wavelength fiber laser set to continuous wave (CW) has a maximum power of 150 W with a Gaussian beam profile. Based on preliminary sintering experiments in both CW and pulsed modes (QCW) a 600 µm spot size was chosen by adjusting the distance from the galvo. To allow sufficient overlap between line scans, a 50% line-scan pitch was initially chosen. An adequate balance was achieved to sufficiently sinter the PbSe yet minimize thermal stress and allow recrystallization of the PbSe. Substrate heating plays a key part in film adhesion. Slow rastering leads to loss of selenium as well as partial melting, balling, ablation, and excessive substrate heating. Scanning too rapidly leads to incomplete recrystallization and high film stress.[33]

Significantly different conditions were used for QCW (quasi pulsed-wave) experiments due to the high pulse energy, leading to a more rapid material heating and cooling cycle. This could help minimize selenium loss buts could potentially lead to higher film stress compared to CW. This may, however, minimize the need for substrate cooling and loss of selenium during the laser sintering. Preliminary results necessitated a lower power be used (24 W average, 165 W peak) with a tighter raster pitch due to the short pulses and heat dissipation (85% overlap and a scan speed of 100mm/sec).[33]

2.4 Results and Tailoring of Laser Sinter Deposition of PbSe Thin Films

The ball milling process successfully and consistently produced a repeatable PbSe NC powder in colloidal form. Initially, it was not known if laser sintering would require a narrow size distribution of PbSe NCs. An experiment was performed using centrifugal processing to selectively drop out specifically sized crystals. Figure 12 shows the results of this experiment.

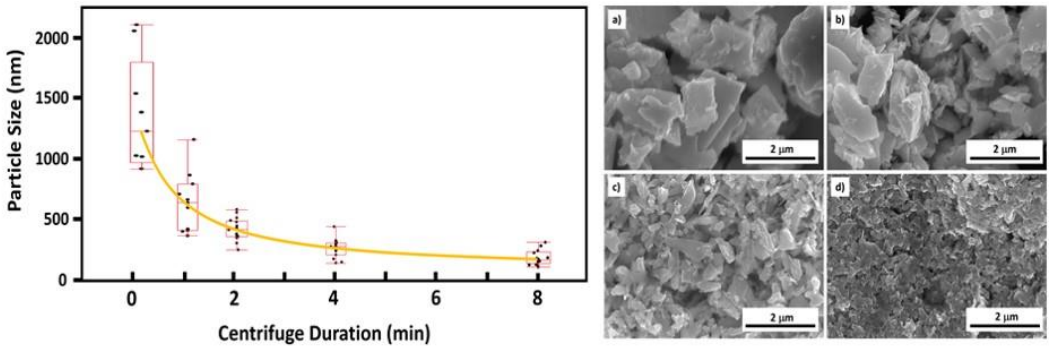

Centrifuge (min)	Number (counts)	Mean (nm)	Std Dev	Std Err Mean	Lower 95%	Upper 95%
0	9	1342.1	446.1	148.7	999.2	1684.9
1	11	687.6	220.3	66.4	539.6	835.6
2	16	414.0	81.1	20.3	370.8	457.2
4	15	308.7	74.9	19.4	267.2	350.2
8	17	172.5	48.6	11.8	147.5	197.4

Figure 12: Results of particle segregation through centrifugal separation. Images are all at the same magnification and show particle size segregation following (a) 1 min, (b) 2 min, (c) 4 min, and (d) 8 minutes in a centrifuge.[33]

PbSe NC separation by size was successfully achieved; however, later experiments revealed that a broad NC size dispersion was beneficial for forming a densely packed film of PbSe powder. The tight packing of varying sizes of PbSe NCs produces a more dense and uniform film following laser sintering. For this reason, this process was interesting but found to be unnecessary. A more detailed description of this experiment and results is available in reference [33].

As mentioned previously, the 1070 nm wavelength allowed the most morphological control and superior film-substrate adhesion due to the 1070 nm absorption into silicon. Figure 13 shows how the 1070 nm laser can tailor the morphology by substrate temperature control and laser parameters. This allowed the PbSe film morphology to vary from an equiaxed grain type to an elongated columnar grain type.[33]

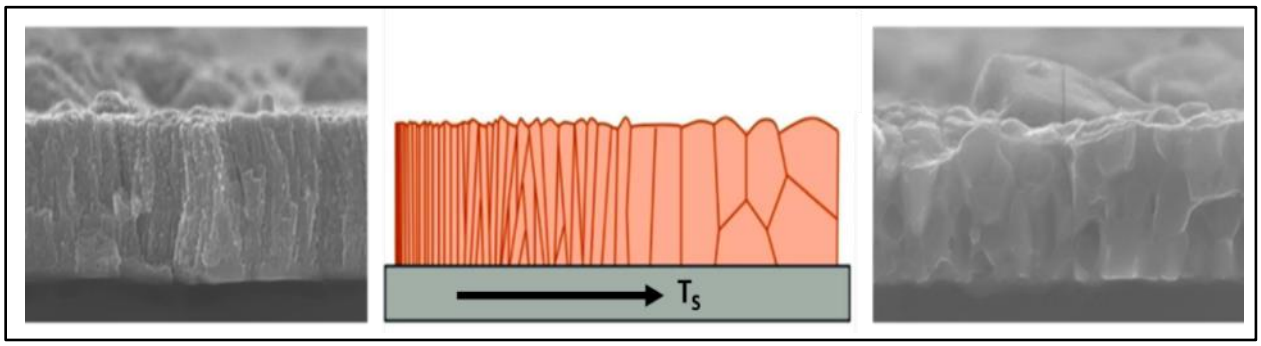

Figure 13: SEM cross-sections of LSD films of PbSe showing the variation of grain morphologies following laser sintering of PbSe using a 1070 nm laser with fast laser scan (100-500 mm/s) for reduced substrate heating (left) versus slow laser scan (25-100 mm/s) with in-situ substrate heating.

Tailorable morphology, as well as spatial control, are one of the key benefits of the LSD process as well as in-situ doping. Figure 14 below shows top-down SEM images of some of the tailoring allowed with PbSe.

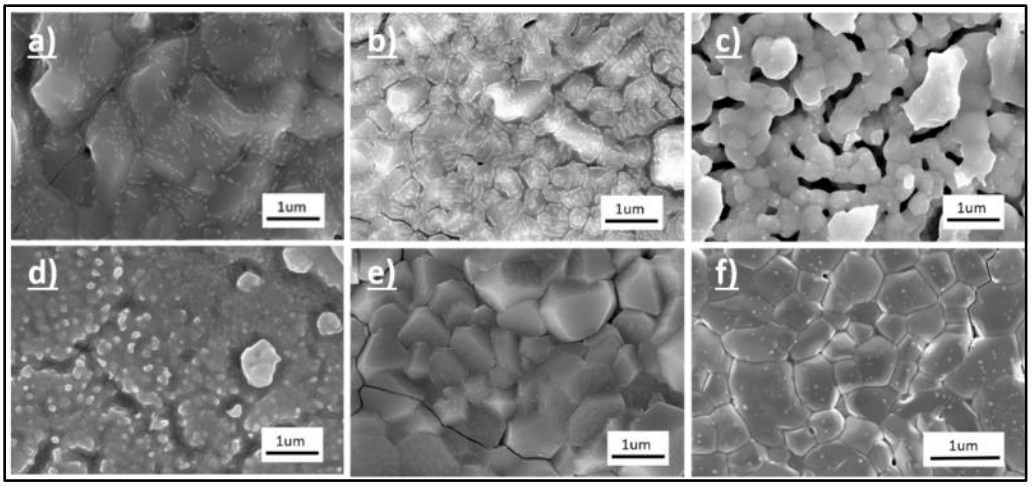

Figure 14: SEM images of PbSe morphology tailoring with layer sintering, a) Smooth (UV treated), b) nano-textured (, c) porous, d) columnar, e) equiaxed, f) KI doped. All images are at the same magnification. Image a through c are from higher laser power to lower, d and e are fast scan (columnar grains) and slow scan (equiaxial grains), respectively, and f shows the influence of potassium iodide incorporation.

2.4.1 Comparison between CBD and LSD deposited thin films of PbSe

The ability to tailor film morphology using the LSD process and the choice between using either continuous (CW) or pulsed wave, also known as quasi-continuous wave (QCW), allows many parameters to control specific properties. In the case of PbSe, where selenium is volatile at high temperatures, minimizing heating with rapid sintering using a pulsed laser reduces selenium loss and thermal shock. Figure 15 shows top-down SEM images of a thin film of PbSe produced by CBD[11] and LSD[33] side by side. The parameters for producing this film are listed in Table 5.

Table 5: Laser parameters of the 1070 nm IPG sintering process used to produce the film in Figure 15 (left).

Mode	Spot Size (µm)	Laser Power (W)	Scan Rate (mm/s)	Linescan Pitch (µm)	Substrate temp (°C)
QCW	600	165.0 (Peak)	100.0	100.0	35.0
CW	600	49.0	3.0	300.0	35.0

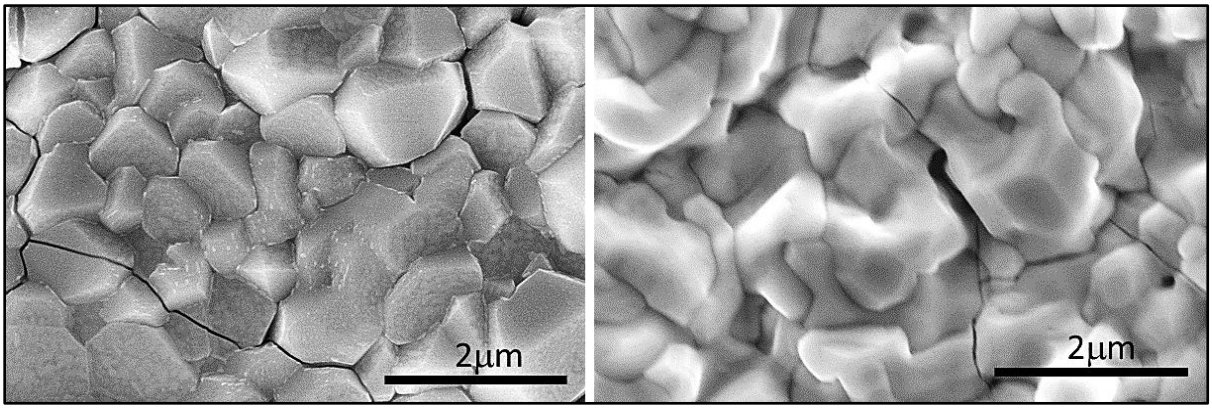

Figure 15: Side-by-side comparison between LSD (left)[27] and CBD (right)[12] deposited thin films of PbSe.

2.4.2 LSD PbSe Thin Film Composition

SEM inspection was the primary tool for determining physical film quality; however, energy dispersive spectroscopy (EDS), focused ion beam (FIB) and transmission electron microscopy (TEM) was also used for determining composition, microstructure, and allowed site-specific cross-sections. Top-down and cross-sectional EDS were used throughout this work to confirm both stoichiometry and composition profile through the full film thickness. Figure 16 shows an EDS line scans showing the consistent Pb to Se ratio through the full thickness of this 1.6 μm film.

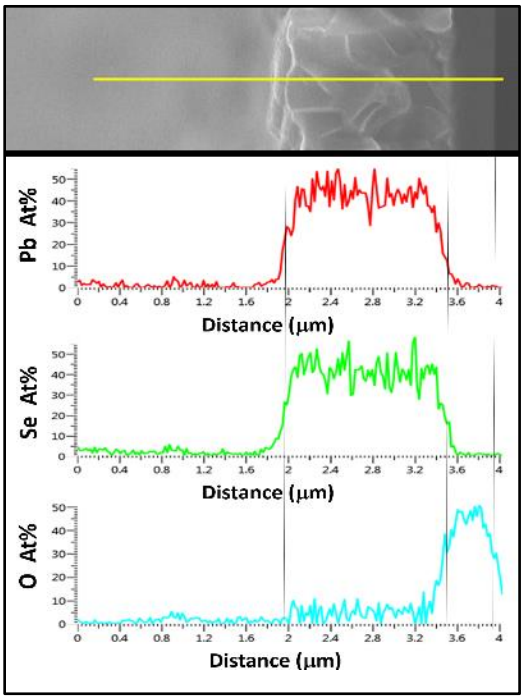

Figure 16: Linescan EDS through laser-sintered PbSe cross-section indicating uniform stoichiometry

Top-down and cross-sectional energy dispersive spectroscopy (EDS) indicated a balanced stoichiometry was maintained and was proven effective for detecting when and if selenium loss occurred (Figure 16 and Table 6). This correlated nicely with Hall Effect measurements. When significant selenium loss occurred, the majority of carrier concentrations were toggled from *p*-type to *n*-type.

2.4.3 Electrical Characterization (Resistance, Mobility, and Carrier Density)

A precision current source meter and Ecopia Hall Effect four-point probe system (described above) were used to determine sheet resistance across voltage ranges for films with sheet resistance varying between 500 Ω/*sq* (post-sintered) and 30 MΩ/*sq* (fully sensitized). A Keithley 2400 Source-meter was used to sweep current versus voltage (I-V) and determine linearity. The I-V measurements indicated electrical contact properties (ohmic vs. Schottky) and the presence and polarity of *pn* junctions. Laser-sintered samples consistently resulted in linear I-V between +/- 20V, and no evidence of any across sample pn junctions or Schottky barriers were evident.

Table 6 below shows the electrical parameters of both CBD and laser-sintered samples. The mobility of laser-sintered PbSe was consistently lower. Based on electrical measurements, thermal annealing results, and TEM analysis, it is concluded that this is due to a combination of film density, crystalline defects produced during the ball milling process, and the lack of a passivated surface. The film density is increased, and the resistivity decreased with repeated subsequent laser sintering scans. Repeating the

sinter scans and rotating the raster orientation successfully improved sample uniformity (morphology and resistance), and lowered the resistivity (from 0.58 Ω·cm to 0.17 Ω·cm). A more detailed explanation will follow in Chapter 6.

Table 6: Hall measurements on laser-sintered thin films and comparison with CBD process[11]

Sample	Carrier Type	Carrier Concentration (/cm^3)	Mobility (cm^2/V·s)	Resistivity (Ω·cm)	Thickness (μm)	Stoichiometry %Pb/%Se
CBD (As-deposited)	p-type	7.1x10^{17}	41.6	0.16	1.5	49.5/50.5
Laser-sintered	p-type	4.5x10^{17}	19.3	0.58	1.6	49.1/50.9

Additionally, TEM and selected area electron diffraction (SAED) patterns confirmed that the laser sintering process successfully recrystallizes the PbSe (Figure 17).

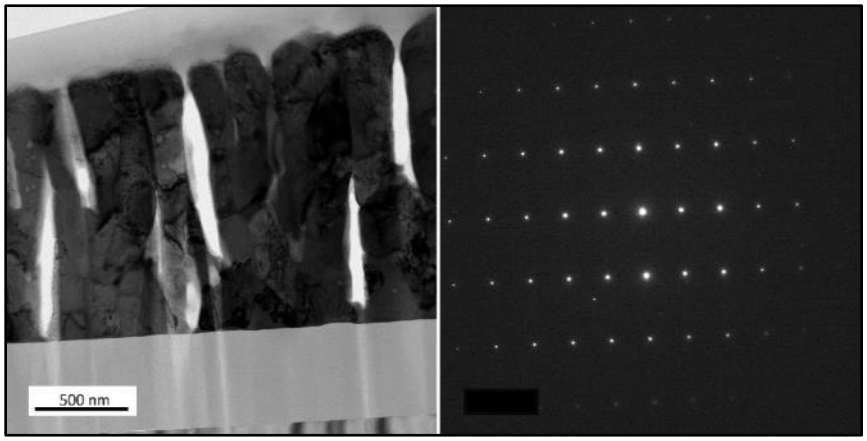

Figure 17: TEM and Selective Area Electron Diffraction (SAED) of the columnar grains of PbSe showing complete recrystallization of PbSe grains following laser sintering.

2.4.4 Effect of Thermal Annealing of Post Laser Sintered Films

As described in the experimental section, XRD peak shift and peak broadening are strong indicators of lattice stress. In this experiment, a thermal annealing treatment was performed to identify any relaxation or change in lattice stress. No strong correlation between XRD peak width and thermal annealing was observed. While peak broadening can indicate the presence of film stress, changes in peak width also indicate changes in grain size, which can change with thermal annealing. Peak shifts, however, are not related to grain size, and it was found that ball milling and laser sintering may introduce film stress.

The XRD spectrum for samples showed all the expected characteristic PbSe peaks (Figure 25). The silicon peak from the substrate (not shown in Figure 25) provides a strong reference point for accurately determining peak shifts for PbSe. Table 7 below shows peak shifts relative to silicon between post-sintered samples and those exposed to an extended anneal (4.5 hours @ 475^o C). This shift is subtle but consistent across multiple PbSe peaks and suggests that uniform film stress was reduced. This also indicates that samples exposed to KI (drop cast in 6.0 μM) exhibited larger peak shifts. This supports the theory that KI impacts the recrystallization of PbSe by acting as a flux. The relative percent shift is within the instrument error; however, it is consistent and proportional across the three primaries PbSe peaks [(111), (200), and (222)]. Both the samples with and without KI exhibited an equivalent shift for the (022) peak. To confirm the influence of KI on grain growth, grain measurements were taken with SEM (20 kx

magnification) before and after the thermal anneal (Figure 18). After a short anneal (1.5 hrs at 475° C), grains exposed to KI (6.0 μM drip cast) grew, on average, 60%, while grains without KI only grew 12%.

Table 7: Data showing characteristic peak shifts relative to silicon for samples with and without KI.

2θ Shift in $x10^{-3}$ degrees				
	(111)	(200)	(222)	(220)
w/ KI	17.69	6.32	23.87	10.23
w/o KI	6.21	2.1	10.84	9.99
ratio	2.85	3.01	2.20	1.02

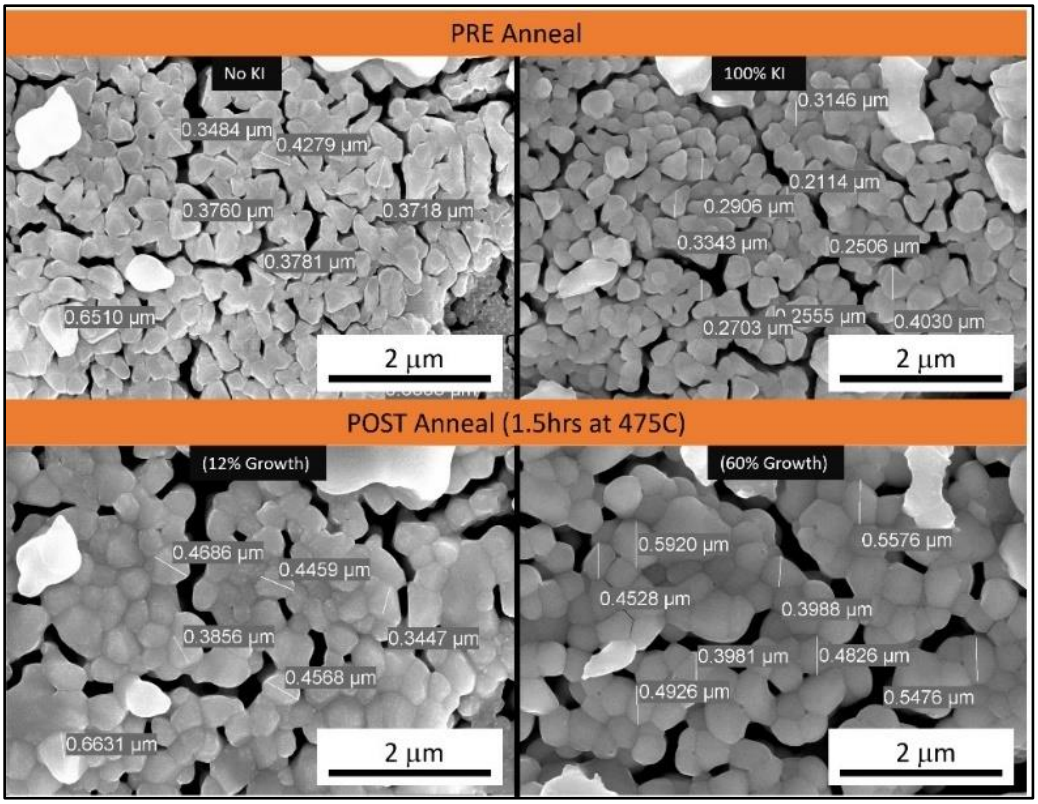

Figure 18: SEM with site-specific measurements of the influence of KI on grain growth during an anneal. These images are all taken in the same field-of-view before (top) and after (bottom) a 90-minute inert anneal at 475° C. They show how the grains grow and merge with KI (right) versus without KI (left) following the anneal. The films incorporated with KI show a substantial increase in grain growth (12% versus 60% increase).

(The preceding sections 2.1 – 2.4 were written by the author of this thesis and reproduced from ref. [33] *with permission from the Journal of Alloys and Compounds)*

2.5 Conclusion

This work successfully introduces a novel new method for forming a polycrystalline thin film of PbSe, not reported by any other research group as of the time of its publication. As a result, a provisional joint patent application between the University of Virginia and the Department of Navy has been submitted for the LSD process. This works shows that not only can LSD sufficiently reproduce CBD equivalent thin films of PbSe (chemically, compositionally, morphologically, and electrically), but the LSD process can

address and improves CBD. The LSD process is spatially tailorable, improves substrate adhesion, offers rapid laser treatments that can expand the understanding behind PbSe, and offers a tool for the experimental fabrication of thin PbSe films. The process is now repeatable; however, the biggest factors in film quality are dependent on the ball milling and centrifuge process producing a tightly packed pre-sintered film as well as the correct dosing of potassium iodide before laser sintering. This process is by no means limited to the PbSe material set. We have shown that this novel method has many advantages over others and can be used to advance the knowledge of the photoresponse mechanism of PbSe. Further exploration for new applications for this and other materials sets will be pursued.

CHAPTER 3: Sensitization of LSD Deposited PbSe Thin Films

3.1 Introduction

3.1.1 Background

PbSe thin films require oxidation followed by iodization (sensitization process) to enable an MWIR photoresponse by incorporating and activating iodine in the polycrystalline PbSe film, within and in-between the individual PbSe grain.[43] The oxidation followed by iodization significantly improves the PbSe thin film photoresponse, but the mechanism is not well understood. The combination of oxygen and iodine incorporation in PbSe thin films is considered important.[12,27] The controlled formation of lead selenite ($PbSeO_3$) is also believed to enable the photoresponse, while iodine is understood to impact the recrystallization of PbSe grains, reduce activation energy in forming $PbSeO_3$, and may also contribute to the photoresponse.[44,45] Golubchenko et al. reported the presence of iodine in PbSe reduces the formation temperature of oxyselenites by 100° C and assists in the recrystallization of underlying PbSe grains.[12,27] Some groups have demonstrated reversing the order in a hybrid sensitization process where iodization is performed before oxidation, although oxygen is used as a carrier gas for the iodine.[45–47] The high MWIR photoresponse achieved by many researchers using vastly different methods supports the claim that (1) oxygen and iodine play a very interactive symbiotic role and (2) the as-deposited PbSe film morphology and microstructure determine the sensitization conditions necessary for maximizing the MWIR photoresponse.

3.1.2 Sensitization of PbSe Thin Films

As described in previous sections, the generic sensitization process for PbSe is broken down into two thermal process steps. Most often, the first step is thermal oxidation or annealing in air at a temperature between 280° – 480° C followed by a second thermal step of iodization performed at a lower temperature of 285° – 325° C. During this step, iodine interacts with the previously formed oxidized PbSe (lead selenite), and a surface layer of PbI_2 is formed. The PbI_2 layer that forms on the surface during iodization necessitates this temperature to remain below the melting point for PbI_2 of 410° C. The oxidation and iodization process is shown in Figure 19.

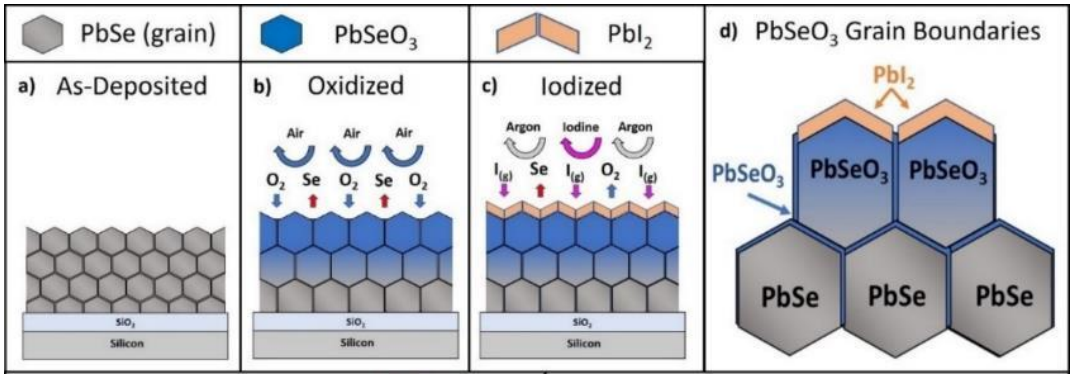

Figure 19: Schematic of the generic sensitization process for each step. (a) as-deposited polycrystalline PbSe, (b) Oxidation of PbSe, to form $pbSeO_3$ (c) Iodization of PbSe, and (d) simplistic depiction of inter-grain oxide barrier. NOTE: These schematics are not to scale; however, an increase in PbSe grain size does occur throughout the thermal sensitization process. Iodine is also incorporated in PbSe grain boundaries and is not shown.

The current understanding is that the fully sensitized PbSe films (500 - 1,500 nm thick) are most often comprised of polycrystalline equiaxial grains (200 - 500 nm). The film is composed of a top layer of PbI_2, a transition layer of unknown composition (prior to this work) with little understanding of its influence on the MWIR mechanism, and a polycrystalline PbSe base layer. The base-layer grains are suspected of being coated with lead selenite which enhances the photoconductivity by producing electron traps.[12,27]

Little is understood about the transition layer between the PbI_2 and the PbSe base layer; however, some groups have reported Pb:Se:I-based or Pb:Se:O:I-based compound in this transition layer that may impact the photoconduction of PbSe thin films.[12,29,30] These trinary and quaternary phases are reported in the cited literature as being crystalline in structure with molar fractions varying greatly from the surface of the film (primarily PbI_2) down to the base-layer (primarily PbSe, coated with oxygen and iodine). Jang et al. did not report oxygen in his transition layer but describe how the trinary phase influences photoconduction by diffusing electrons down into the PbSe to suppress holes under dark conditions, leading to high dark resistance.[12] Upon IR illumination, the electrons from this ternary phase are trapped at grain boundary trap sites along with photogenerated electrons. Kumar et al. reported significant high-resolution transmission electron microscopy (HRTEM) analysis with electron diffraction data.[29,30] Kumar reported the crystalline properties and the molar fraction through the quaternary phases layer revealing Pb:Se:O:I diffraction patterns and lattice spacing.

Previous works for the sensitization of PbSe-based photodetectors report varying conditions for oxidation and iodization and report the conditions that maximize the photoresponse for their particular film. The goal of this work is to provide a detailed fundamental understanding of the impact of oxidation on iodization and provide data on changes in morphology, chemical composition, and structure of the film under different sensitization conditions. Furthermore, this work aims to provide a general guideline to optimize the IR photoresponse as well as conditions that are detrimental to IR photoresponse. The IR photoresponse mechanism is complex, and the literature shows various proposed mechanisms. Our paper aims to show the optimum material configuration for high photoresponse and provides some insight. Our results show that the oxidation and sensitization process provide higher photoresponse due to (a) the formation of the PbI_2 surface passivation layer (b) infrared absorption by the PbSe thin film (c) the formation of $PbSeO_3$ and $Pb_3Se_2O_6I_2$ controls the necessary PbSe film thickness for efficient infrared light absorption and controls the iodine concentration in the PbSe (d) low levels of iodine may be present in the PbSe thin films which may induce electron traps.

3.2 Experimental Setup

3.2.1 Sample Preparation

The laser sintering method, as described in previous work, was used to fabricate the PbSe thin films.[33] Before laser sintering, the film is a loosely packed layer of ball-milled PbSe crystallites with a huge surface-to-volume ratio. A small dose of KI is introduced by drip casting KI dissolved in methanol (0.18 μM). All samples in this work were deposited by drip-casting KI before laser sintering as described in the previous work[33]; however, KI incorporation was omitted from experiments when appropriate, such as for control samples (no iodine) when exploring the impact iodization has on grain growth and morphology.

3.2.2 Sensitization of PbSe Thin Films

The thermal sensitization processing was performed using a customized INSTEC HCS602SG-PM (INSTEC Corp.) temperature-controlled probe system and chamber, capable of both cooling to -190° C and heating to 600° C (Figure 20 a, b, c). The oxidation step was performed in the INSTEC chamber at 460° C for varying durations with ambient air as an oxygen source. The iodization process was performed by sublimating solid iodine pellets heated to 105° C. Argon gas was used to transport the iodine vapor through a heated glass tube to a custom chamber insert milled from a solid silver block fabricated by INSTEC. The PbSe sample was heated to 325° C inside the custom iodization chamber for varying durations (Figure 20 d and e).

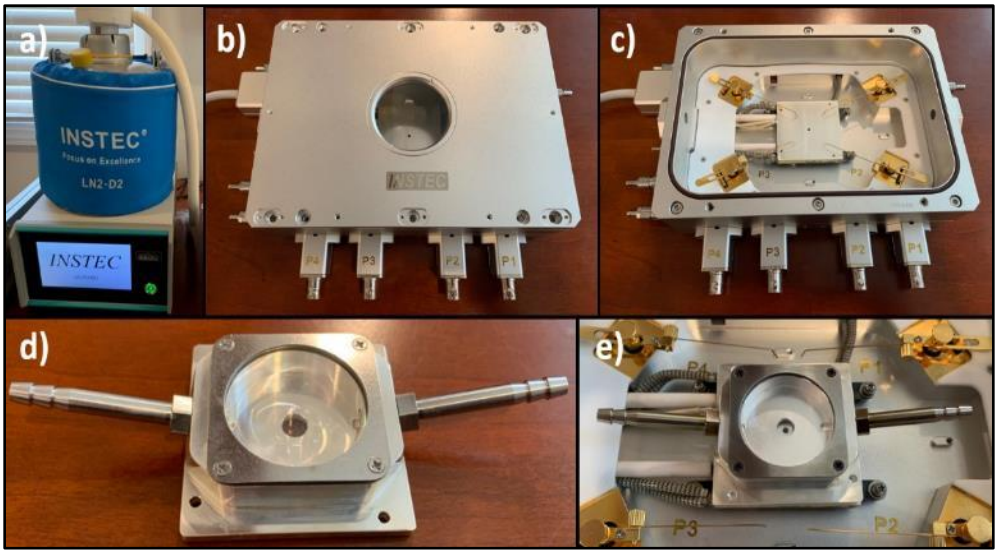

Figure 20: Images of (a, b, c) INSTEC temperature-controlled probe chamber (-190° - 600° C @ 150° C/min rate). This is used to perform sensitization of PbSe films (oxidation & Iodization). A custom iodine corrosion-resistant chamber is shown with iodine gas inlets (d, e).

3.2.3 Characterization of PbSe Thin Films

The deposited thin film characteristics were analyzed at each stage of the process through extensive top-down and cross-sectional scanning electron microscopy (SEM), energy dispersive spectroscopy (EDS), x-ray diffraction (XRD), and Raman spectroscopy. The transformation from as-deposited (laser-sintered), oxidized, and iodized were compared under varying conditions and analyzed to better understand the interactions between these process steps and their impact on producing highly MWIR sensitive thin films. The following equipment was used for this characterization provided by the University of Virginia Nanomaterials Characterization Facility (NMCF): Helios Dual-Beam FIB/SEM/EDS/STEM, Rigaku SmartLab X-ray Diffractometer (XRD), and Renishaw INVIA Confocal Raman. The Helios SEM was used for high-resolution inspection of the films (top-down and cross-section) as well as Energy Dispersive Spectroscopy (EDS) for film composition. The SEM was operated at 8 kV and 1.9 nA. The XRD system is equipped with a Cu anode (1.54 Å wavelength) and operates at 40 kV and 44 mA. Both 514 nm and 785 nm lasers were evaluated in the Raman spectroscopy analysis; however, the 514 nm was found to provide ideal penetration depth and better sensitivity to the surface of the film.

Once the PbSe film is fully sensitized (oxidized and iodized), the MWIR photoresponse was measured. The figure of merit for measuring the photoresponse was obtained using an I-V sweep test often called *Delta-R or DelR (ΔR)*. DelR is the percent difference in film resistance between dark (R_D) and illuminated (R_L) conditions ($\frac{(R_D - R_L)}{R_D}$). For this test, an 18 mW/cm^2 MWIR light source illuminated the sample through a 3-5 μm optical filter. The data was collected using a Keithley 2400 source meter.[33] A diagram of the circuit setup is shown in Figure 21.

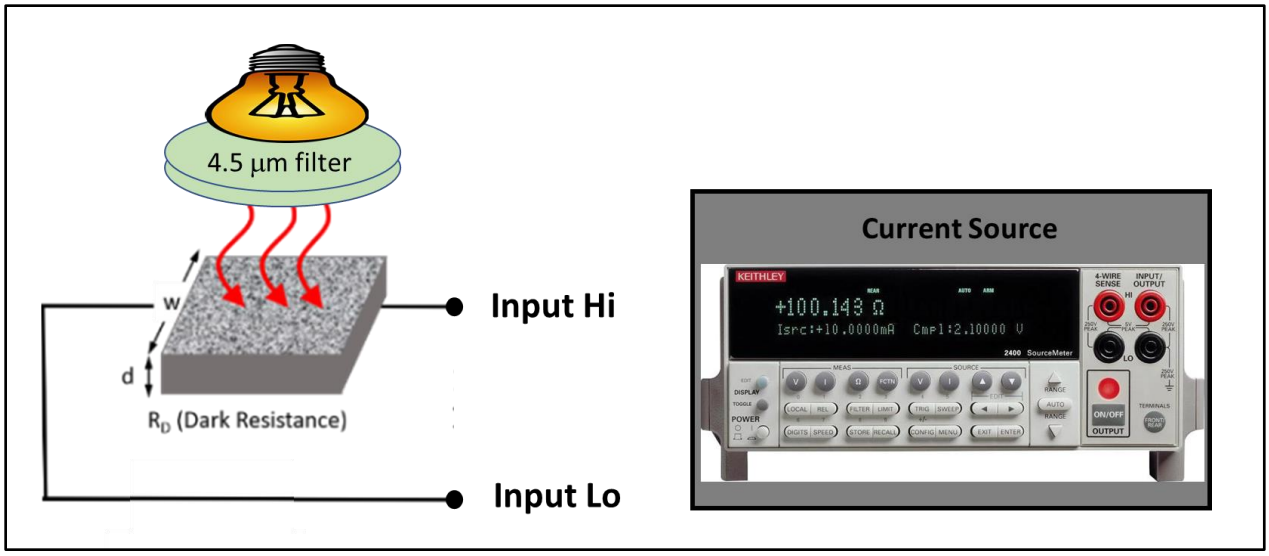

Figure 21: Diagram of the DelR photoresponse measurement under illumination. A 4.5 µm (+/-500 nm) filter illuminates the sample with 18 mW/cm^2. A Keithley 2400 Sourcemeter is used to sweep a voltage (typically +20 to -20 volts) and measure the current. This is performed under dark and illuminated conditions and the percent difference in resistance is DelR.

3.3 Oxidation Studies

3.3.1 Morphology

The changes in morphology as a result of the oxidation time of *as-deposited* PbSe thin films were investigated. The oxidation process induces both chemical and morphological changes; however, the primary morphological changes are a result of the thermal anneal as opposed to the result of oxidation. As-deposited PbSe thin film samples, without any KI content (no potassium iodide), were annealed at 460° C for 0, 6, 12 minutes, and the top-down and cross-sectional morphology and grain size were measured. The *as-deposited* PbSe thin film morphology shows round/spherical grains in a porous and columnar form. The average grain size is 42 nm. Following 6 and 12 minutes of oxidation, the morphology shows round/spherical grains but densified from porous and columnar to equiaxial merged grains. The average grain size increased to 242 nm. Cross-sectional SEM shows that regardless of oxygen incorporation, which primarily occurred in the top half of the film, the grain size and morphology changed consistently throughout the film. This suggests that the dominant transformation in morphology is due to thermalization rather than oxidation.

3.3.2 Composition

A composition study was performed on oxidized samples followed by detection of the elemental distribution throughout the film thickness using cross-sectional EDS line scans and complemented with Raman spectroscopy. The relative *elemental distribution* data is correlated with Raman spectroscopy measurements to better understand the material *composition distribution*.

The EDS line scans (Figure 23) show a nominal amount of oxygen near the surface in the as-deposited PbSe film before any thermal oxidation (0 minutes). Although the laser sinter deposition (LSD) is performed in an inert gas-filled (argon) chamber, some level of surface oxidation occurs during laser sintering. Oxidation for up to 6 minutes at 460° C forms a uniform $PbSeO_3$ layer (400-500 nm) and preserves the Pb:Se stoichiometric ratio throughout the entire thin film. The primary reaction is shown in equation (6). Oxidation durations beyond 6 minutes begin to volatilize free selenium from the surface of the film to produce PbO_x, and the Pb:Se ratio begins to increase as selenium escapes the film as a gas. These reactions are shown in equations (7), (8), & (9). Notice the greater selenium loss as a result of extended oxidation duration (yellow arrows) in Figure 23.

Raman spectroscopy of the same samples was then performed with a 514 nm laser source to determine the bond type and compositions of the PbSe thin film following the various oxidation times. The 514 nm laser was specifically chosen due to the shallow penetration depth in PbSe, as observed by the lack of a silicon substrate peak (520 cm^{-1}) and the presence of a silicon peak when illuminated with a 785 nm laser. The Raman study (Figure 24) confirms the EDS data showing that initially, $PbSeO_3$ forms and oxidation durations longer than 6 minutes begin to lose Se and form Se-poor lead selenite and PbO_x. The as-deposited film initially exhibits characteristic Raman peaks for PbSe at 136, 274 & 793 cm^{-1}.[48,49] The weak characteristic $PbSeO_3$ peak at 94 cm^{-1}, for the as-deposited sample, is likely the nominal surface oxidation from sample preparation. The signal below 100 cm^{-1} is obscured by the grating lower limit. Following progressively longer oxidation durations, peaks at 118, 361, and 790 cm^{-1} confirm the presence of $PbSeO_3$.[50] The resolution of the Raman system is approximately 4 cm^{-1}; however, deconvolution was used to delineate between the PbSe peak at 793 cm^{-1} and the $PbSeO_3$ peak at 790 cm^{-1}. Finally, as an excessively long oxidization duration occurs, the presence of PbO peaks appear at 145 cm^{-1} and 807 cm^{-1}.[51] The 807 cm^{-1} peak is subtle and was only seen as a shoulder for the sample oxidized for 30 minutes. X-ray photoelectron spectroscopy (XPS) confirmed the presence of PbO on the surface of oxidized PbSe.[52]

3.3.3 Structure

X-ray diffraction (XRD) spectroscopy of *as-deposited* PbSe shows a stoichiometrically balanced (Pb:Se = 1:1) forms of lead selenite $PbSeO_3$ following *oxidization* for 6 minutes @ 460° C (Figure 25). This is consistent with the EDS line-scan results from the previous section. As oxidation durations extend beyond 14 minutes, selenium-poor forms of lead selenite such as $Pb_3O_2(SeO_3)$ begin to dominate, as reported previously by Jang et al., and a transition to a polycrystalline form of PbO_x can occur with excessively long oxidation times.[48]

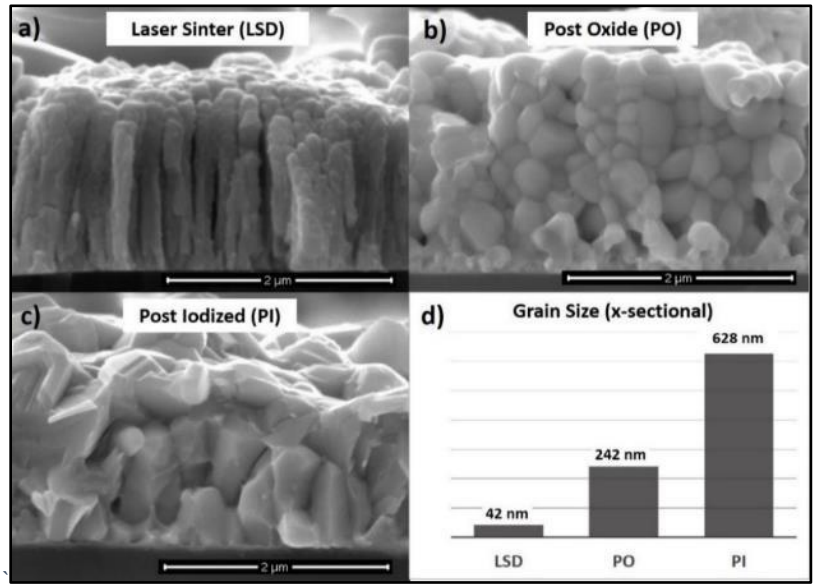

Figure 22: Scanning Electron Microscope images of grain size and morphology changes for a) as-deposited (PbSe), b) after oxidation for 6 min @ 460° C, c) after iodization of oxidized films for 6 min @ 460° C + iodization for 4 min @ 325° C, and d) comparison of grain size measurement data in (a) to (c).

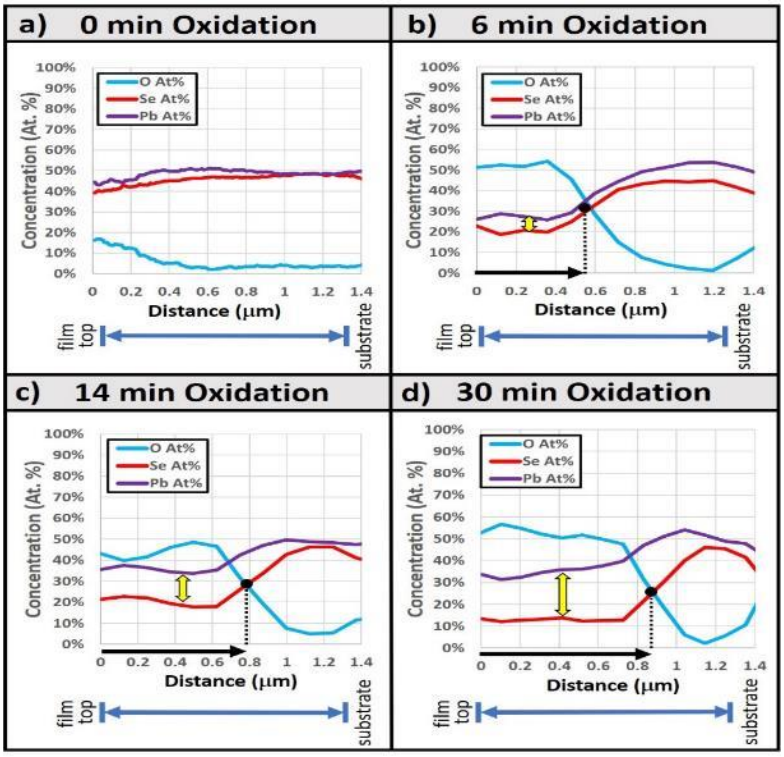

Figure 23: Cross-sectional Energy Dispersive Spectroscopy (EDS) line-scans of films prepared at various oxidation times a) as-deposited (no oxidation), b) 6 min, c) 14 min, and d) 30 min oxidation at 460° C. The greater selenium loss is observed as a result of extended oxidation durations (yellow arrows). NOTE: The EDS contribution of the silicon (substrate) profile was omitted.

Oxidation Reactions:

$$2PbSe + 3O_2 \rightarrow 2PbSeO_3 \quad (6)$$

$$4PbSe + 6O_2 \rightarrow 2PbSe_2O_5 + 2PbO \quad (7)$$

$$6PbSe + 9O_2 \rightarrow 2Pb_3O_2(SeO_3) + 4SeO_2(g) \quad (8)$$

$$2PbSe + 2O_2 \rightarrow PbSeO_3 + PbO + Se(g) \quad (9)$$

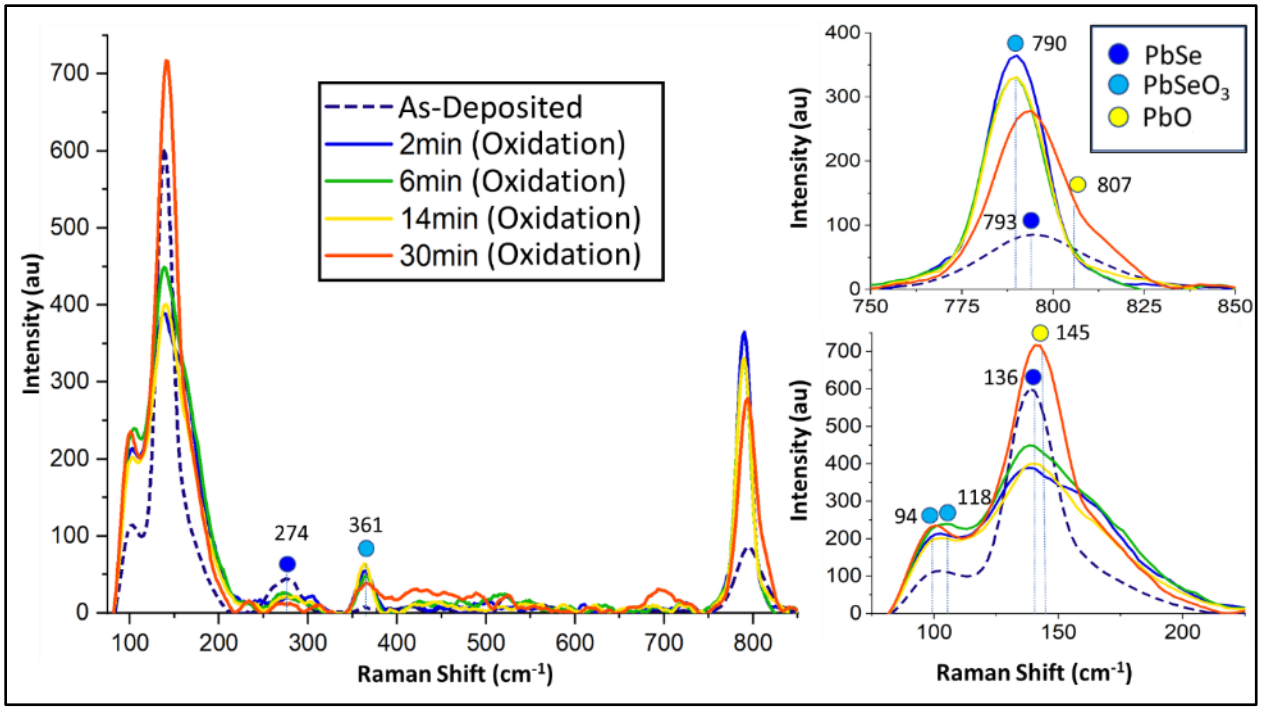

Figure 24: Raman spectroscopy of PbSe thin film oxidation at various times, as-deposited (no oxidation), 2 min, 6 min, 14 min, and 30 min oxidation at 460° C. This was used to determine the compositional make-up of film under different oxidation conditions. The first PbSe peak is observed at 793 cm^{-1}, then after 2 minutes, a strong peak for $PbSeO_3$ is observed at 790 cm^{-1}, then the $PbSeO_3$ peak decreases as PbO concentrations increase on the surface.[11,48,49,51–53]

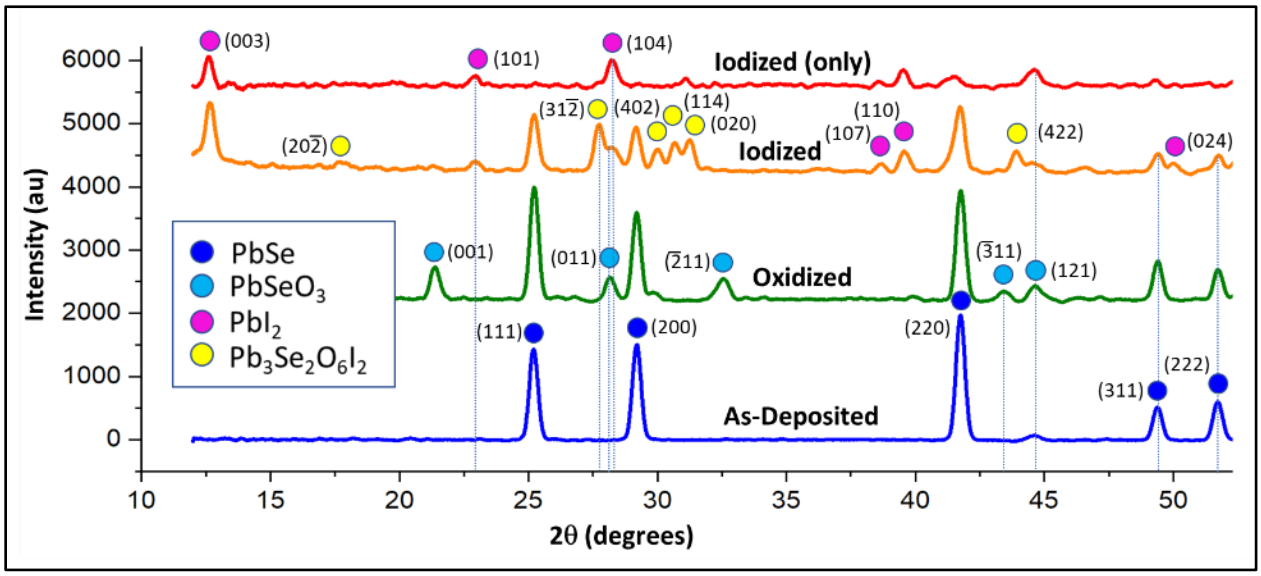

Figure 25: X-ray Diffraction of thin films of PbSe through the deposition and sensitization process [as-deposited, Oxidized (4 min @ 460° C), Iodized (iodization for 4 min @ 325° C after oxidation for 6 min @ 460° C), and iodized only for 4 min. at 325 ^0C. (without oxidation]. XRD ICDD Reference Code: [PbSe:00-006-0354] [$PbSeO_3$: 00-015-0471] [PbI_2: 98-007-7325] [$Pb_3Se_2O_6I_2$:98-042-2641]

3.4 Iodization Studies

3.4.1 Morphology

We measured the morphology changes of a PbSe thin film following a standard sensitization process proven to produce a high MWIR response (6 min oxidation @ 460° C + 4 min iodization @ 325° C). In the previous section, it was shown that oxidation (alone) increases grain size by nearly 6x (42 nm – 242 nm) and densifies the entire film stack to reduce porosity. Other researchers have reported that iodine promotes recrystallization of PbSe and reduces the formation temperature of oxyselenite by 100° C.[44,45]

Both top-down and cross-sectional SEM results revealed similar structural changes following the *standard* sensitization recipe described above. Although the iodine must diffuse top-down in what is now a multi-layered film ($PbSeO_3$/PbSe) and iodization is performed at 325° C (135° C lower than oxidation), the entire film stacks morphology and grain structure are transformed by 4 minutes of iodization (Figure 26 a). SEM cross-sections show a 260% increase (242 -> 628 nm) in grain size, but most notable is that significant structural changes occur due to iodization, transitioning from a round/spherical grain shape to a highly planar faceted grain interface. This is directly a result of the iodine and appears to influence the full film stack despite iodization occurring primarily in the upper part of the film. Given the grain boundaries are suspected of playing an important role in improving photoresponse, the planar faceting likely improves the inter-grain coupling and raises the question as to how iodization influences the grain boundaries of the base-layer of PbSe and if iodine is present at these grain boundaries.

3.4.2 Composition

Previous studies revealed that the high (> 30% ΔR) MWIR photoresponse for PbSe thin films occurs when oxidized for 6 minutes at 460° C and iodized for 4 minutes at 325° C. For this reason, the same samples were taken directly from the oxidation time study (0, 6, 14, and 30 minutes of oxidation at 460° C), and all samples were iodized for 4 minutes at 325° C to determine the impact of varying oxidization times. Figure 26 reveals the EDS line-scan results for the different oxidation conditions with a fixed iodization duration of 4 minutes at 325° C. The sample without any oxidation showed signs of rapid iodization, and iodine diffused through nearly the entire film in just 4 minutes. The regions in this sample where iodine concentrations were highest showed nearly zero selenium suggesting the reaction in equations (10) and (6) rapidly occurs when *pure* PbSe is exposed to iodine at 325° C, and the film is converted to PbI_2.

Iodization under the same conditions through a protective lead selenite ($PbSe_{(1-x)}O_x$) layer formed during the prior oxidation process (Figure 26 b-d) results in a surface layer of PbI_2 and a gradient of iodine concentration. Recall from the oxidation time study (Figure 23), that an extended oxidation duration of greater than 6 minutes produces a selenium-poor lead selenite layer. The PbI_2 layer becomes proportionately thicker than would occur in a stoichiometric $PbSeO_3$ layer (Figure 26 b) under the same iodization conditions (Figure 26 c-d). This suggests that selenium-poor lead selenite ($PbSe_{(1-x)}O_x$) and lead oxide (PbO_x) will iodize much more rapidly, similar to that of pure PbSe, to produce a thick PbI_2 layer. The thick PbI_2 results in a thin PbSe base-layer and is detrimental to achieving a high MWIR photoresponse. This reaction is represented in equations (12) and (13).

A second-time study similar to that which was done for oxidation was performed for iodization following a 6-minute oxidation step at 460° C to form the previously determined 400 - 500 nm $PbSeO_3$ layer necessary to adequately protect the underlying PbSe base-layer. Equation (14) represents the chemical reaction for $PbSeO_3$ during iodization which is believed to be a slower, more uniform, and thus more controlled reaction. Recall that the 6-minute oxidation recipe also best preserves the Pb:Se stoichiometric balance throughout the film stack. The oxidized PbSe thin films were iodized at 325° C for 0, 1, 2, 4, 6, and 8 minutes. For this study, Raman spectroscopy was used to better understand the composition transition of the film with a fixed oxidation time and varying iodization durations. The results are shown in Figure 27. Here we show that initially, the characteristic PbSe peaks at 136 and 793 cm^{-1} are present; however, the PbSe and $PbSeO_3$ peaks reduce in intensity as the PbI_2 layer thickness

increases due to the absorption of the 514 nm laser wavelength used for Raman measurements.[48,49] With just a short iodization duration of 1 – 2 minutes, the peaks at 790 cm^{-1} from the $PbSeO_3$ layer begin to diminish below the background, and characteristic PbI_2 peaks increase at 94, 110, and 214 cm^{-1}.[53] The sample processed with 6 minutes of oxidation and just 1-minute iodization showed what appears to be a PbO_x peak at 804 cm^{-1}.[51] This suggests that even 6 minutes of oxidation can produce some PbO_x on the surface; however, it rapidly disappears with iodization durations longer than 1 minute at 325° C.

3.4.3 Structure

X-ray diffraction (XRD) was performed for thin films prepared under two different iodization conditions. First, the iodization of an as-deposited thin film was carried out to confirm the rapid transformation of pure PbSe to PbI_2. XRD confirms that the film has very little crystallinity, and only PbI_2 peaks were observed.

The second condition of iodization for XRD is the standard *sensitization* recipe (described above) and reveals that the intensity of the PbSe and $PbSeO_3$ peaks diminish as the PbI_2 peaks increase. This is expected; however, one new finding is the identification of characteristic XRD peaks for $Pb_3Se_2O_6I_2$ which has not been reported in the scientific literature for IR sensitized PbSe-based detectors. Several researchers have reported a Pb:Se:I-based or Pb:Se:O:I-based compound in this transition layer that may impact the photoconduction of PbSe thin films.[12,30] This compound is only present in PbSe thin films showing highly MWIR photoresponse. This compound is within the transition layer material between the top PbI_2 and PbSe base layer. Jang et al. report that this iodine-incorporated PbSe transition layer on top of the PbSe base-layer provides diffused electrons that cancel out hole concentrations under dark conditions due to electron-hole recombination.[12] The $Pb_3Se_2O_6I_2$ is shown in Figure 25 in the XRD spectrum labeled Iodized. Equation (15) represents the reaction necessary to produce this compound.

3.5 PbSe Sensitization Mechanism

Based on the above analysis, the overall sensitization mechanism that occurs in thin films of PbSe to maximize MWIR photoresponse can be described as follows:

- A 1.2 μm thin film of polycrystalline PbSe requires 6 minutes of oxidation (in the air) at 460° C to produce a 400 - 500 nm layer of $PbSeO_3$ and a similar thickness of PbSe.
- A 400 – 500 nm layer of formed $PbSeO_3$ serves multiple purposes by (1) protecting the underlying PbSe base-layer from rapid iodization and (2) allowing trace levels of oxygen and iodine to diffuse along grain boundaries to recrystallize the PbSe base-layer into a highly ordered and planar faceted grain structure. This incorporates both oxygen and iodine at the grain barriers and increases inter-grain coupling during photoconduction.[52]
- Shorter oxidation durations result in an insufficient $PbSeO_3$ layer thickness to protect the PbSe base layer from the subsequent iodization.
- Longer oxidation durations result in an excessively thick lead selenite layer which is selenium-poor ($PbSe_{(1-x)}O_x$) and a PbO_x surface layer. Both these conditions negatively impact the MWIR photoresponse following iodization by (1) producing conditions for a thick and uncontrollable PbI_2 layer and (2) reducing the PbSe base-layer thickness, causing exceptionally high dark resistance (R_D) and lower infrared light absorption.
- Optimum iodization of 4 minutes at 325° C was determined for its ability to simultaneously perform several roles. Iodization needs to sufficiently diffuse iodine along grain boundaries to recrystallize the PbSe base-layer while simultaneously forming a 100-200 nm surface layer of PbI_2 and a 300 nm transition layer (containing $Pb_3Se_2O_6I_2$) on top of a 400-500 nm base-layer of PbSe. The above configuration produces a film that is passivated by PbI_2 and is composed of a highly conductive stoichiometrically balanced polycrystalline PbSe base-layer. This further supports the claim that iodine *directly* influences the photoconductive effect of PbSe.

- The KI likely contributes to the recrystallization by acting as a fluxing agent but the thermal iodization process is very important.

A comprehensive summary and model of the various oxidation and iodization conditions studied in this work as well as the IR photoresponse is shown in Figure 28. This model was constructed by correlating the elemental distribution analysis (spatial dependent) with the compositional and crystallographic analysis techniques. A comparison between the process conditions and the MWIR photoresponse reveals the parameters necessary to maximize the MWIR photoresponse of PbSe thin films. The conditions for the highest photoresponse were found to be ΔR = 29%, corresponding to 6 min oxidation + 4 minutes iodization (2nd column of Figure 28). This study also shows that there is a narrow process window for oxidation and iodization that would lead to high photoresponse. This study also provides a scientific explanation as to why IR photoresponse decreases outside the optimum process condition.

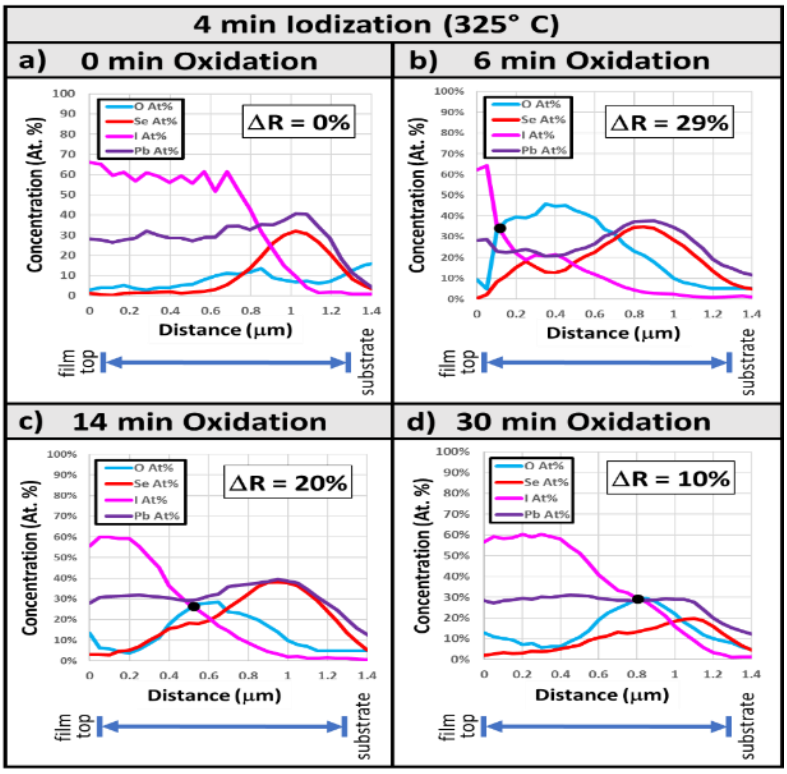

Figure 26: Cross-sectional Energy Dispersive Spectroscopy (EDS) of a) as-deposited (no oxidation), b) 6 minutes oxidation, c) 14 minutes oxidation, and d) 30 minutes oxidation following 4 minutes of iodization at 325° C. The MWIR photoresponse following a subsequent 4 minutes of iodization at 325° C is ΔR = 0%, 29%, 20%, and 10%, respectively. NOTE: The EDS contribution of the silicon (substrate) profile was omitted.

Iodization Reactions:

$$PbSe + I_2 \rightarrow PbI_2 + Se(g) \quad (10)$$

$$2PbSe + 2I_2 \rightarrow PbSeI_2 + PbI_2 + Se(g) \quad (11)$$

$$2Pb_3O_2(SeO_3) + 6I_2 \rightarrow 6PbI_2 + 5O_2(g) + 2Se(g) \quad (12)$$

$$2PbO + 2I_2 \rightarrow 2PbI_2 + O_2(g) \quad (13)$$

$$PbSeO_3 + I_2 \rightarrow PbI_2 + SeO(g) + O_2(g) \quad (14)$$

$$2PbSeO_3 + 2PbSe + 2I_2 \rightarrow PbI_2 + Pb_3Se_2O_6I_2 + 2Se(g) \quad (15)$$

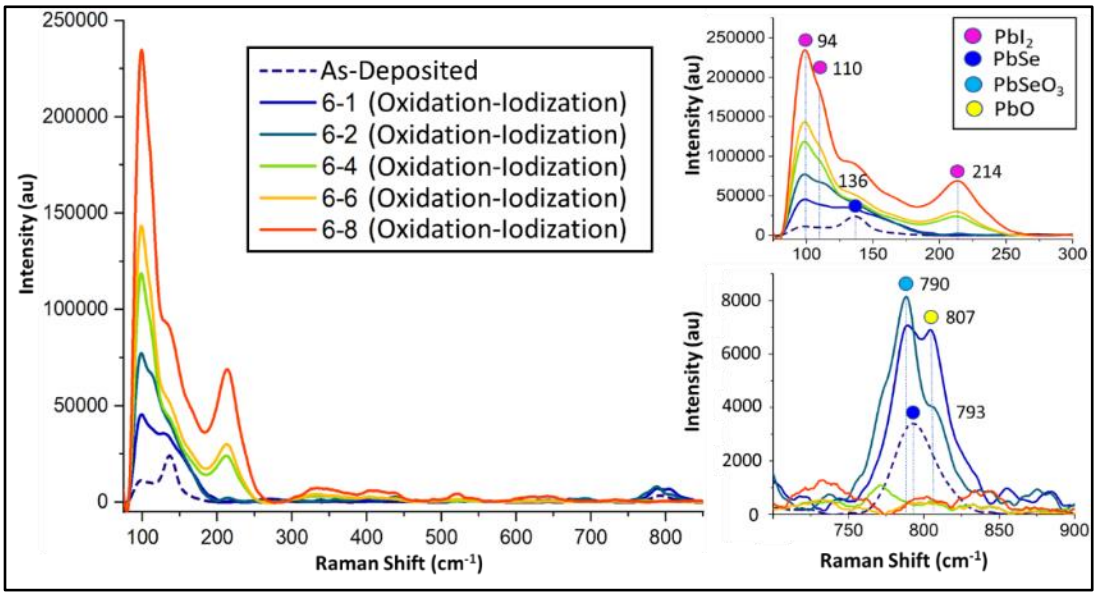

Figure 27: Raman spectroscopy of PbSe thin films as-deposited versus films iodized at 325° C for 1 minute, 2 minutes, 4 minutes, 6 minutes, and 8 minutes following 6 minutes oxidization at 460° C.[11,48,49,51–53] [NOTE: "6-4 (6 min oxidation + 4 min iodization)]

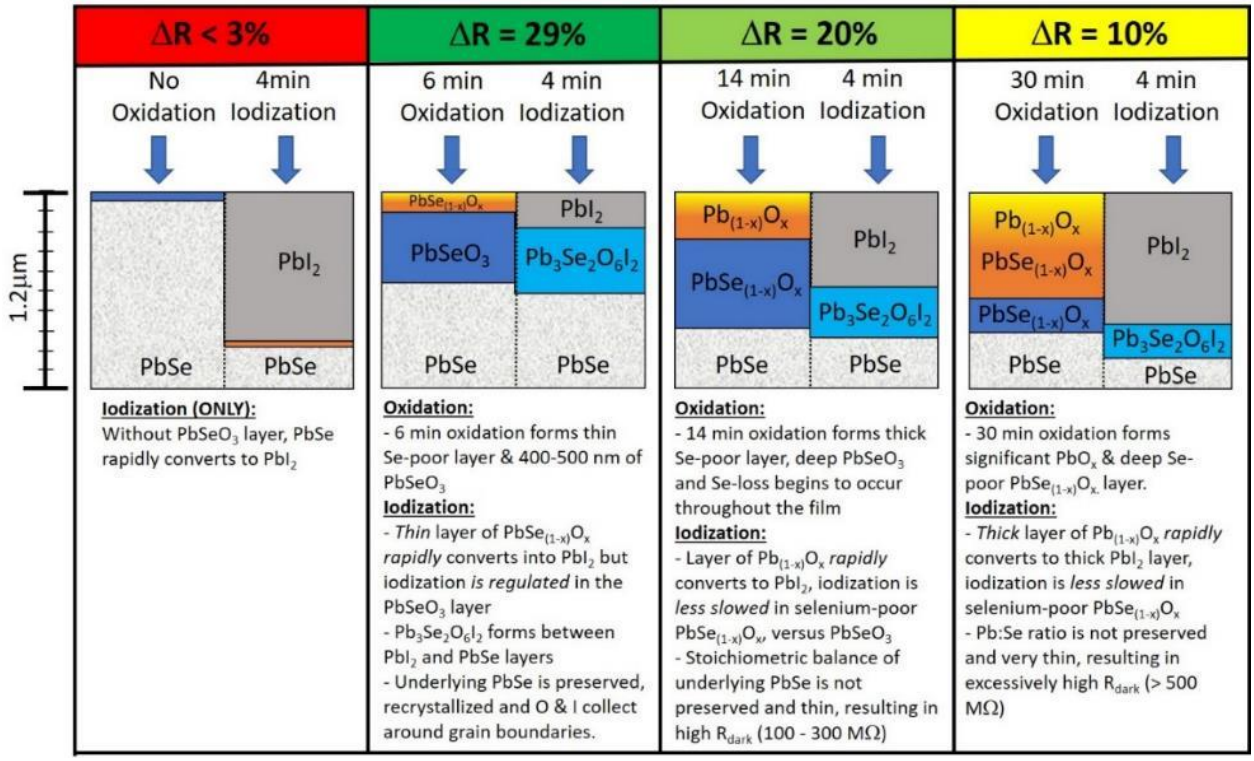

Figure 28: PbSe Sensitization Model for oxidation and iodization developed from integrating SEM, EDS, XRD, and Raman measurement results. The corresponding MWIR photoresponse DelR () is shown for each case. The conditions for the highest photoresponse were found to be DelR = 29%, corresponding to 6 min oxidation + 4 minutes iodization (2nd column).

3.6 Conclusion

The goal of this study is to provide a fundamental understanding of oxidation and iodization processes used for PbSe thin film sensitization for mid-infrared detection. This study shows that there is a narrow process window for oxidation that leads to a high IR photoresponse. This study also provides a scientific explanation of why IR photoresponse decreases outside the optimum process conditions. The optimum sensitization process that led to the highest IR photoresponse, converted the original PbSe thin film of 1.2 μm thickness into a multi-layered film with a 200 – 300 nm thick top layer of PbI_2, a transition layer partially containing $Pb_3Se_2O_6I_2$, and a bottom layer of PbSe of thickness 400-500 nm. Both oxygen and iodine were observed between PbSe grains with TEM in previous works.[52]

The oxidation of PbSe thin films at 460° C produces a surface layer of lead selenite ($PbSeO_3$) with a base layer of polycrystalline PbSe. This study provides evidence that a targeted $PbSeO_3$ layer thickness of 400 nm is needed to (1) restrict the PbI_2 surface layer thickness to less than 200 nm, (2) regulate the iodization process, allowing only trace amounts of iodine to diffuse along grain boundaries and recrystallize the PbSe base-layer, and (3) preserve the stoichiometric balance of the underlying PbSe layer. The 1.2 μm PbSe thin films used in this study required 6 minutes of oxidation at 460° C to produce a 400-500 nm layer of $PbSeO_3$. An optimum process window was observed for the oxidation step whereby initially, 400 nm of $PbSeO_3$ forms with minimal selenium loss in the first six minutes at 460° C; however, significant selenium loss begins to occur with longer oxidation times, and PbO_x forms on the surface. The subsequent iodization process is found to be highly dependent on the thickness and type of oxides formed during oxidation. This work shows that $PbSeO_3$ iodizes to form PbI_2 at a rate of ~100 nm/minute. Both pure PbSe and selenium-poor lead selenite rapidly transform into PbI_2 at nearly 5x the rate of $PbSeO_3$. Consequently, $PbSeO_3$ *regulates* the diffusion of iodine into the film, allowing the iodine to impact the morphology of the entire film and prevent the rapid conversion of PbSe into PbI_2. As such, a narrow window exists in the oxidation process whereby too much, as well as too little oxidation, both result in a thick PbI_2 layer and a thin PbSe base layer. Both conditions result in an excessively high dark resistance (R_D > 500 MΩ) and a reduced MWIR photoresponse due to lower infrared light absorption by thinner PbSe.

This work shows a diffused gradient of iodine reaching the PbSe base-layer to recrystallize it and increases inter-grain coupling by transforming the PbSe structure to a highly planar faceted morphology throughout the entire film stack. While iodine concentrations vary with depth, the iodization process uniformly transforms morphology and increases grain size by 260% (242 -> 628 nm) for the entire film. This work also identifies a new compound ($Pb_3Se_2O_6I_2$) that is formed between the PbI_2 surface and the PbSe base-layer, which is only present in samples with high MWIR photoresponse. The presence of this new compound ($Pb_3Se_2O_6I_2$) is observed in highly photoresponsive PbSe thin films and supports the notion that iodine does indeed play a *direct* role in the photoconduction mechanism.

It is concluded that to maximize the MWIR photoresponse, the overall sensitization processing (oxidation & iodization) must restrict PbI_2 to the surface yet allow oxygen and iodine to diffuse to PbSe base-layer grain boundaries while maintaining the stoichiometric balance of the underlying PbSe layer.

(The preceding sections 3.1 – 3.6 were reproduced from Ref.[54] *, with permission of AIP Publishing)*

CHAPTER 4: Electrical Properties of Sensitized PbSe Thin Film

4.1 Introduction

The electrical properties of LSD deposited PbSe thin films were measured and compared to those of published literature for PbSe deposited by CBD. The primary method for collecting electrical properties is an Ecopia Hall Effect System. Carrier type, concentration, mobility, and sheet resistance were compared. Top-down EDS spectra are used to quantify and compare the overall stoichiometry. All parameters are collected at each step of the process (as-deposited, post oxidation, and post iodization)

4.2 Electrical Properties of As-Deposited PbSe (Unsensitized)

The *as-deposited* carrier type, carrier concentration, mobility, sheet resistance, and stoichiometry for both the CBD and LSD deposited films are shown in Table 8. The stoichiometry data show that film is slightly Se-rich in both samples making the film p-type. The difference in mobility is believed to be due to crystalline damage caused during the LSD process. We will show how subsequent thermal annealing occurring during the oxidation and iodization correct for this and the mobilities and resistance will begin to match. To further support this, it was observed that LSD deposited PbSe films with excessively high carrier concentrations ($> 5 \times 10^{19}$ cm^{-3}) exhibited mobilities below 1.0 $cm^2/V \cdot s$ and further laser treatment reduced the carrier concentration and increased the mobility proportionately.

Table 8: Electrical parameters of as-deposited PbSe from CBD versus LSD deposited thin films.

Sample	Carrier Type	Carrier Concentration (cm^{-3})	Mobility ($cm^2/V \cdot s$)	Resistance (Ω)	Thickness (μm)	Stoichiometry Pb/Se (at. %)
CBD (As-grown)	p-type	7.1×10^{17}	41.6	1,066	1.4	49.5/50.5
LSD (post-Sinter)	p-type	4.5×10^{17}	19.3	3,625	1.6	49.1/50.9

4.3 Electrical Properties of Oxidized PbSe

The sheet resistance of the baseline CBD thin film following oxidation can vary greatly between 50k – 100k Ω□ due to its dependence on the contact method, and temperature and duration of the oxidation process. Our baseline CBD oxidation process is 6.5 minutes at 460° C in laboratory room air. Following this step, the top 50% of the original PbSe is oxidized and converted to one of many forms of PbO_x, SeO_x, and $PbSeO_x$[44]. Table 9 below summarizes the baseline CBD electrical parameters for *oxidized* PbSe thin films and compares them to the capabilities of the LSD process.

Table 9: Electrical parameters of oxidized PbSe from CBD versus LSD deposited thin films.

Sample	Carrier Type	Carrier Concentration (cm^{-3})	Mobility ($cm^2/V \cdot s$)	Resistance (Ω)	Thickness (μm)	Stoichiometry Pb/Se/O (at. %)
CBD (post-Ox)	p-type	6.6×10^{16}	9.2	51k	1.4	21.6/24.9/53.5
LSD (post-Ox)	p-type	1.1×10^{17}	9.8	79k	1.6	18.8/20.8/60.4

4.3.1 Electrical Characterization and Effect of Oxidation Time

Some of these parameters will contrast those reported in the earlier section due to changes made to optimize the LSD deposited film for maximizing the MWIR photoresponse. Experiments and results reported in Chapter 2 were aimed at proving the electrical properties of LSD deposited PbSe could

achieve equivalent parameters to those of CBD deposited thin films of PbSe. Since that reported work, efforts have gone into optimizing the LSD process for maximum MWIR photoresponse, and the impact of the introduction of potassium iodide (KI) before laser sintering is noticeable. The activation of the KI during the thermal processing shift some properties like electrical resistance. This was done for the benefit of improvement in the carrier concentration, morphology, and film density. The impact KI has on the film density and morphology is the primary reason the DeltaR figure of merit improved from ~14% to over 31%. This is due to the higher density film produced with LSD when KI is added. The reason is that a more uniformly dense film allows for a more uniform and controllable oxidation and iodization process.

This experiment is aimed at determining trends. Optimization of the electrical parameters was not considered here and will be covered in Chapter 6. The following figure shows the trends of key electrical properties of PbSe through the oxidation duration (time). An Ecopia Hall Effect system was used to determine carrier type and collect carrier concentration, carrier mobility, and sheet resistance across various oxidation times.

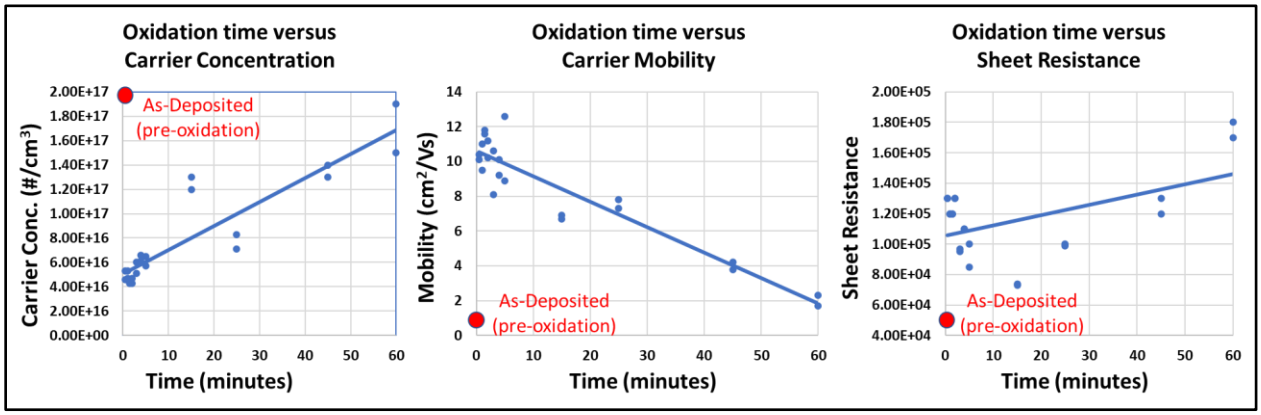

Figure 29: Oxidation time (460° C) experiment and the impact on electrical parameters.

For each of the electrical parameters shown in Figure 29, a red dot denotes the typical value for that respective parameter before oxidation (as-deposited or laser-sintered). Notice the trends for carrier concentration are almost linear (log y-axis), yet within the first few seconds, the p-type carrier concentration consistently drops from ~1.0 x 10^{18} /cm^3 to ~7.0 x 10^{17}/cm^3 and then slowly trends upward. Later will find that the optimum oxidation time is ~4-6 minutes at 460° C. As for the mobility versus oxidation time, the mobility drops linearly as well as oxidation time. Also, notice the immediate increase in mobility compared to as-deposited. The mobility increases nearly an order of magnitude immediately from ~1 cm^2/V·s to ~11 cm^2/V·s. Interestingly enough, the sheet resistance is not linear versus oxidation time but instead is almost parabolic, with a spike up from time zero (as-deposited) and a gradual drop followed by an asymmetrically gradual increase. The immediate change within the first few seconds is likely a mix of crystalline defects annealing out, volatilization of potassium iodide or free iodine, melting of any PbI_2 formed from the KI during laser sintering (T_m of PbI_2 is 410° C), and oxidation of the PbSe. The PbSe film before oxidation is a matte gray color and immediately turns amber as it transitions to vibrant blue as it oxidized and loses selenium from the surface. The chemical reactions of oxidation are presented in sections 4.3 and 4.4.

4.4 Electrical Properties of Iodized PbSe

The sheet resistance of the baseline CBD thin film following iodization can also vary greatly between 2M – 1G Ω□ based on the contact method, annealing temperature, and duration of the iodization process. Table 10 below summarizes the baseline CBD electrical parameters for *fully sensitized* PbSe thin films and compares them to the LSD process. The films match properties and MWIR response comparably.

Table 10: Electrical parameters of fully sensitized PbSe from CBD versus LSD deposited thin films.

Sample	Carrier Type	Carrier Concentration (cm^{-3})	Mobility ($cm^2/V{\cdot}s$)	Resistance (Ω)	Thickness (μm)	Stoichiometry Pb/Se/I/O (at. %)
CBD (post-Iodization)	p-type	1.5×10^{14}	11.7	26.8M	1.4	29.2/18.8/25.4/26.6
LSD (post-Iodization)	p-type	6.2×10^{13}	16.4	76.5M	1.6	21.7/17.1/30.2/31.0

It is not until the PbSe film is fully sensitized (oxidized and iodized) that it will exhibit a substantial MWIR photoresponse. The first figure of merit for measuring the photoresponse is with an I-V sweep test often called *Delta-R*. Delta-R is quite simply the percent difference in resistance between dark and illuminated resistance. Despite the varying semiconductor layers (PbI_2, $PbSeO_3$, PbSe), the I-V response is linear and gold-coated probes or silver paint provide ohmic contacts. Delta-R can be performed with a simple 2-point probe; however, due to the potential for high impedance between the contact and the PbI_2 surface layer, 4-point probe techniques are recommended when metal contacts are not formed. A diagram of the circuit setup is shown in Figure 21.

4.5 Conclusions

The differences between some of the electrical parameters for the *as-deposited* CBD versus LSD deposited PbSe films such as mobility (μ) (41.6 vs 19.3 $cm^2/V{\cdot}s$) and sheet resistance (R_s) (1,066 vs 3,625 Ω□), respectively, were corrected by the oxidation anneal step. Following oxidation, the mobilities between the two films were nearly identical (9.2 vs 9.8 $cm^2/V{\cdot}s$) and the delta in R_s reduced significantly (51k vs 79k Ω□). This suggests the anneal may have reduced or repaired any crystalline damage produced during the laser sintering. The two films appear to be physically and electrically comparable.

CHAPTER 5: Optical Properties of Sensitized PbSe Thin Film

5.1 Introduction

The optical properties of LSD deposited PbSe thin films were measured and compared to the intrinsic values for PbSe. IR absorption data can be used to extract useful information such as optical band gap E_g via Tauc plots and validated with photoluminescence (PL) as well.

5.2 Optical Characterization of Sensitized PbSe

5.2.1 Determination of Semiconductor Bandgap for LSD Deposited PbSe

Photoluminescence (PL) is collected using a Nicolet iS50 FTIR from Thermo Fisher modified for detecting PL with an external light source and an MCT-A detector. The samples are illuminated with a 15mW, 650 nm red laser. The optical band gap of intrinsic PbSe is ~0.28 eV. The PL spectrum in Figure 30(a) confirms the peak wavelength and energy correspond to the optical band gap of PbSe (0.29 eV). The asymmetry of the PL spectra of the fully sensitized PbSe thin film, skewing towards higher energies may suggest the presence of components of PbSe nanoparticles with quantum dot properties.

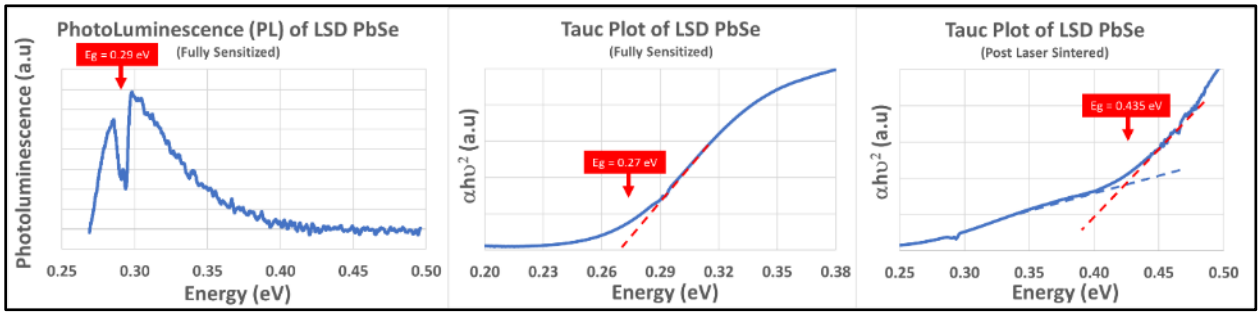

Figure 30: Photoluminescence (left) and Tauc plots (middle) of LSD deposited PbSe film (fully sensitized). Tauc plot of unsensitized (right). The dip in PL is from CO_2 in the air.

The same Nicolet iS50 was used to collect infrared absorbance spectra of PbSe thin films at various stages of the LSD and sensitization process. The absorbance spectra are used to confirm the optical bandgap of the LSD deposited PbSe film by using the Tauc plot method [55]. Figure 30 (b) shows a Tauc plot composed of the IR absorption spectra of a fully sensitized Pbe film produced using the LSD deposition method. The absorption spectra confirm that the optical bandgap of the fully sensitized PbSe film is 0.27 eV. The unsensitized film exhibited an abnormal, but not uncommon absorption profile. Baseline correction of the Tauc plot for the unsensitized film suggests there may be nanoparticles in the post LSD film with confinement properties. This should be confirmed in future work with TEM imaging of samples.

5.2.2 Infrared Absorption and Reflection Spectra for LSD Deposited PbSe

The infrared transmission and absorption properties are not well characterized for traditional CBD deposited thin films. This work aims to characterize and share the transmission, absorption, and reflection characteristics of Laser Sinter Deposited thin films of PbSe at each step of the sensitization process, as-deposited (laser-sintered), oxidized, and iodized (fully sensitized) as well as determine if KI has any impact.

Infrared (IR) absorption spectra were collected with a Thermo Fisher iS50 FTIR system. The spectra were collected and compared between laser-sintered (as deposited) and oxidized samples to see the impact these steps have on the relative IR absorption of the PbSe film. The silicon substrate background was removed. Samples of each step were prepared with and without potassium iodide (KI) to determine whether KI impacts the absorption spectra. Figure 31 shows the spectra under each of these conditions. The relative IR absorption improves for both cases following oxidation; however, the sample exposed to KI showed a 48% increase (0.58 to 0.86) in IR absorption between 3.0 - 4.8 μm following oxidation. While the samples without KI show only a nominal increase in IR absorption of ~4%. The samples with KI also show the absorption peak is maximized at ~3.8 μm which coincides with 0.33 eV. The shift from the 0.28 eV optical bandgap of PbSe to this 0.33 eV absorption peak may be due to the transition layer's influence on the overall film optical bandgap maximum absorption. Lead selenite ($PbSeO_3$) and lead iodide (PbI_2) are coating the PbSe grain and may also be incorporated into the PbSe lattice. Their bandgaps are E_g = 3.17 eV and E_g = 2.41 eV, respectively. A notably broad and flat spectrum of the samples without KI is observed and supports the notion that iodine in the form of KI improves the absorption and photoresponse.

Figure 32 shows the IR absorption spectra for laser-sintered, oxidized, and iodized (fully sensitized) all with KI doping. A slightly smaller improvement is observed between the laser-sintered and oxidized, however, the absorption spectra were consistent and remained unchanged between oxidization and iodization.

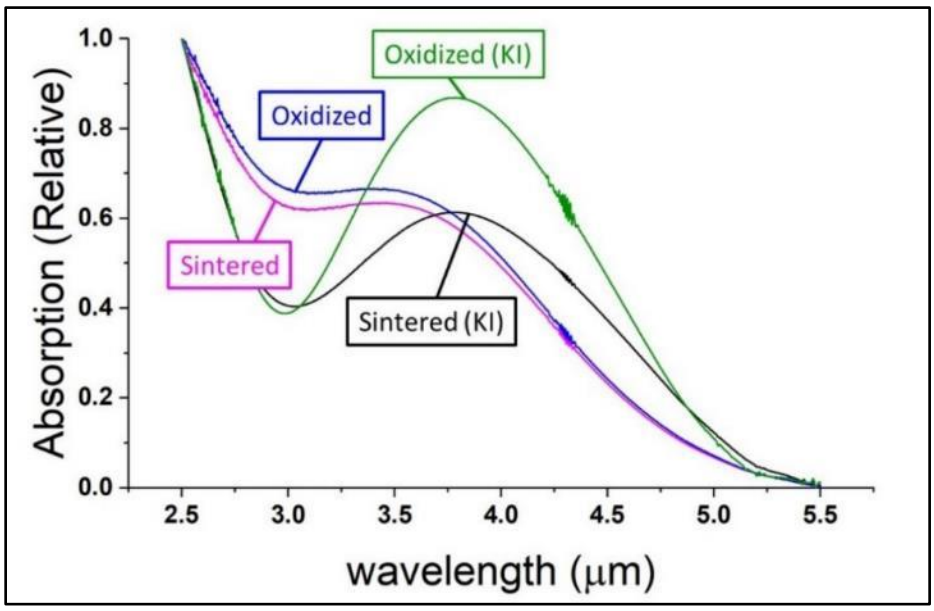

Figure 31: Infrared absorption spectra for sintered (w/ and w/o KI) and oxidized (w/ and w/o KI)

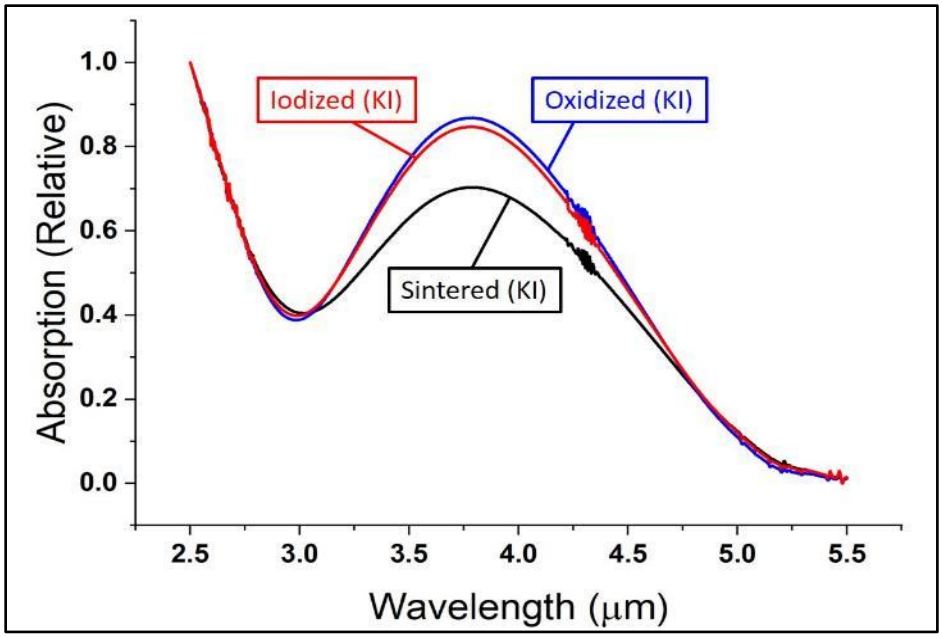

Figure 32: Infrared absorption spectra for sintered, oxidized, and iodized (w/ KI).

A separate study was performed to determine the reflection of the PbSe film at each respective step. The results showed an 18% reflection at 3.3 μm for laser-sintered, and the reflection was reduced to 8% for oxidation and 4% for iodized samples. This implies that a minimal amount of IR reflection occurs after sintering, and is reduced substantially by ~56% and 78%, respectively, from the post sintered reflectivity for oxidation and iodization.

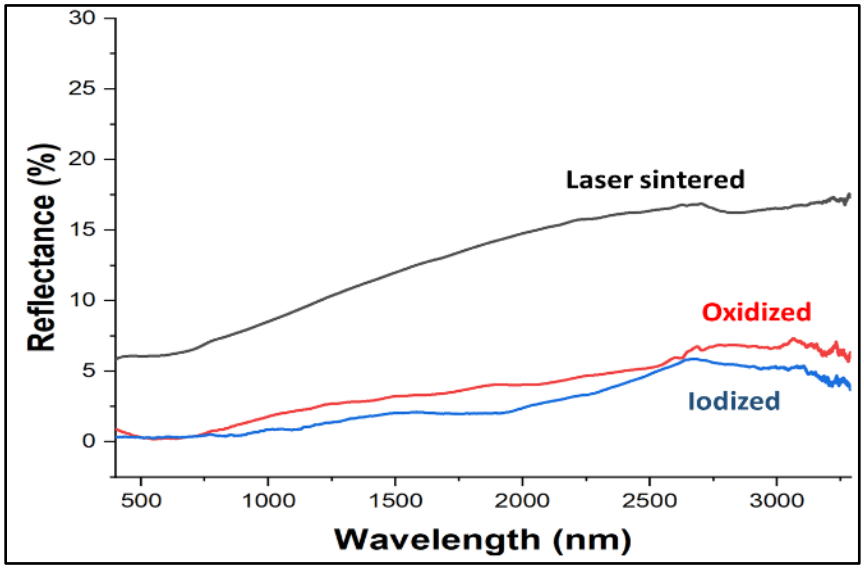

Figure 33: UV-VIS-NIR reflection spectrum for laser-sintered, oxidized, and iodized PbSe films.

5.3 Conclusion

The goal of this work is to confidently determine whether the optical properties of the laser sinter deposited thin films of PbSe respond as expected according to the documented literature and alternative deposition method. The intrinsic optical band gap of bulk PbSe is 0.27 eV. Two separate analytical methods were used to determine and confirm the optical band gap of LSD deposited thin films of PbSe.

Both photoluminescence (PL) and IR absorption spectra (Tauc method) revealed an E_g of 0.29 eV and 0.27 eV, respectively. These values were found on LSD deposited PbSe film after full sensitization.

The PL spectra for the fully sensitized PbSe film were asymmetric, with a tapered tail skewing towards the higher energy (shorter wavelength) direction. It is unclear what caused this but it could be an indication of some component of nanocrystals in the film with quantum dot properties (blue shift due to larger E_g). The results of PL measurements on post-laser-sintered (unsensitized) and post oxidized failed to show a PL response. This is consistent with unsensitized, and oxidized CBD deposited PbSe thin films.

The Tauc plot for the post-laser-sintered film suggests a possible bandgap of 0.435 eV when using the baseline correction method [55]. It is unclear if this baseline method is valid; however, the combination of PL and Tauc results support the notion of some component of quantum confinement due to the presence of NC in the LSD deposited film.

The combination of absorption and reflection spectrum for laser-sintered, oxidized, and iodized confirms that the IR absorption increases 48% with the addition of KI between 3.0 – 4.7 μm for oxidized samples before sensitization. This also shows that the absorption improvement remained following the iodization of PbSe samples with KI. Lastly, the reflectivity of the films reduced considerably by ~56% and 78%, respectively, from the post sintered reflectivity for oxidation and iodization.

CHAPTER 6: PbSe Thin Films and the Role of Potassium Iodine Incorporation

6.1 Introduction

As mentioned, the sensitization process is necessary to achieve a high mid-wave infrared (MWIR) response of PbSe, and despite decades of research, there is still debate as to the role of various process steps and how they interact to enable such high room-temperature photoresponse. Sensitization of PbSe can be broken down into two steps and require high-temperature thermal processing (between 280° C – 480° C) to incorporate and induce a reaction with (1) oxygen and (2) iodine into the thin film. The way these elements are introduced, their interactions, and the many spatially varied compounds have multiple purposes and are difficult to fully understand. The morphology, stoichiometry, and film density play a significant role in how these processes work and are the primary reason for variations in researchers' results. To further convolute the understanding, additives such as potassium iodide (KI) are introduced during film deposition and are reported to enhance MWIR photoresponse by as much as 300%, compared to samples without KI.[1–5]

Typically, the first step following deposition of a pure PbSe thin film is thermal oxidation (annealing in the air), often occurring between 425° C to 460° C. The current understanding is that oxygen diffuses into the PbSe and forms one of many oxyselenite ($Pb_xSe_yO_z$) compounds. The highest photoresponsive films generally oxidize the top half of the film, leaving a pristine polycrystalline PbSe underneath. XRD is widely used to identify the types of polycrystalline phases of PbO_x, SeO_x, and $Pb_xSe_yO_z$.[4,6] Following oxidation, iodization is necessary to trigger the photoconductive characteristic of PbSe.

The iodization process is another thermal process in an iodine vapor environment, usually at a lower temperature between 285° C to 325° C. This process forms a PbI_2 surface layer, and the presence of iodine in the PbSe reduces the formation temperature of oxyselenites as well as reduces the temperature of recrystallization of the underlying PbSe.[7,8] The melting temperature of PbI_2 is 402° C, and a controlled concentration of oxygen and iodine in and around the underlying PbSe grains is thought to be critical for maximizing the MWIR photoresponse. The presence of iodine at grain boundaries may also assist in the recrystallization of PbSe. This is supported by the PbI_2 – PbSe system eutectic phase diagram[7–9].

Potassium iodide (KI) is commonly introduced into the CBD bath during PbSe thin film deposition.[1] The understanding is that KI is a stable source of iodine that can easily be incorporated into the CBD bath chemistry and allows a low dose (< 1 at. %) of iodine in PbSe thin films. It is unclear how much iodine is necessary and its role. One of the goals of this work is to use the rapid sintering of laser processing to provide an understanding of how KI influences the PbSe grains and photoresponse. Golubchenko et al. reported that the presence of iodine in PbSe reduces the formation temperature of oxyselenites (forms of $PbSeO_x$) by 100° C and assists in the recrystallization of underlying PbSe grains.[7,8] Other iodine-containing additives and methods for iodine doping PbSe before thermal iodization have been reported as having a high impact on grain morphology, recrystallization, and improved IR photoresponse.[10,11] The rapid melt and a cool cycle of the pulsed laser allow the unique ability to introduce and experiment with KI. Laser sintering has the advantage of rapid sintering and laser-induced reactions between the KI and the PbSe crystals. Laser sinter processing also minimizes any selenium loss that occurs in furnace annealing, or even rapid thermal anneal (RTA) due to short heating and cooling times.

The role of KI incorporated during thin film deposition versus the iodine gas reaction after the thermal oxidation step is different, but interacting. It is well accepted that iodine plays multiple roles beyond forming the PbI_2 layer that forms on the surface and acts as a passivation layer. This study investigates the role of KI in PbSe thin films and its impact on photoresponse.

The PbSe thin films deposited in this study used Laser Sinter Deposition (LSD) as described in our previous research papers.[12] This deposition method is ideal for experimentation for several reasons. The laser sintering process is rapid and can introduce film stress that can be reduced with subsequent thermal

annealing in argon. The inherent laser-induced stress provides the unique ability to observe the impact Potassium Iodide (KI) has on film stress and morphology not possible with other deposition methods.

6.2 Experimental Setup

The PbSe thin films were deposited using Laser Sinter Deposition (LSD) as described in our previous research papers.[12] PbSe thin film samples were exposed to varying concentrations of drip-cast potassium iodide (KI) before laser sintering, as well as control samples without KI. Three different concentrations of KI dissolved in methanol were introduced into the PbSe films (Low-KI 1.8 μMol, Med-KI 18 μMol, and Hi-KI 180 μMol) before laser sintering. Samples were dipped into the respective KI solution and dried at room temperature for 30 minutes. The impact of KI on morphology is particularly apparent with the rapid heating and cooling of the laser sintering process.

Materials characterization for this work was performed after each step of the sensitization process using a Helios UC G4 (Dual Beam FIB-SEM) with an Oxford Energy Dispersive Spectroscopy (EDS) detector to observe the morphology and determine the topdown and cross-sectional elemental composition of the film. A Themis 200 kV Transmission Electron Microscope (TEM) provides high-resolution EDS and determination of the microstructure of the individual PbSe grains and interfaces between grains. A SmartLab X-Ray Diffractometer (XRD) provides crystallographic information, and X-ray Photoelectron Spectrometer (XPS) provides surface chemistry and composition. A Thermofisher iS50 Fourier-transform infrared spectroscopy (FTIR) system provides optical (spectral) transmission information, and Raman Spectrometer (Raman) provides evidence of film composition through the depth of the film. An Ecopia HMS-3000 Hall Effect measurement system was used to determine semiconductor electrical properties (majority carrier type, mobility, and resistivity). Thermal processing (annealing, oxidization, and iodization), as well as temperature versus electrical resistance, was accomplished using a custom INSTEC (HCS602SG-PM) Temperature Controlled Probe Chamber (-190° to 600° C, + ΔT 150° C/min)

The MWIR sensitization process performed in this work is similar to that described for the fabrication of CBD MWIR devices. The oxidation is accomplished using an INSTEC Inc. temperature-controlled chamber set to 460° C and exposed to the fume hood atmosphere. The second step is iodization, where solid iodine is sublimated in a temperature-controlled glass container at 105° C. Argon carrier gas is used to transport the iodine vapor through glass tubing to a custom INSTEC chamber, where the oxidized PbSe sample is heated to 325° C.

Potassium Iodide (KI) has been used as an additive in chemical bath deposited films of PbSe, but its role is not well understood. In this chapter, we provide a better understanding of the role of KI in photoconductive PbSe thin films and show that low levels of KI densify the PbSe film, increase grain size, reduce film stress/cracking, and improve IR absorption. The KI incorporation converts round equiaxed grains to highly faceted grains. PbSe films with KI showed 30x higher electrical resistance (RD) under dark conditions, leading to reduced lower dark current and improved photoresponse.

6.3 Material Characterization for Optimization of Film Properties

6.3.1 Laser-Sintered PbSe Films

Samples were prepared using the four KI conditions (*No-KI*, *Low-KI*, *Med-KI*, and *Hi-KI*) described above. Following laser sintering, SEM inspection revealed the PbSe film with *No-KI* was highly porous and much less dense compared to all samples treated with KI (Figure 34). The grains successfully sintered to recrystallize uniformly in size; however, there are significant gaps between the clusters of PbSe grains for the *No-KI* samples. Beginning with the *Low-KI* and progressively larger KI concentration, the size and connectivity between grains increased, and the film surface roughness reduced proportionately. While *all* samples in this study were sintered using the same laser parameters, varying laser parameters were unsuccessful in compensating for the impact of KI in uniformly densifying the PbSe film. The margin

between sintering and ablation is too narrow to produce large-area fully densified PbSe thin films without KI.

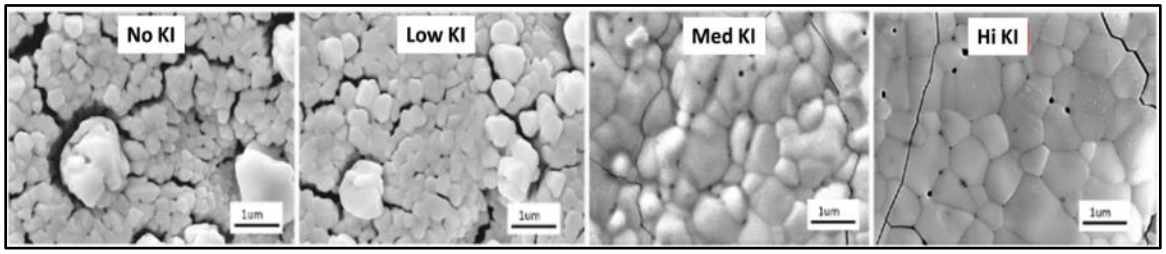

Figure 34: Top-down SEM image of laser-sintered PbSe films under the same conditions with different KI doses. KI promotes a more dense and smooth film with larger and more consistent grains.

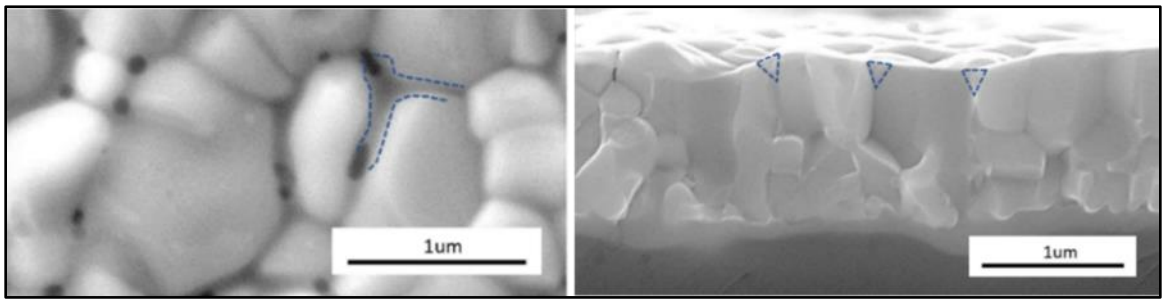

Figure 35: High magnification SEM image of a Med-KI sample following laser sintering. A dissimilar material or phase of PbSe appears to be present between grains (left). Cross-sections imagers highlight the dissimilar materials between grain PbSe grains (right).

Samples from the *Med-KI* appear to have a continuous surface with very few cracks or gaps. The voids seen in the No-KI and Low-KI films are evidence of incomplete sintering, as the PbSe grains are not connected. The voids do not significantly affect the conductivity since they are confined to the surface based on the cross-section studies; however, the voids can impact the uniform diffusion of oxygen, and Iodine during the sensitization process. A dense, closed PbSe surface is necessary to maximize the photoresponse. The small fine cracks, seen in the Hi KI sample do not seem to impact film photoresponse; however, this suggests some film stress may exist from the laser sintering process. Laser processing parameters could be optimized further to minimize the surface crack formation. The film stress, as a result of laser sintering, was reported in our previous works.[33] The subsequent thermal anneal steps (oxidation and iodization) closed the fine cracks and reduced the film stress (reported in the next section).

A dissimilar secondary electron contrasting material or a mixed phase of PbSe and KI appears to be present between the PbSe grains as a result of the KI addition. Figure 35 shows a higher magnification SEM image highlighting the contrasting material. The sample shown in Figure 35 was prepared for transmission electron microscopy (TEM), and cross-sectional TEM-EDS identified the material between grains as a mixture of an amorphous $PbSeO_{(1-x)}I_x$ and PbI_2. TEM-EDS mapping shows a concentration of iodine and oxygen along grain boundaries (Figure 36 & Figure 37). This suggests that introducing KI to PbSe followed by rapid thermal processing decomposes the KI to chemically react with the PbSe.

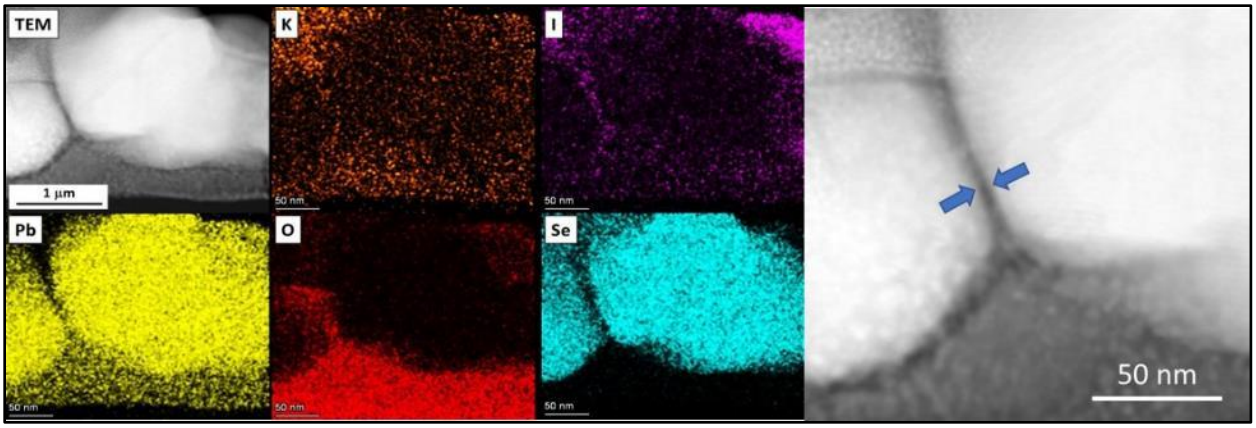

Figure 36: Transmission electron microscope (TEM) Energy Dispersive Spectroscopy (EDS) map of the Med-KI sample following laser sintering. The presence of both oxygen and iodine between grains where evidence of PbSe remains suggests that PbI_2 and $PbSe_{(1-x)}O_x$ may be forming from the exposure to KI. The right-most figure shows a high magnification TEM image where iodine and oxygen are confirmed to be present in the EDS (left).

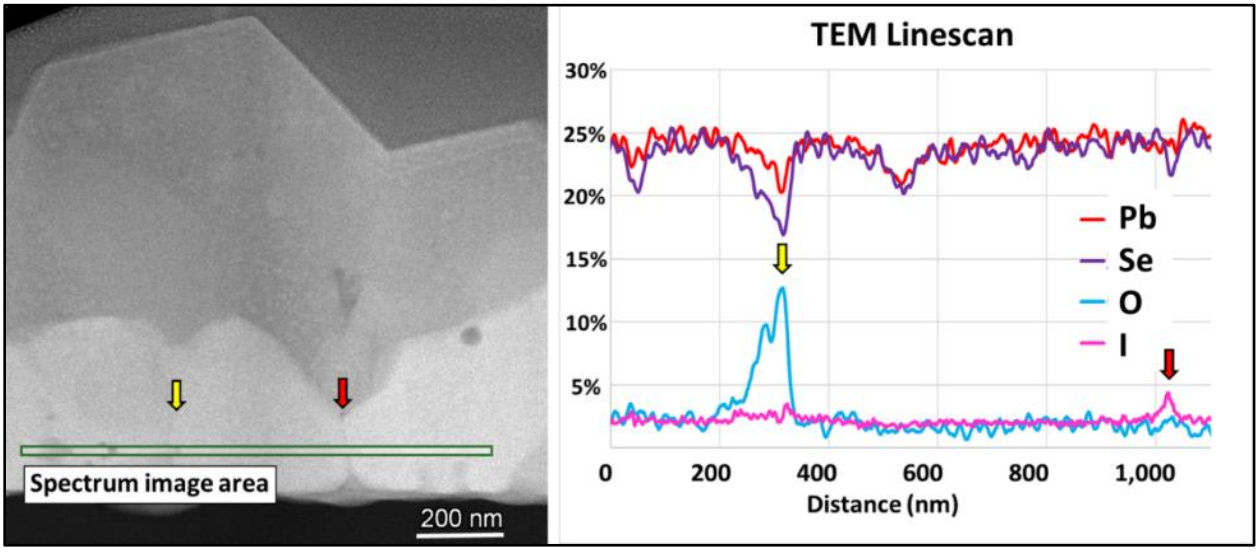

Figure 37: TEM EDS line scan of grain boundary following laser sinter of a PbSe film with Med-KI. This shows both oxygen and iodine exist at grain boundaries. The TEM-EDS linescan (right) highlights the presence of oxygen and iodine at grain boundaries corresponding to the colored arrows on the TEM image (left)

6.3.2 Thermal Sensitization of PbSe Thin Films

(a) Annealed Under an Inert Atmosphere

The rapid sintering that occurs during laser processing induces cracks that suggest the presence of high stress in all samples. The density of cracks and severity is inversely proportional to the KI exposure. The next experiment contrasts the difference between the inert atmosphere annealing of samples with and without KI. Samples with and without KI were annealed in the INSTEC chamber purged with argon to minimize oxidation.

Figure 38 shows a topdown SEM image of the morphology of samples with *No-KI* (Left) compared to *Med-KI* (right) following a 5-minute inert anneal at 460° C. The sample with *No-KI* remains porous with round equiaxed grains containing voids and cracks. The samples exposed to KI consistently exhibit highly faceted grains with no evidence of pores and significantly less cracking, indicating recrystallization and

film densification with less stress. The PbSe recrystallizes as a result of the presence of iodine along grain boundaries from the decomposition of KI, which acts as a flux. The iodine reduces the melting point of PbSe and more readily recrystallizes.[44,45]

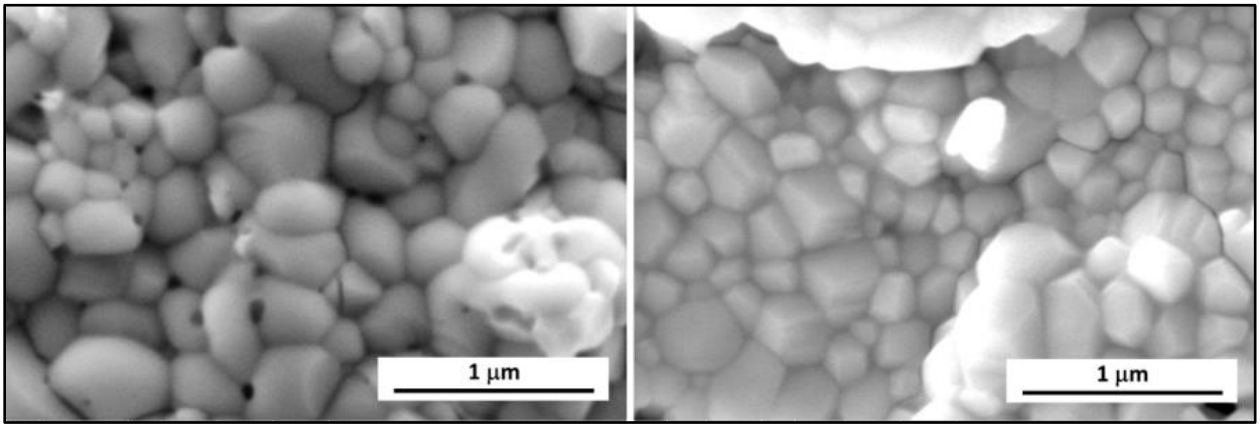

Figure 38: SEM images of PbSe film without KI (left) and with KI (right) following an inert atmosphere thermal anneal (5 min @ 460° C). The samples without KI are porous and fractured with round equiaxed grains. The sample with KI is more smooth and less fractured with highly faceted grains.

Table 11: Energy Dispersive Spectroscopy (EDS) of samples shown in Figure 38 and Figure 39. These results suggest that KI, or decomposed constituents, might be coating the PbSe grains and reducing susceptibility to oxidation, even during inert annealing at 460° C for 5 minutes. The oxygen quantities below 1 at. % are below the detection level for EDS quantification and are equivalent to zero.

Post Anneal (argon)			
Concentration (at %)	As Prepared	Laser Sintered	
		without KI	with KI
O	6.0	6.4	0.7
Se	45.8	44.3	46.3
I	0.0	0.0	0.7
Pb	48.3	49.3	52.3

Top-down EDS revealed the *as-prepared* PbSe (pre-laser-sintered) and the laser-sintered with *No-KI* films both contain ~6 at. % of oxygen *following* inert anneal at 460° C in argon (Table 11). The sample with *Med-KI*, however, shows only 0.7 at. % oxygen following the same inert anneal. This implies that the low levels of residual oxygen in the INSTEC chamber react with pure PbSe (without KI) to form $PbSeO_3$, and the samples with *Med-KI* are less susceptible to oxidation (less surface area). This further confirms that KI coats the PbSe grains, regardless of laser sintering, and creates a barrier to premature oxidation. This, combined with the increased density of the films with KI (fewer voids and cracks), contributes to producing a more uniformly, topdown thermal oxidation and iodization during the subsequent thermal sensitization steps. The oxygen quantities below 1 at. % are below the detection level for accurate EDS quantification and are equivalent to zero.

X-ray Diffraction (XRD) of the samples shown in Figure 38 revealed that samples with KI show only the intrinsic XRD peaks expected for PbSe (Figure 39). In contrast, the XRD of the sample without KI revealed $PbSeO_3$ despite the purging of the chamber with argon.

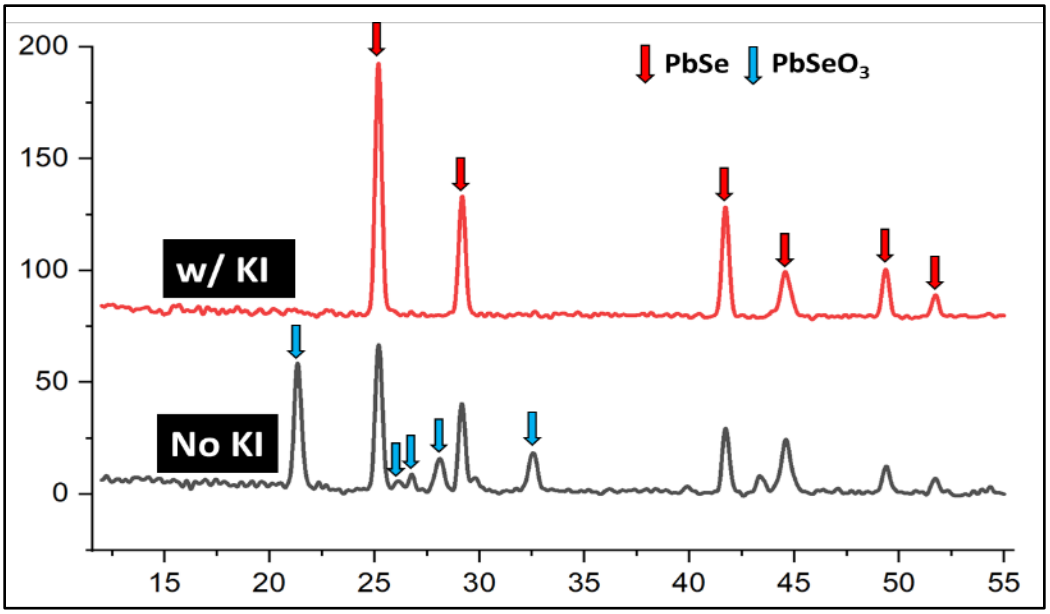

Figure 39: X-ray Diffraction of samples with KI and without KI following an inert anneal in argon at 460° C for 5 minutes. The sample with KI only shows intrinsic PbSe peaks (red arrows), while the sample without KI shows some evidence of oxidation (blue arrows).

Raman spectroscopy of samples with and without KI, and before and after inert anneal are shown in Figure 40. The Raman signal for both the samples laser-sintered with KI (black) and without KI (green) show only PbSe characteristic peaks (138 cm^{-1} and 793 cm^{-1}). The signal is much weaker for the sample with KI. There is no significant overall change in the Raman signal *intensity* for PbSe peaks following the inert anneal for the sample without KI; however, evidence of oxidation is confirmed by the presence of $PbSeO_3$ characteristic peaks at 361 cm^{-1} and 790 cm^{-1}. In contrast, the Raman signal for the sample with KI following the inert anneal shows a marked difference in the overall PbSe signal intensity at both 138 cm^{-1} and 793 cm^{-1}. There is some evidence of surface oxidation for both samples following inert anneal; however, much less for the sample with KI. This further supports the notion that KI may be encapsulating around the PbSe grains and reducing the susceptibility to oxidation before thermal oxidation when $PbSeO_3$ is intentionally formed under improved control on a denser film. The presence of the iodine, introduced by decomposed KI, forms a PbI_2 coating around the grains before thermal oxidation, improving crystallization, and may be preserved throughout the sensitization process. If one role of iodine is to recrystallize the base-layer of PbSe, low concentrations of KI exposure during film deposition greatly reduce the role of the *thermal* iodization process (following oxidation) in forming a passivation layer. Without KI, the thermal iodization process alone must simultaneously form a PbI_2 passivation layer as well as diffuse low levels of iodine to the underlying PbSe base-layer to recrystallize grains and form both $PbSeO_3$ and PbI_2 grain barriers.

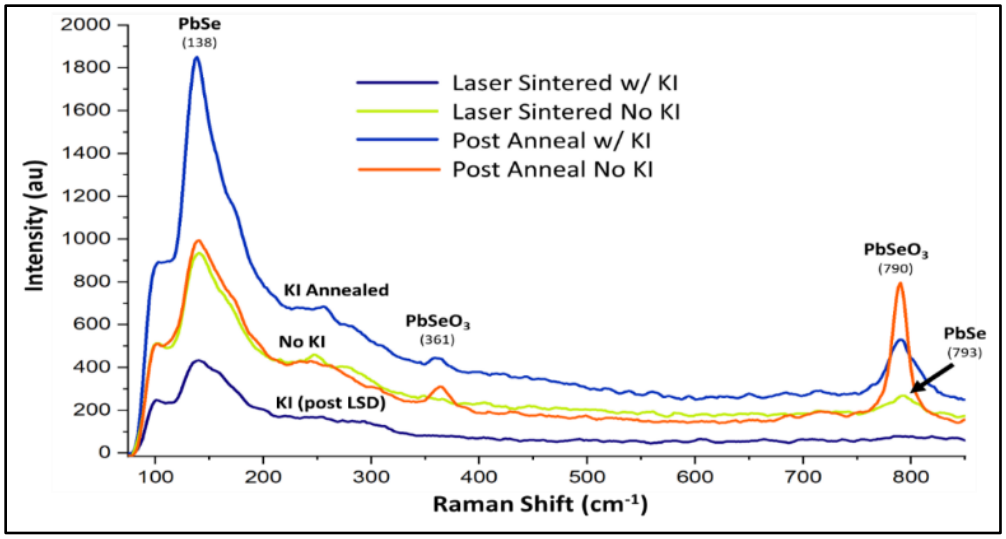

Figure 40: Raman spectroscopy of PbSe samples following laser sintering and an inert anneal at 460° C. The PbSe characteristic peaks are evident on all samples; however, no difference in intensity is seen in the sample without KI after annealing except for the presence of lead selenite ($PbSeO_3$). The sample laser-sintered with KI, however, shows a marked difference in the PbSe peak intensity after the inert anneals and shows some evidence of lead selenite on the surface.

X-ray photoelectron spectroscopy (XPS) was performed on samples with and without KI following laser sintering, and an inert anneal described above. XPS is extremely surface sensitive and is limited to the top ~10 nm of these films. The results are consistent with topdown and cross-sectional EDS via SEM and TEM. The XPS study shows that samples with KI appear to have a surface coating of PbI_2 and are consistently less susceptible to oxidation in an inert atmosphere (Table 12). The sample without KI exhibited $PbSeO_3$ and PbO on the surface as a result of oxidation and the loss of selenium. Whether the source of oxygen is from native oxide, residual moisture, or residual oxygen within the chamber, all samples without KI have a significantly higher concentration of oxygen. Further work is necessary to understand this.

These results suggest PbSe films containing KI are less suspectable for being oxidized when exposed to low concentrations of oxygen at high temperatures. In addition, potassium levels are below the detection levels for XPS and suggest the potassium is desorbed from the surface or diffuses deep into the film. Additional chemical analysis done using XPS showed that PbI_2 is present in patches on the surface of the PbSe films following inert annealing. XPS analysis provides an accurate chemical confirmation for PbI_2.

Table 12: X-ray Photoelectron Spectroscopy (XPS) analysis of surface composition. Oxygen levels on the surface of the sample without KI are significantly elevated while the selenium is reduced due to out-gassing.

XPS of Argon Annealed PbSe		
	No KI (at. %)	KI (at. %)
Pb	27	39
Se	12	18
O	61	41
I	0	2
K	0	0

(b) Annealing Under an Oxygen Atmosphere

The following experiment focuses on the difference in PbSe thin films with and without KI formed by laser sintering deposition (LSD) following thermal oxidation at 460° C in an oxygen environment for 5 minutes. No noticeable difference is observed in top-down SEM inspection between the films with and without KI following oxidation. X-ray Diffraction (XRD) was then collected for samples with KI and without KI following oxidation at 460° C for 5 minutes (Figure 41). The sample with KI primarily shows intrinsic PbSe peaks (red arrows) with some signs of oxidation in the $PbSeO_3$ peaks. The KI peaks are

from the recrystallized KI on the surface of the periphery of the film, outside of the laser-sintered area. The sample without KI shows significant oxidation peaks for $PbSeO_3$ (blue arrows). This supports the previous EDS and Raman data suggesting the KI reduces the formation of $PbSeO_3$ by oxidation.

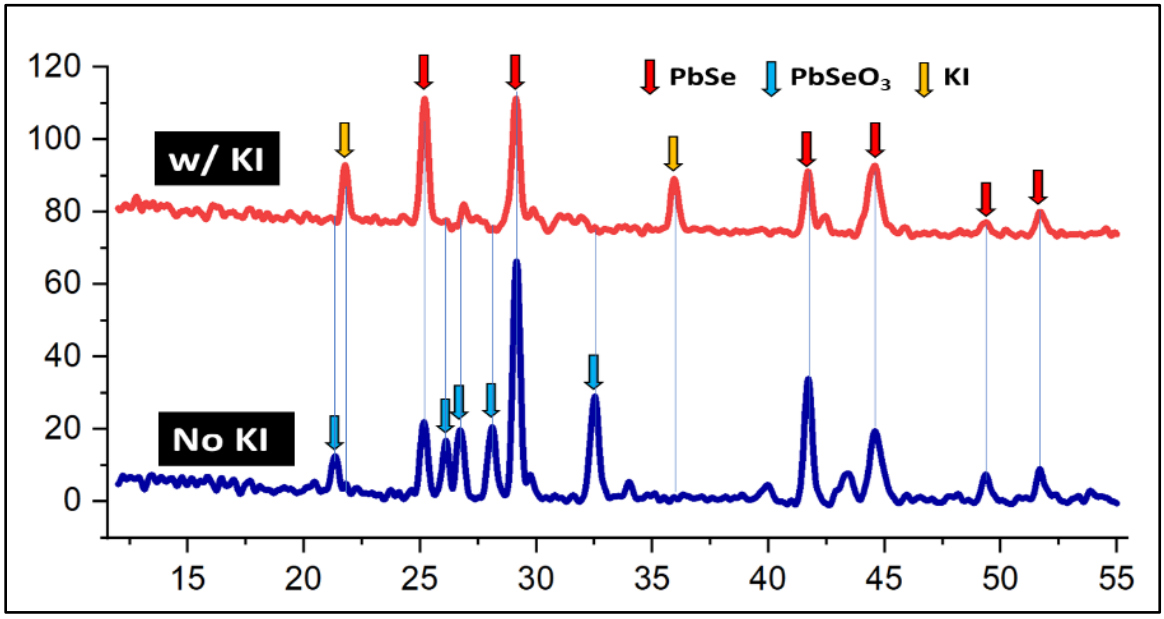

Figure 41: X-ray Diffraction of samples with KI and without KI following oxidation at 460° C for 5 minutes. The sample with KI primarily shows intrinsic PbSe peaks (red arrows) with some signs of oxidation, while the sample without KI shows significantly more oxidation (blue arrows). The KI Peaks (labeled in orange) are not representative of the overall PbSe film. These are from crystallized KI on the surface of the sample and ONLY around the periphery of the sample (outside of the laser-sintered area).

(c) Iodization of Oxidized PbSe

The same samples from Figure 34 that were then oxidized at 460° C for 6 minutes in the custom INSTEC chamber were then iodized at 325° C for 4 minutes. Figure 34 shows the significant influence KI exposure has on the morphology following laser sintering, and Figure 38 shows the impact of KI on recrystallization (fluxing) following an inert anneal. The impact of KI is further amplified in the crystallization of the top PbI_2 layer following thermal iodization (Figure 42). The thermal iodization process forms a top layer of PbI_2 regardless of the exposure of KI; however, the PbI_2 crystallite size is proportional to the KI concentration. A smooth and fractured continuous layer of PbI_2 is observed on the *Hi-KI* sample. This is likely the result of the reduced reaction temperature iodine has on PbSe in the formation of both $PbSeO_3$ and PbI_2. The KI recrystallizes the PbSe and begins to form PbI_2 even before oxidation.

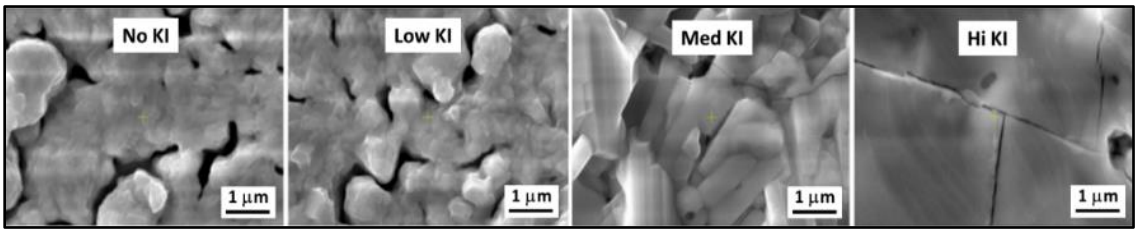

Figure 42: Top-down SEM image of fully sensitized PbSe films prepared under the same conditions with different KI concentrations. KI introduced before laser sintering has a significant impact on oxidation and iodization.

Cross-sectional EDS mapping reveals the distribution and uniformity of oxygen for samples with and without KI (Figure 43). Previously, we have shown that the PbSe films with KI are denser, less porous, highly faceted, and have a smoother surface. The SEM-EDS maps shown in Figure 43 reveal the impact that KI has on densifying the PbSe film and how oxygen and iodine diffuse more uniformly into the

polycrystalline thin film following full sensitization. The less-dense and porous film with *No-KI* have random pockets of high concentrations of oxygen and iodine deep into the film. The more dense and highly faceted PbSe film with KI shows an ideal top-down distribution of oxygen.

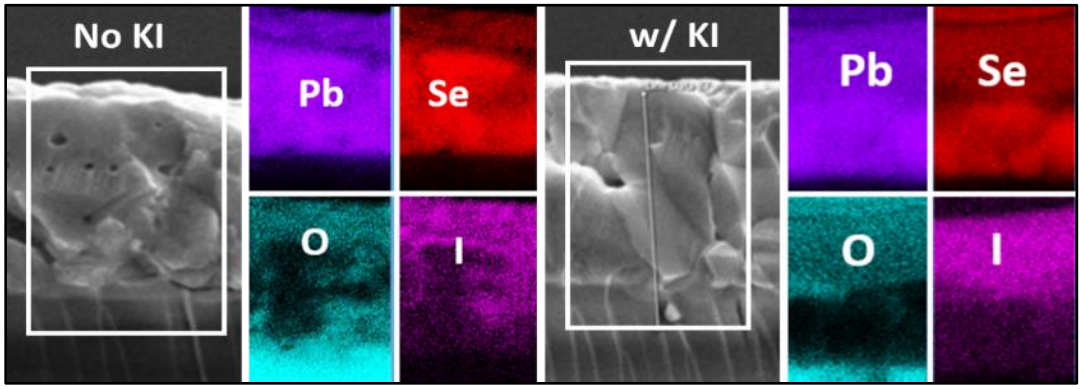

Figure 43: EDS mapping of Pb, Se, O & I following oxidation (6 minutes @ 460° C) and iodization (4 minutes @ 325° C) of laser-sintered PbSe films with No-KI (left) and with Med-KI (right). Films with KI oxidize and iodize more uniformly (topdown) than samples with No-KI.

6.3.3 Impact of KI on Optical and Electrical Properties

Samples prepared using different concentrations of KI and *No-KI* were used to study the optical absorption characteristics of laser-sintered PbSe films on silicon substrates. Immediately following laser sintering, the infrared transmission spectrum was collected using FTIR. The transmission spectra were compensated to account for the silicon substrate. Figure 44 shows that PbSe films exposed to KI have a trend for improved IR absorption proportional to KI concentration. Annealing and oxidization of identically prepared samples (red) showed improvement in absorption as well. The improved absorption is believed to be due to a denser film as a result of the KI. All samples in the infrared transmission characterization followed a similar spectral characteristic except for the Hi-KI sample. Top-down and cross-sectional EDS of the Hi-KI sample following laser sintering show a significantly different film composition due to the high level of KI incorporation that forms a PbSe + KI compound throughout the film. As a result, this Hi-KI sample exhibits a higher absorbance but also results in excessively high dark resistance with ionic conduction characteristics. Both characteristics are detrimental to achieving a high IR photoconductive film. Lower levels of KI are preferred with improved IR photoconductive performance.

A separate study of the electrical resistance versus temperature was performed to identify any difference between samples with and without KI. The electrical resistance was monitored through the temperature ramp as well as during steady-state oxidation in air at 460° C (Figure 45). All samples with KI show a unique characteristic electrical resistance versus temperature profile during the temperature ramp-up. Multiple transitions occur at 80°, 140°, 200°, & 220° C for samples with KI only. This suggests a phase change and/or chemical reaction. More work is necessary to understand these reactions. All samples with KI exhibited elevated electrical resistance proportional to dose compared to samples without KI.

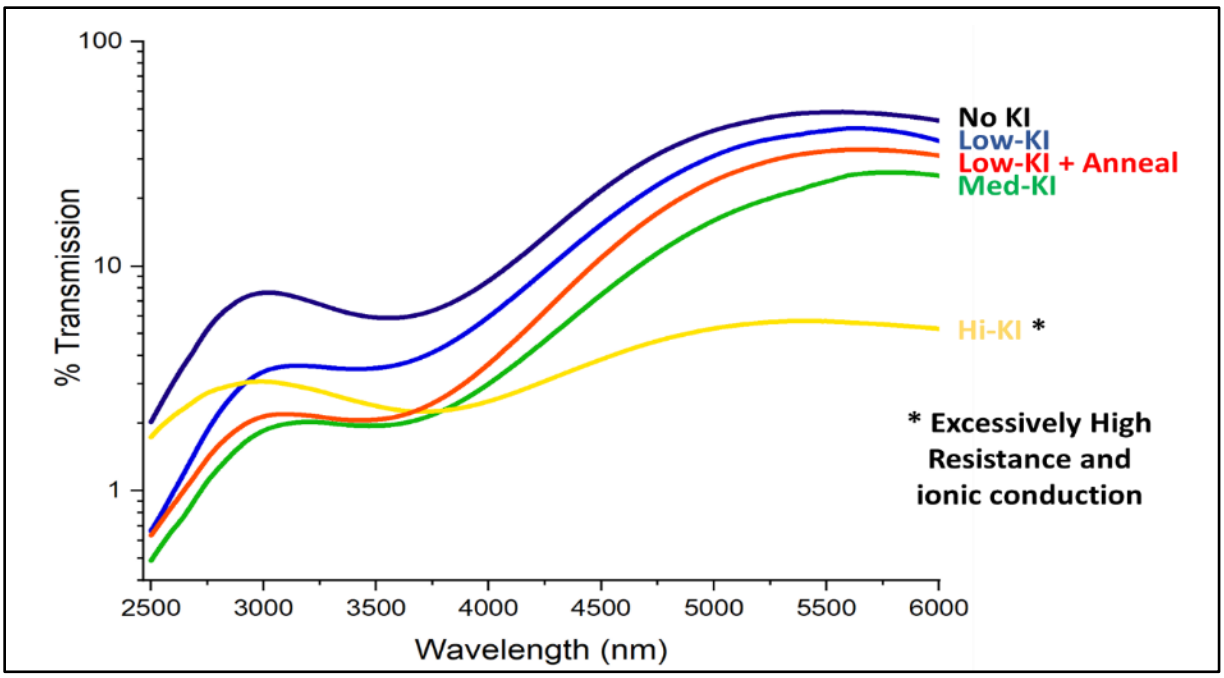

Figure 44: Infrared transmission spectrum of PbSe thin films having different concentrations of KI following laser sintering. This shows that the IR absorption of PbSe films increases proportionally to KI concentration. Annealing and oxidation show some evidence of higher IR absorption as well. The improved absorption is believed to be due to a denser film as a result of the KI.

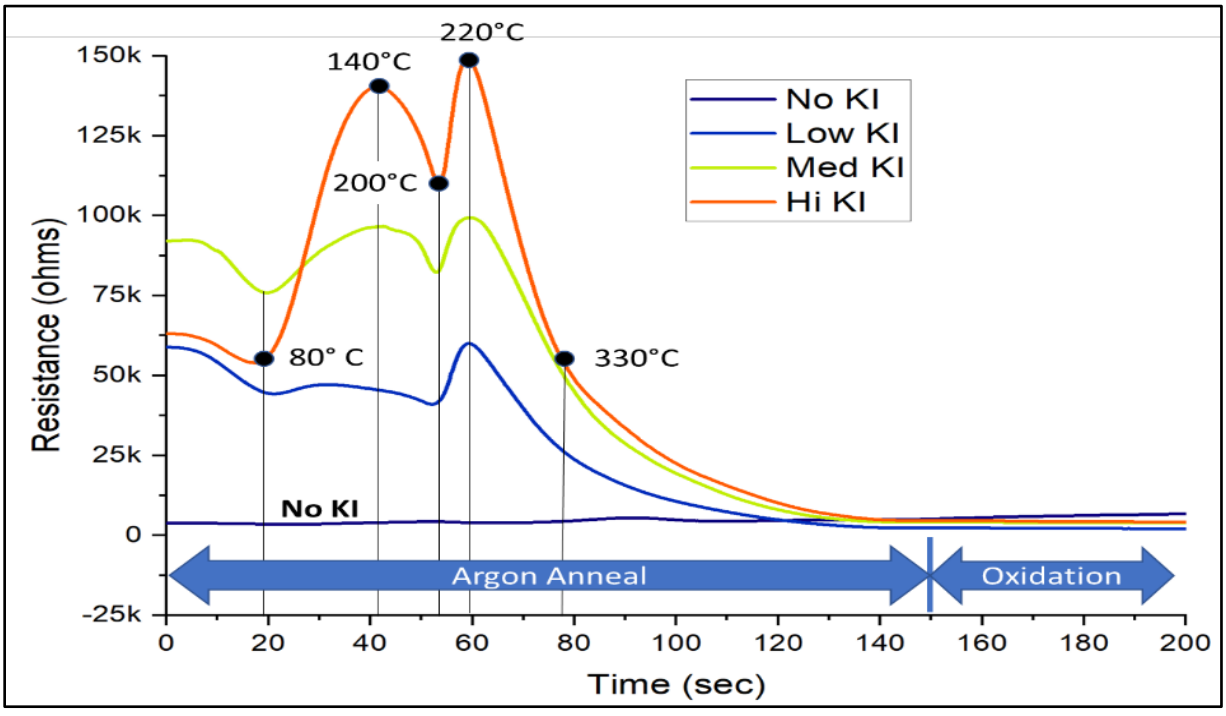

Figure 45: Electrical Resistance versus temperature ramp during inert anneal (in Argon). No-KI (aqua blue). All Samples with KI followed a similar characteristic profile during the temperature ramp. (right). Following the temperature ramp, all samples exhibited a similar linear profile after ramp, during oxidation at 460° C. Vertical lines at 80° C (19 sec), 140° C (42 sec) 200° C (53 sec), 220° C (59 sec) and 330° C (78 sec) are shown to help understand the relationship between ramp-up time and temperature. These curves are indicative of chemical changes in the film.

The Ecopia 4-point probe system was then used to measure the carrier type, carrier concentration, and mobility of PbSe films. All samples were annealed in an inert gas during the temperature ramp, followed

by oxidation at 460° C for 6 minutes. All films, regardless of KI, were p-type, and the carrier concentration was reduced with increased KI concentration (Table 13). The mobility and resistivity increased with higher KI concentration. The KI concentration corresponding to the maximum photoresponse is *Med-KI*. The *Hi-KI* concentration resulted in excessively high dark resistance following oxidation and iodization and exhibited a slow response indicative of ionic conductivity characteristics. PbSe films with *Med-KI* show ~30x higher dark electrical resistance (R_D) following oxidation versus *No-KI*, leading to ~100x reduced carrier concentration and improved photoresponse. Mobility was similar between samples, except for the *Hi-KI*, which has significantly higher. Following iodization, the *Hi-KI* sample dark resistance (R_D) is greater than 10 Giga Ohms

Table 13: Hall Effect Measurement following argon anneal + oxidation and 460° C.

Argon Anneal + Oxidation	Carrier Concentration (cm^3)	Mobility ($cm^2/V{\cdot}S$)	Resistivity Ω·cm
No KI	5.80E+18	4.5	0.3
Low KI	1.20E+17	4.8	11
Med KI	3.60E+16	6.1	32
Hi KI	2.00E+16	19.7	12

***Optimization of KI concentration for high MWIR* Photoresponse**

The ideal oxidation and iodization recipes were determined by a design-of-experiment (DOE). The maximum photoresponse of PbSe without KI was limited to a DelR between 8% - 15%. Figure 46 shows top-down SEM images (with oxidation and iodization times) of the PbSe films following the oxidation DOE. The impact on MWIR photoresponse for a one-step LSD film versus a two-step LSD film is shown on the right of Figure 46. The one-step LSD film introduces a single dose of *Low-KI* followed by laser sintering, oxidation, and iodization (described above). The maximum DelR achieved with the one-step KI (*Low-KI*) was 12.8%. The two-step LSD film is identical except introduces a 2nd *Med-KI* dose followed by a 2nd laser sintering. The two-step process results in a significant improvement in the MWIR photoresponse (Figure 46).

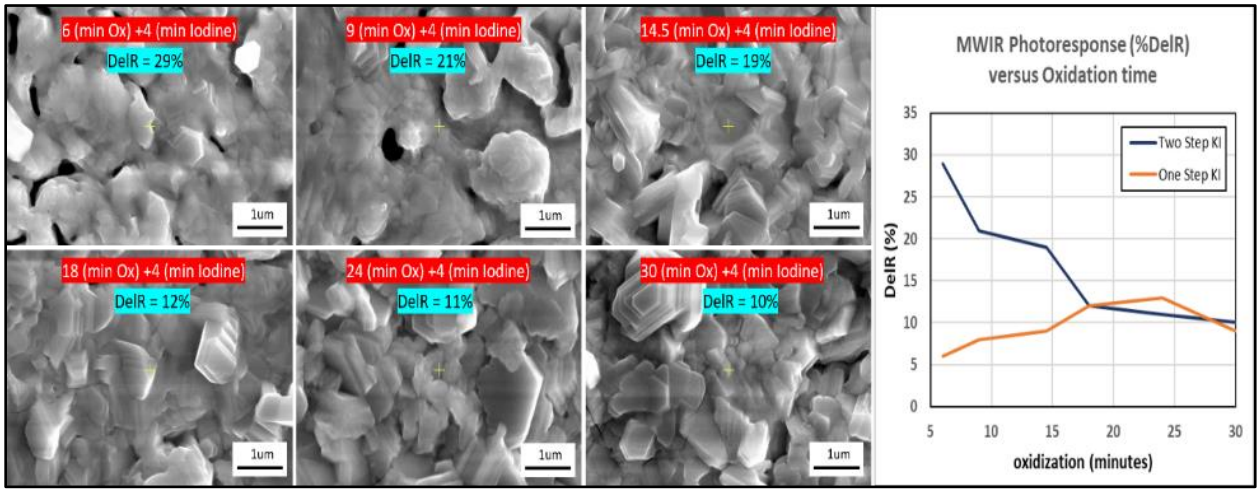

Figure 46: Top-down SEM images of PbSe samples produced by LSD with the 2-step KI dosing described above and processed through different oxidation times (left), and the right image shows a plot of MWIR response (%DelR) vs. oxidation time for single and two-step KI process.

6.4 Conclusion

Iodine plays many roles in the sensitization of PbSe, including, but not limited to, lowering the temperature of recrystallization of the PbSe grains, forming $PbSeO_3$ and PbI_2 coating on PbSe grains, and forming a PbI_2 surface passivation layer. Relying on a *single* thermal process for the diffusion of iodine to effectively achieve these roles on a 1-micron thick polycrystalline thin film is challenging. Introducing a

low level of iodine early in the deposition process through the use of KI, maximizes the photoresponse and improves repeatability.

This study confirms that potassium iodide (KI) introduced during the film deposition dramatically improves film densification through the lowering of the temperature for recrystallization by acting as a flux for the PbSe. The introduction of KI in the as-prepared films allows the decomposition of KI during the laser sintering process to form iodine which recrystallizes the PbSe thin film, increases film density, improves optical absorption, and electrical properties. The most obvious impact of KI is in the recrystallization and densification of the film, however, these results show that the early introduction of KI encapsulates the PbSe grains with a PbI_2 layer during the laser sintering process that helps to improve the subsequent thermal sensitization and inter-grain coupling. The more dense and highly faceted PbSe grains, as a result of KI, regulate the diffusion of oxygen and iodine to improve the formation of the uniform layer thickness of PbI_2, $PbSeO_3$, and the PbSe base-layer.

We report how introducing KI modifies the PbSe morphology and improves the MWIR photoresponse, but also demonstrate how a 2-step KI process can further improve the MWIR photoresponse by 300% compared to that of a 1-step KI process. These findings, and those previously reported, show similarities between the early introduction of KI to that of the thermal iodization (final step of thermal sensitization) process.[54] The key benefit of KI is the controlled distribution of low levels of iodine throughout the film during deposition. The KI decomposes to more controllably impact the morphology and interface between grains of the lower part of the PbSe film. The early introduction of KI simplifies the thermal iodization step by recrystallizing the base-layer of PbSe and enabling the formation of $PbSeO_3$ and PbI_2 at grain boundaries. The role of the later thermal iodization step is then simplified to the formation of a PbI_2 passivation layer. Neither thermal iodization nor the introduction of potassium iodide was able to provide a high photoresponse alone. The combination of the two was necessary to maximize the photoresponse of these films.

(The preceding sections 6.1 - 6.4 were written by the author of this thesis and reproduced from ref.[52] with permission from the Journal of Alloys and Compounds)

CHAPTER 7: Novel Laser Processing of PbSe Thin Films

7.1 Introduction

The following are laser processing techniques that will be considered for use in device fabrication. Each of which is summarized in Table 14.

Table 14: Summary of laser processing types, concepts, effects, and motivations

Laser Process	Results and Achievements	Added Benefit	
Laser Sinter Deposition (LSD)	• Deposit uniform & precise film (500 nm to 2 μm) • Laser sinter to form tailorable polycrystalline thin film	Process Integration for consecutive treatments	Laser definable Pattern (spatial)
Insitu-patterning	• laser defined pattering to eliminates photolithography • Selective layer patterning (PbSe, Metal, Contacts)		
Improve CBD Film Adhesion	• Chemical Bath Depositon (CBD) sufffers from film adhesion (delamination) • Laser Treatment improves adhesion of ALL traditional depositon methods		
Surface Treatment	• Surface texturing and smoothing • Selective passivation & annealing		
Carrier Conversion	• Convertes majority carrier type (p-type → n-type) • improves mobility 500%		
Selective Depth Sintering (SDS)	• produces bottom-up vs top-down sinter → structure/doping gradient • Seals surface of porous thin films		
Laser Dicing	• Enables wafer dicing, simplifying device fabrication • Allows successive laser treatments (LSD dep → laser patterning → dicing)		

7.2 In Situ Patterning

To further reveal the benefits of laser processing, this work shows how laser processing can not only simplify the deposition of thin films but can also be utilized to eliminate the necessity for photolithography to define and pattern device structures. This work has already shown how laser treatment can be used to deposit a tailorable thin film with unique textures and surface treatments, but laser processing can also be used to selectively ablate and pattern different materials. The combination of 1070 nm (IR) and 355 nm (UV) lasers can be used in a single chamber to both form a thin film and surface treatments as well as pattern devices and metal traces/contacts. The 355 nm laser is capable of selectively ablating the PbSe film without damaging the substrate or the integrity of the thin SiO_2 layer insulating the silicon substrate. Figure 47 shows SEM images of the result of in-situ patterning of PbSe. Figure 47 (b) shows how the 100 nm SiO_2 insulator remains undisturbed with the removal of all evidence of the PbSe thin film. Both individual lines or clearing of large areas can be achieved rapidly, immediately after LSD processing without the need for photolithography. This can be done in an inert chamber if oxidation is a concern.

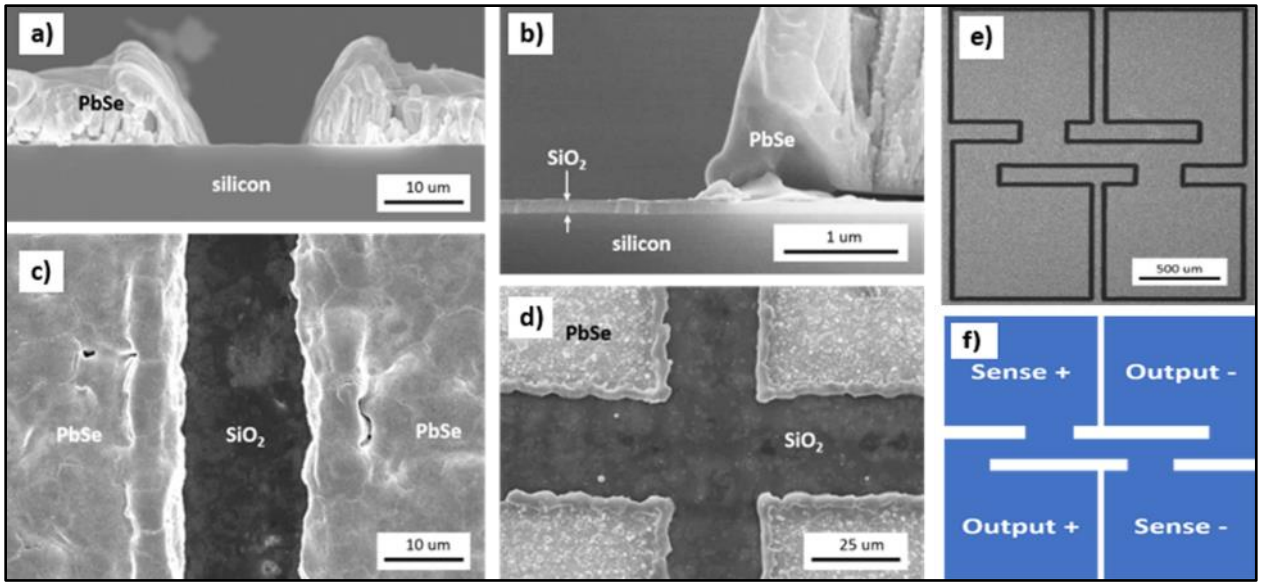

Figure 47: SEM cross-section (a,b) and top-down (c,d,e) images of in situ patterning of PbSe using a 355 nm laser to selectively ablate thin films without damaging the substrate of SiO_2 isolation. 4-point Van Der Pauw test structure layouts (e,f)

To further characterize and measure the electrical and optical properties of this PbSe thin film, the 355 nm laser was utilized to form test structures and define discrete photodetector devices. Figure 47 (e-h) shows two common Van Der Pauw test structures used to measure sheet and line resistance of thin films. Figure 47 (g) shows an example of an 80 x 80 μm test structure that can be defined without the need for the costly and time-consuming photolithography process.

The edge-bead of the laser-defined line in Figure 47 (a) is an artifact of the 355 nm laser patterning. This can be minimized but is an unavoidable product of laser patterning. This edge-bead is found to be Pb-rich and thus has a higher electrical conductivity than that of the 1070 nm LSD-formed film. This may pose a problem when defining small MWIR photoresponsive devices, as the lower resistance of the edge-bead may impact the performance. To mitigate this concern, the argon purge of the chamber was replaced with oxygen. The result is an oxidized edge bead (Figure 48) which has a much higher resistance than the PbSe film (as-deposited). The oxidized edge-bead more rapidly converts to a highly resistive PbI_2 during the subsequent sensitization process. This is only a concern if laser patterning is performed before sensitization.

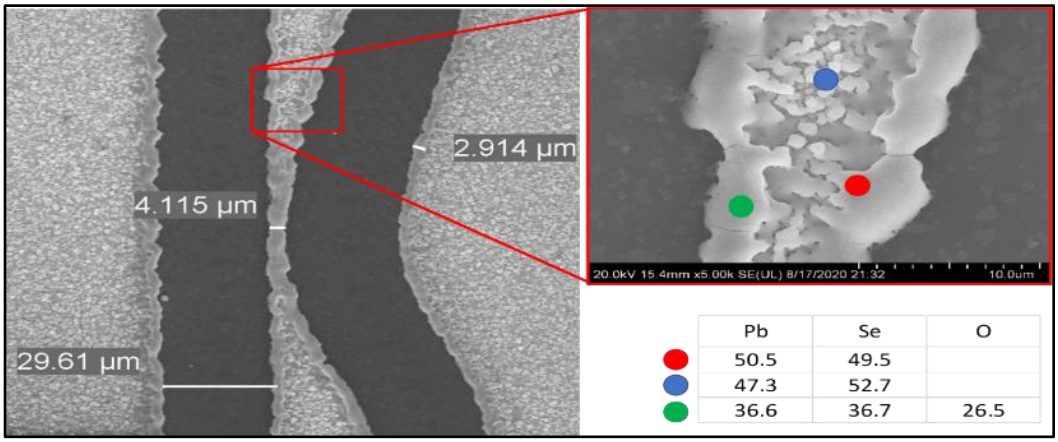

Figure 48: SEM and EDS results of 355 nm (UV) patterned PbSe (pre-sensitized) showing in-situ oxidation of the edge-bead to mitigate the highly conductive (Pb-rich) edge of patterned structures. The upper right image shows the concentration of Pb, Se & O (at.%) and reveals that the edge bead is oxidized by exposure to air during sintering, eliminating its effect on film conductivity.

Similar laser ablation selectivity can be achieved between a 100 nm sputtered layer of gold (Au) and the SiO_2/silicon substrate. The results are shown in Figure 49.

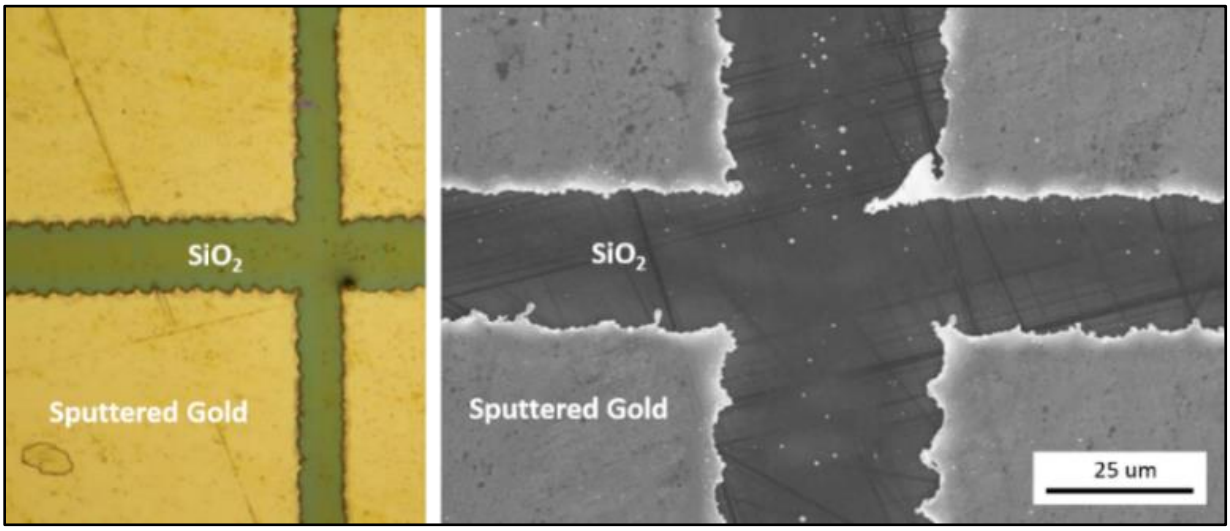

Figure 49: 355 nm (UV) patterned 100 nm layer of Au on SiO_2. The optical image on the left shows ~100 nm of sputtered gold on SiO2 after selectively laser ablating the gold without damaging the substrate. SEM image on the right more clearly shows the completeness of the ablation and even shows the roughness SiO_2 has little, if any, impact from the laser.

Selective laser patterning of metal without disturbing the underlying PbSe can be used if sufficient selectivity can be achieved. This requires high selectivity of the laser for the metal over the underlying film with some margin for error. The following work shows how a 100 nm layer of sputtered gold (Au) can be selectively laser patterned with the same 355 nm (UV) laser. Conveniently, MWIR sensitized PbSe has a chick PbI_2 passivation and provides a large margin in Au patterning. However, the SEM imaging and EDS line-scan results (Figure 50) show that little margin is necessary as the 355 nm laser can ablate the 100 nm layer of Au without disturbing the underlying PbSe.

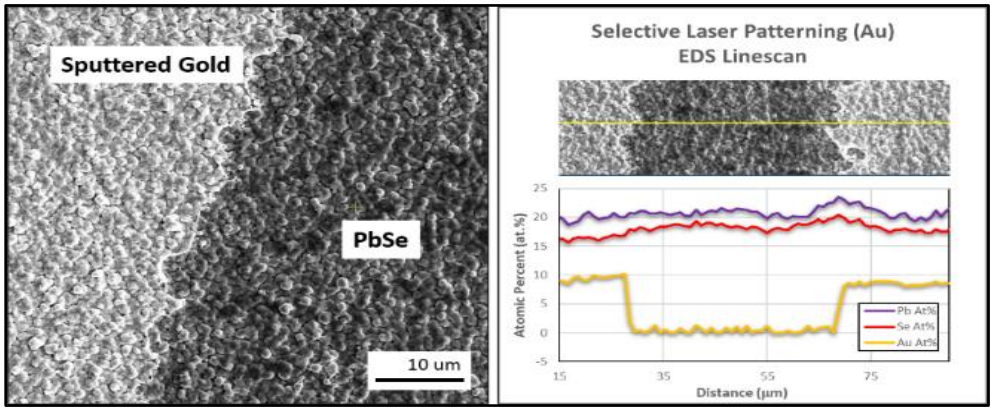

Figure 50: SEM images (left) and EDS line-scan (right) results showing high selectivity between the ablation of 100 nm of Au and the underlying PbSe.

7.3 Improved Film Adhesion for CBD Films

Chemical bath deposition (CBD) suffers from film adhesion due to the chemical nature of the wet processing and lack of surface texture on the substrates, usually SiO_2. This has resulted in manufacturers pre-treating their wafer surfaces by roughening or other processing that takes additional time and expense. Still, CBD suffers from delamination.

The laser sinter deposition process has been shown to improve the film adhesion for tightly packed nanocrystals following the ball milling and centrifuge process, but laser processing is not restricted to LSD. Similar laser processing proves to be effective for improving the adhesion of even tradition deposited PbSe films. Figure 51 shows a wafer with PbSe deposited via chemical bath deposition with no substrate treatment. A very simple tape method was used to show how a small area of the CBD deposited film treated with laser sintering can have significant improvement in the film adhesion.

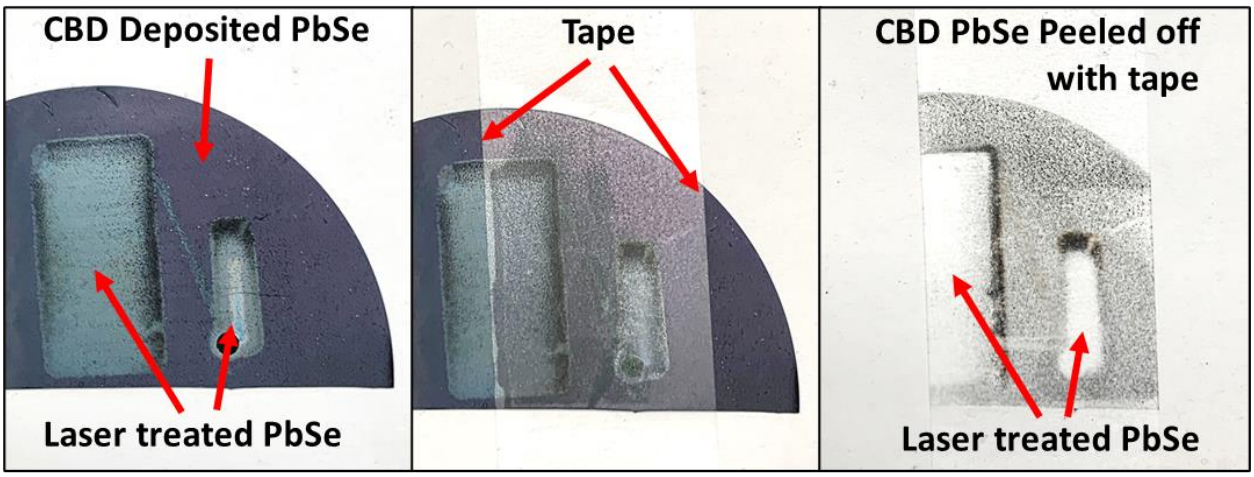

Figure 51: Optical images of a wafer with a 1 μm thick layer of PbSe deposited with the chemical bath deposition (CBD) method. A small area was treated with laser sintering (left rectangle) followed by a simple adhesion test with tape (center). The rightmost images show the results of the tape upon removal. The area treated with laser showed almost zero loss of film transfer to the tape. The area with only CBD deposited (untreated by laser) was nearly removed entirely.

7.4 Surface Treatment

Another very powerful capability of the LSD process is that a variety of laser wavelengths can be chosen based on the wavelength-dependent absorption depths and rapid heating to accomplish more than just full-film sintering. By using shorter wavelengths with shallow penetration depth and short pulses, laser treatment can be applied to smooth the surface and change the morphology, globally or in select regions. The choice between surface treatment in inert gas versus oxygen can help maintain stoichiometry or passivate the surface and protect the underlying materials to reduce porosity. A rough surface can promote light scattering and improve absorption in a thinner film, while a smooth surface might increase reflectivity or improve conductivity in specific regions. Figure 52 shows examples of how surface roughening can be achieved with a 1070 nm (IR) laser, and a 355 nm (UV) laser can be used to progressively smoothen the surface by increasing the power. The 355 nm laser ONLY sinters the top 100-200 nm of PbSe, so the underlying film remains unchanged. Slower scan rates can sinter to deeper levels. The potential for rapid and selective oxidation is demonstrated in Figure 48 of section 7.2 In Situ Patterning.

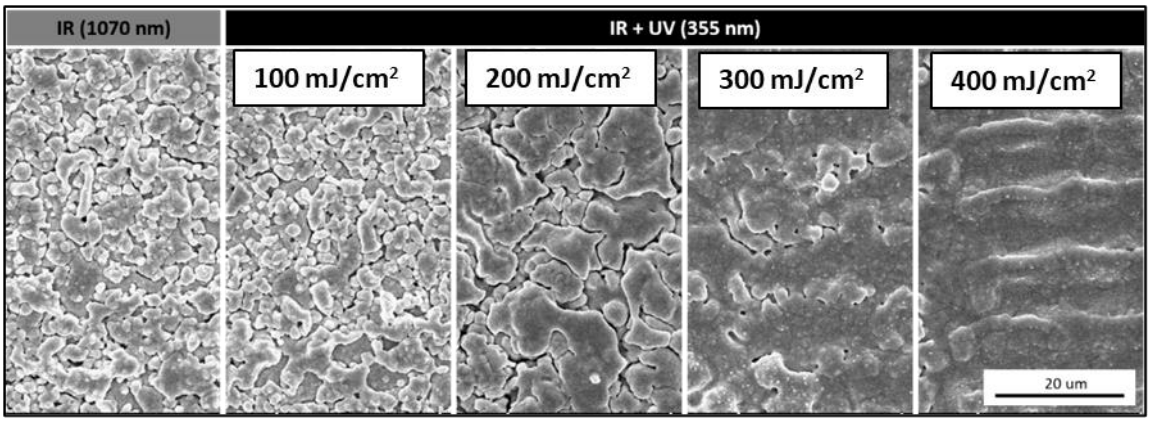

Figure 52: (Low magnification) Top-down SEM images of a textured IR (1070 nm) PbSe surface with progressively increased 355 nm (UV) laser (100 mJ/cm² - 400 mJ/cm²) treatment to smoothen the surface.

7.5 Carrier Conversion of PbSe (p-type → n-type)

One interesting discovery in this work is the unique ability to selectively and spatially transition a p-type PbSe thin film from p-type to n-type using the 355 nm (UV) laser. This is accomplished by forming a PbSe film with the 1070 nm laser, followed by subsequent laser treatment with multiple scans of the 355 nm laser. The 355 nm laser energy sinters the film top-down in contrast to the 1070 nm laser sintering bottom-up. [34,54] Repeated scans at reduced power convert the majority carrier type from p-type to n-type. This was found to be very repeatable and confirmed on the Ecopia Hall effect system (Table 15). It is believed to be due to selenium loss.

Table 15 shows the film properties of the IR (only) sinter and the IR + UV sinter, which converts the carrier type from p-type to n-type. The mobility (μ) increases, and the sheet resistance (R_s) reduces. This may be the result of the 355 nm laser volatilizing the PbSe film to reduce the selenium content. This agrees with the fact that Se-rich PbSe is p-type and Pb-rich PbSe is n-type. Interestingly enough, the carrier concentration does not dramatically change, however, the carrier concentration does consistently increase with carrier type conversion. This could potentially be used to convert regions of semiconductive PbSe to a metal lead conductor.

Table 15: Table showing the hall measurement data of carrier conversion using laser treatment. Each sample is measured before and after UV treatment and shows a consistent change.

	Pre UV Laser Treatment						Post UV Laser Treatment					
SN#	Sinter Type	Carrier type	N_A (cm^{-3})	μ (cm^2/V·s)	R_s (Ω□)	ρ (Ω·cm)	Sinter Type	Carrier type	N_D (cm^{-3})	μ (cm^2/V·s)	R_s (Ω□)	ρ (Ω·cm)
SN1	IR	p-type	4.90E+18	6.1	1740	0.21	UV	n-type	-8.40E+18	41.1	150	0.018
SN1	IR	p-type	4.70E+18	6.8	1637	0.21	UV	n-type	-9.90E+18	33.6	155	0.019
SN2	IR	p-type	4.00E+18	8.6	1468	0.18	UV	n-type	-1.20E+19	25.1	162	0.02
SN2	IR	p-type	2.40E+18	8.4	2599	0.31	UV	n-type	-1.50E+19	26.9	158	0.016
SN3	IR	p-type	1.00E+18	8.3	4980	0.7	UV	n-type	-4.70E+18	80.7	82	0.01
SN3	IR	p-type	1.00E+18	3.9	5900	0.8	UV	n-type	-4.90E+18	24.5	256	0.05

7.6 Selective Depth Sintering (SDS)

Another laser treatment is what is known as selective depth sintering. The wavelength, power, and scan speed parameters can be tuned to allow bottom-up sintering as seen with the 1070 nm (IR) laser on PbSe or very shallow sintering using a 355 nm (UV) laser. With the 355 nm laser, a top-down sinter as shallow

as 50 nm was achieved. Figure 53 (a) shows an IR sintered film with columnar grains with a rough surface. Figure 53 (b) shows a top-down sinter using the 355 nm laser at a fast scan and low power. The columnar morphology of the underlying film is maintained, yet the top ~200 nm of PbSe has been sintered and smoothened. The delineation between the two sintered layers is difficult to see. To better demonstrate the effect of SDS, a much thicker, porous film (6.5 μm thick) was IR sintered, followed by UV surface treatment. The delineation is seen in Figure 53 (c,d).

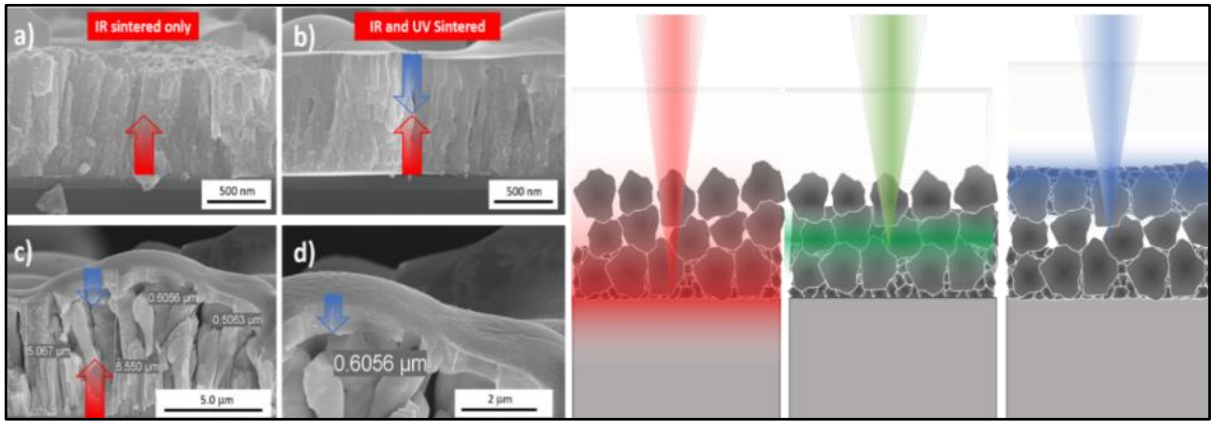

Figure 53: SEM cross-sections showing selective depth sintering (SDS). (a) shows the bottom-up sinter of IR, (b, c, d) shows the top-down sinter of UV. The schematic on the right represents the concept of selective depth sintering. Longer wavelengths penetrate deeper into the film and interact with different interfaces. (a) shows a 900 nm thin film of PbSe before any UV treatment. (b) shows the surface smoothening as a result of the shallow absorption of the 355 nm UV laser. (c) and (d) repeat this on a much thicker PbSe film to better show the shallowness of the UV treatment. Notice the 355 nm laser only sinters the top 600 nm, leaving a buried film of porous PbSe.

7.7 In Situ Laser Dicing

Another benefit of laser processing is the ability to integrate several laser processes. Wafer dicing can be performed with the same 355nm (UV) laser inside the same chamber as other treatments consecutively. For example, after laser sintering a film, surface treating specific areas for unique properties, pattering a metal conductor, and PbSe MWIR devices, one can potentially also score or dice the wafer. The 200 laser passes (Figure 54) for ~30 seconds successfully cut the wafer 150 μm, allowing a simple cleave to separate the adjacent die.

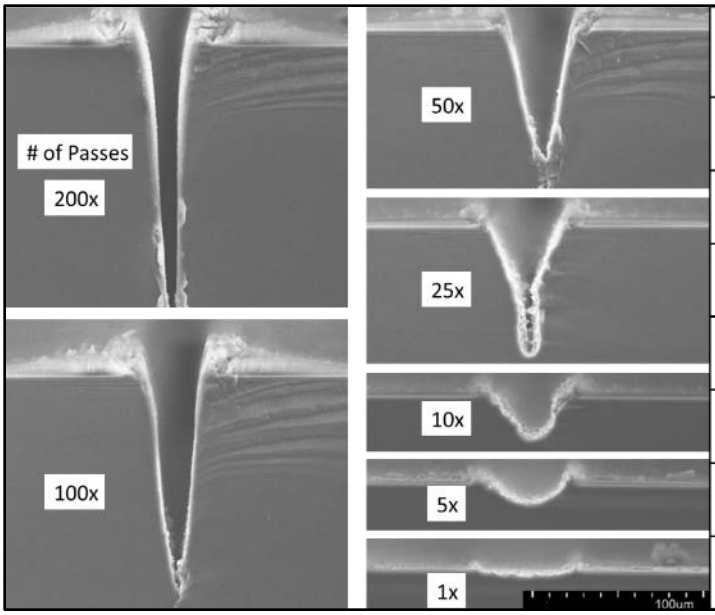

# of Passes	Cut Depth (mm)
200	160
100	128
50	94
25	60
10	27
5	12
1	4

Figure 54: SEM cross-section images of laser-assisted wafer dicing. This is not a new concept but adds to the benefits of integrating laser processing into a single system.

CHAPTER 8: PbSe Thin Film Detector Fabrication and Characterization

8.1 Introduction

8.1.1 Background

Significant efforts were spent developing the Laser Sinter Deposition (LSD) process in determining a process window for producing high MWIR responsive thin films of sensitized PbSe. The LSD process is a completely new method for consistently producing a uniform thin film of polycrystalline PbSe. Many researchers who have attempted laser sintering have struggled with material balling, percolating, and lack of sintering uniformly across larger areas. There is a small margin between sintering and melting and LSD is the first to accomplish this. The combination of the PbSe material, targeted film thickness (700 nm - 1.2 μm), laser parameters (wavelength, power, pulse width, rep-rate, etc.), substrate choice (silicon), and even SiO_2 thickness were just some of the variables considered. The final SiO_2 thickness plays a critical role in the balance between sintering the film and moderating the absorption and heat dissipation through the substrate. The targeted optical, electrical, and physical parameters were based on the *as-deposited* polycrystalline PbSe thin film produced by the CBD process (refer to Chapters 4 - 5).

Once an acceptable process window was determined for repeatable PbSe thin film deposition, the sensitization process (oxidation and iodization) was optimized (Chapter 6) to account for the interactions between the two thermal process steps. Additional work on selective laser patterning of PbSe and the laser-defined metallization (Chapter 7) is necessary for setting up a process flow for forming functional MWIR detectors. The following work will focus on forming large area (> 1 mm^2) discrete MWIR photodetectors using *only* laser processing to form the film, and define features without the need for photolithography.

8.1.2 Device Photoresponse Parameters

This work integrates the LSD deposition process and laser processing tools described in the previous section into a repeatable process flow for fabricating fully sensitized PbSe thin film, depositing metal contacts, and characterizing the MWIR photoresponse. The following results show that an LSD deposited film can show a high photoresponse in a multitude of figures of merit, including DelR (defined previously), Responsivity (R), Quantum Efficiency (QE), Noise Equivalent Power (NEP), and Detectivity (D*). The overall progress and current stage of the process development flow and methodology are highlighted in blue in Figure 55.

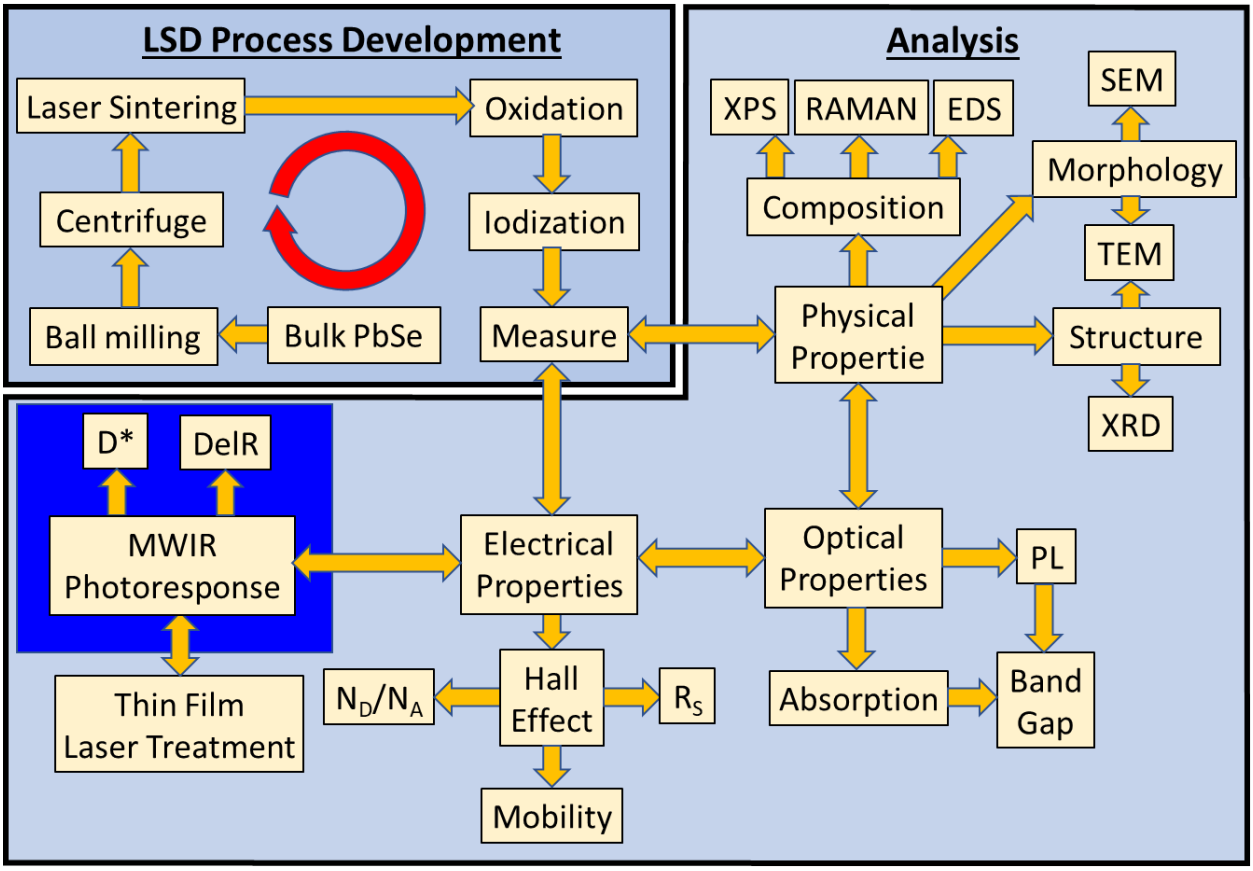

Figure 55: Similar to Figure 5, this process flow shows the current stage and progress. This section focuses on the deep blue highlighted steps. All other steps have been completed up to this point.

8.2 Fabrication and Device Performance Evaluation

8.2.1 Figures of Merit

a) Photoconductivity Measurements

Since PbSe is a photoconductive type of photodetector, it has linear current-voltage characteristics. This means the most common figure of merit, referred to as Delta Resistance (DelR), is a very good method for characterizing the photoresponse. DelR is the change in resistance as a response to a set illumination standard (described previously in Figure 21). We have already reported in Chapter 6, that a DelR of greater than 29% was achieved for the large area thin films of PbSe (without metal contacts). The percent difference in resistance between dark resistance (R_D) and illuminated resistance (R_L) is graphically shown in the form of an I-V sweep (Figure 4, right) and an improved DelR reported in the following section. As described in previous sections, DelR (ΔR) is the percent difference in film resistance between dark (R_D) and illuminated (R_L) conditions.

$$DelR(\%) = \frac{R_{dark} - R_{illuminated}}{R_{dark}} x\ 100 \quad \textbf{(16)}$$

b) Responsivity (R)

The responsivity of a photodetector is simply the voltage (or current) per Watt of illuminated light per unit area at the surface of the sample and is in units of (V/W or A/W).

$$Responsivity = \frac{V_{dark} - V_{illuminated}/\text{detector area}}{Illumination\ Power/area} \quad \textbf{(17)}$$

c) Quantum Efficiency (QE)

Quantum Efficiency, more specifically, the external quantum efficiency is a measure of the ratio of electrons in response to the incident light source flux in photons. The QE is directly related to Responsivity in units of A/W. Both the QE and spectral responsivity are a function of the wavelength of the photon and are calculated as follows.

$$QE_\lambda = \frac{R_\lambda \cdot \mathrm{h} \cdot \mathrm{c}}{\lambda \cdot \mathrm{e}} = \frac{R_\lambda}{\lambda} x(1240 \cdot \frac{W \cdot nm}{Area}) \qquad \textbf{(18)}$$

λ is wavelength in nm, h is Planks constant, c is the speed of light in a vacuum, and e is the elementary charge.

d) Noise Equivalent Power (NEP)

The Noise Equivalent Power is in units of ($W \cdot Hz^{-1/2}$) and, as the name suggests, is the noise power density. Noise Equivalent Power (NEP) is used to determine the random thermal noise of the detector per square root of the equivalent noise bandwidth (ENBW). The ENBW is often chosen to be 1 Hz, however, this value is defined by the system used to measure the thermal noise of the detector. In this case, a Stanford Research SR-830 lock-in amplifier is used to perform this measurement and uses an ENBW of 2.6 Hz.

$$NEP = \frac{Noise\ Spectral\ Density\ /\sqrt{\Delta f}}{Responsivity} \qquad \textbf{(19)}$$

e) Specific Detectivity (D*)

The Detectivity often referred to as the specific detectivity or D-star (D*), is the reciprocal of the NEP and is normalized by the square root of the product of the area of the detector and ENBW. Detectivity is a figure of merit used for characterizing the performance of photodetectors of different sizes and is measured in units of $cm \cdot Hz^{1/2}/W$. In honor of the creator of this unit, Robert Clark Jones, it is also referred to in units of *Jones*.

$$Detectivity = = \frac{\sqrt{Detector\ Area}}{NEP} \qquad \textbf{(20)}$$

8.2.2 Figure of Merit Measurement Equipment

The equipment used for measuring these figures of merit is a Keithley 2400 Source-meter, 5 mW 1555 nm laser diode (ML925B45F) and 30 mW 2700 nm fiber laser (LFL2700), GW INSTEK (AFG-2125) waveform generator used to modulate (chop) the light source, a Thor labs optical chopper and a Stanford Research SR830 Lock-in Amplifier with SR570 Low-noise Current Pre-amplifier. An INSTEC HCS602SG-PM probe system was used to monitor and maintain temperature. For the Responsivity versus wavelength and temperature measurements, an IR-301 Blackbody Temperature controller from Infrared Systems Development, a Keithley Source-meter 2601B, and a custom Process Evaluation Chip system (PEC) with built-in liquid nitrogen (LN) Dewar was used. The PEC system is a vertically mounted socket that accepts LCC08423 packages holding infrared detectors for photoresponse characterization. The system can vacuum seal the sample to eliminate condensation during reduced temperature testing.

8.2.3 Device Fabrication and Device Geometry Considerations

The samples used in this characterization were prepared and sensitized using the methods and recipes described in Chapter 6. The two primary types considered are both planar (lateral) thin film devices (1) rectangular with parallel pads and (2) a device with interdigitated pads (comb layout). The difference is the configuration of the contact pads and channel length for the active area versus the short channel of comb structures. In both cases, photolithography is unnecessary due to the simple pad design and scale, therefore, the PbSe thin film was deposited using the LSD process. Then the pads were defined using the 355 nm UV laser to produce shadow masks followed by plasma sputtered gold (Au) or gold-palladium (AuPd) contacts of between 75 - 100 nm thickness. Figure 56 shows a schematic of the two device

configurations (left), examples of laser cut stencil masks (middle), and an optical image example of a comb structure device (right).

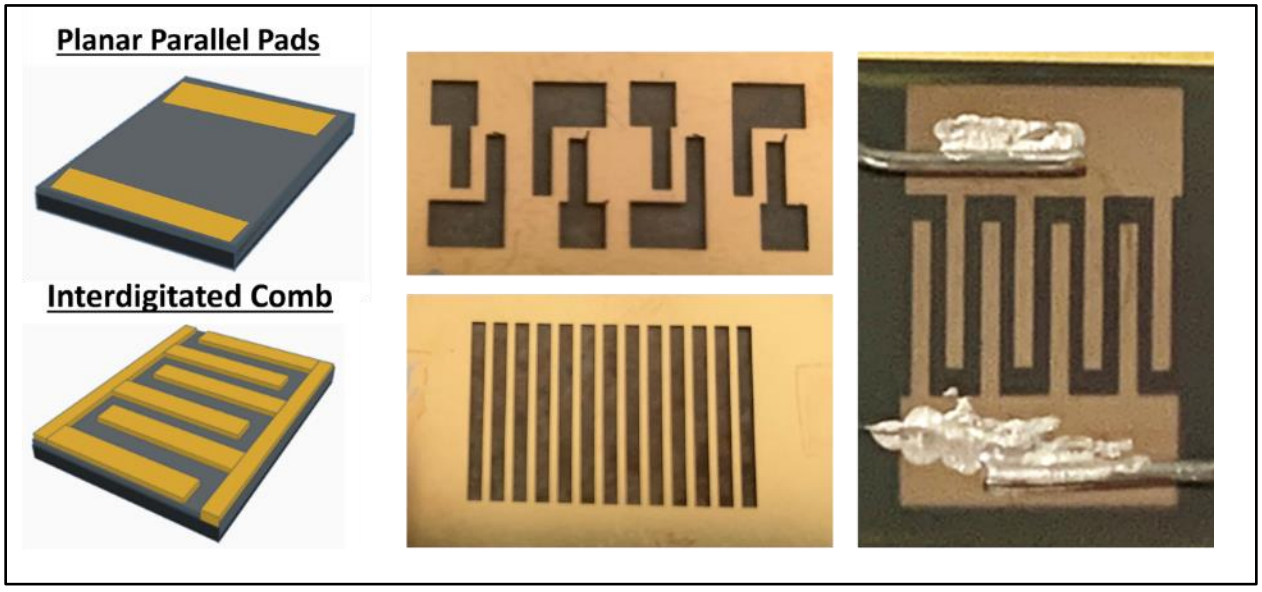

Figure 56: MWIR Device layout types, planar parallel plates (upper left) and interdigitated comb pads (lower right), laser fabricated shadow mask designs with the 355 nm UV laser (middle), and the final plasma gold deposited to define metal pads.

For detectivity (D*) and Noise Equivalent Power (NEP) testing, the small parallel plate design was chosen because it is much more efficient to use a small active area to avoid extraneous light entering the outside area and causing an increase in noise.[56] Responsivity versus wavelength and temperature was later performed on the comb design due to connectivity to the socket required for the PEC tester.

8.2.4 Device Performance Evaluation

As a result of the work reported in Chapter 6, the LSD process and subsequent thermal sensitization have become repeatable for achieving a photoresponse of a *minimum* of 15% DelR, and as high as 35.7% on samples fabricated using the LSD process. There is still a large amount of sample-to-sample variation as well as batch-to-batch. The biggest variable for achieving consistent yield is in achieving uniformly high densification of the film during laser sintering. This directly impacts the photoresponse for the fabricated PbSe thin film device. For this to be achieved, ball milling, centrifuge deposition, and potassium iodide doping are critical steps. Each step introduces variability that can compound if not done consistently. Figure 57 shows an example of the highest recorded DelR film using the LSD process, measured at a DelR of 35.7%.

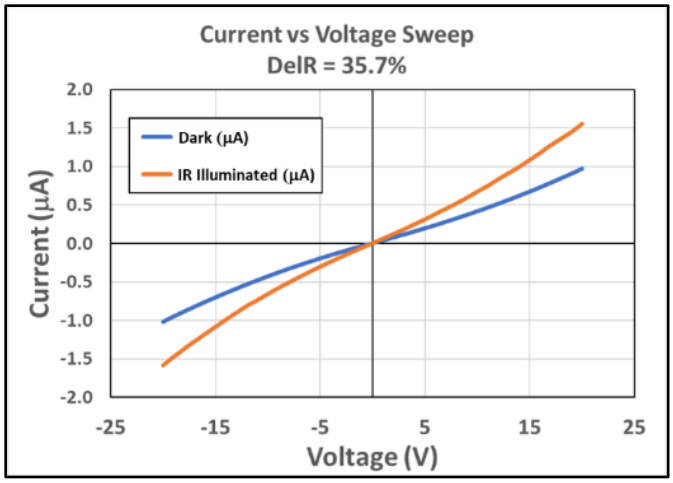

Figure 57: Current vs. Voltage of the highest measured DelR value of 35.7% illuminated at 18 mW at 4.5 µm (+/- 500 nm) wavelength.

The Responsivity and Quantum Efficiency versus wavelength were measured on a comb device design as shown in Figure 58 (left). These results are shown in Figure 59 and measured using the Process Evaluation Chip system (PEC) with a Black Body illumination source, a series of optical filters, and a Keithley 2601B source meter.

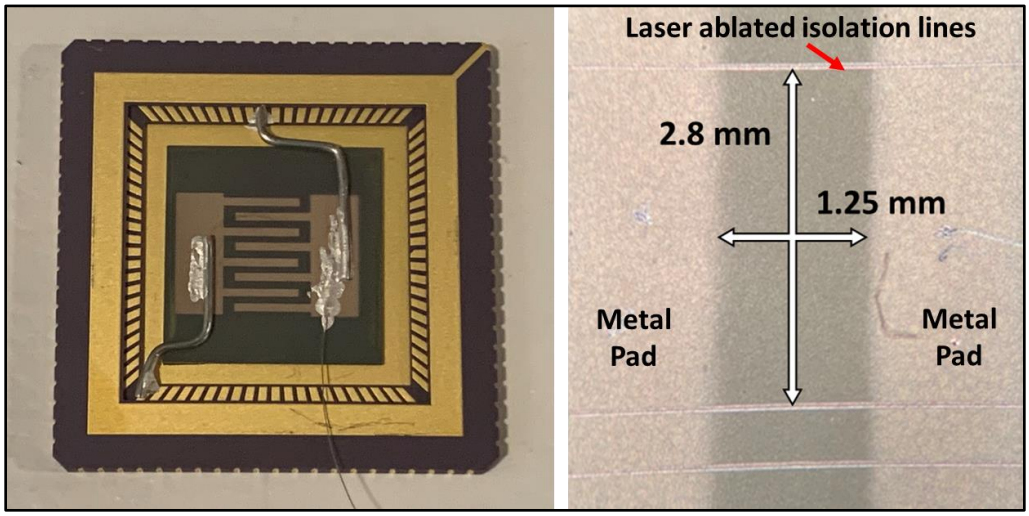

Figure 58: Optical image of the comb design photodetector packaged in an LCC08423 purchased from Spectrum Semiconductor Materials (left) and the small parallel pad device (right). The active area of the larger comb device is 0.5 cm^2 and the smaller parallel contact pad device has an active area of 3.5 mm^2.

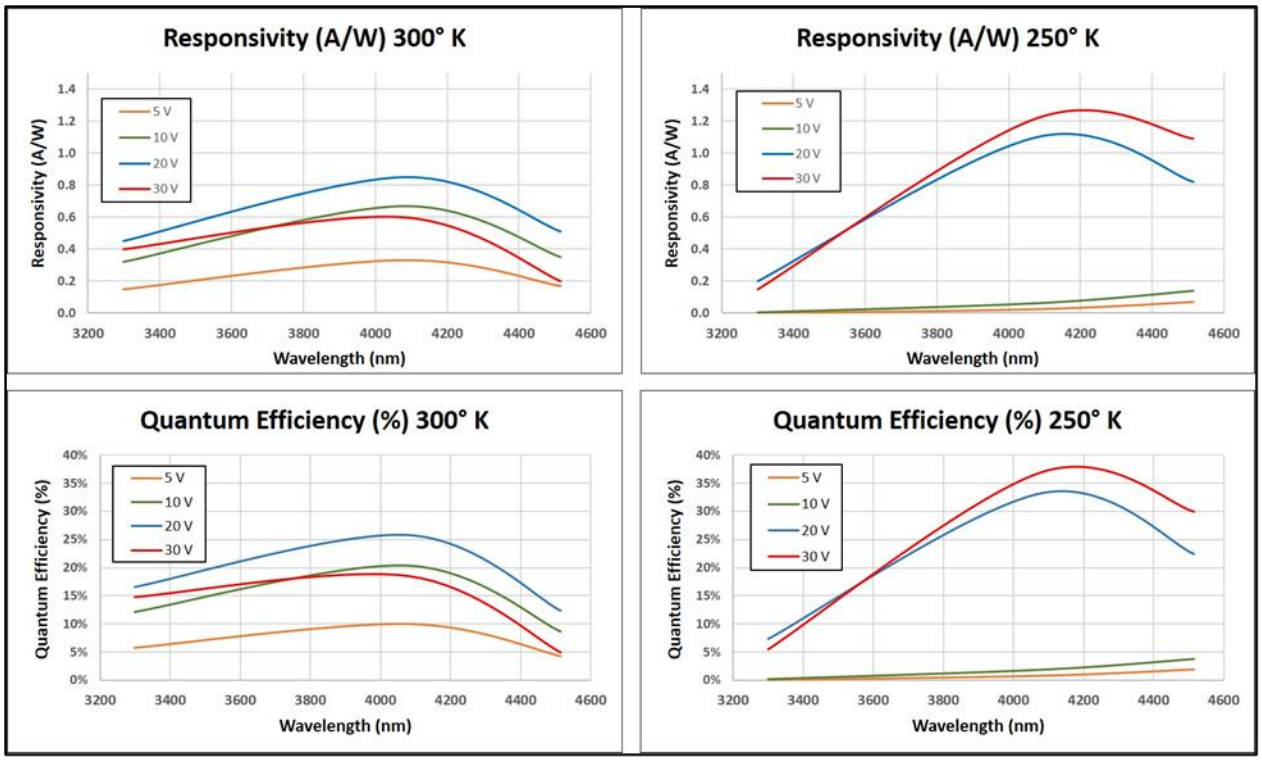

Figure 59: The measured Responsivity (R) and Quantum Efficiency (QE) of the LSD fabricated PbSe thin films. The different curves are for different bias conditions on the device under test (DUT). The responsivity at room temp (300° C) and cooled (250° C) are shown (top) and the respective quantum efficiency are shown as well (bottom). A maximum responsivity of 0.84 A/W and QE of 25.6% was measured at 300° K when biased at 20 volts.

The Responsivity versus wavelength at 300° K is proportional to bias voltage until a threshold of 30 volts is tested. It is not clear why the 30-volt bias shows a degradation of the Responsivity and Quantum Efficiency, but it is believed to be the result of localized heating of the active area. The Responsivity and Quantum Efficiency are proportional as shown in equation 18, therefore the curves are shown in Figure 59 responsivity (top) and quantum efficiency (bottom) follow similar trends. Measurements for both were collected at room temperature (300° K) and cooled to 250° K. As evident, both measurements show a dependence on voltage bias, and below 10 volts and above 20 volts, at room temperature, reveal a voltage bias window for maximum photoresponse and quantum efficiency. This agrees with the literature as many commercially available PbSe detectors are tested with a bias of 15 – 20 volts. The responsivity range observed of between 0.34 to 0.84 A/W is comparable to that seen by other researchers working on a novel method of forming PbSe thin films. Many research groups report their responsivity data in arbitrary units or report responsivity of markedly different size detectors, making it hard to compare; however, Yang et al. reported a similarly scaled PbSe detector (1 cm^2) with typical values for responsivity of between 0.32 to 0.81 A/W.[57]

The detectivity (D*) and noise equivalent power (NEP) were then tested on a small 1.25 mm x 2.8 mm active area parallel plate device as shown in Figure 58 (right). The results are shown in Figure 60 below. A peak D* of 1.01 x 10^9 ($cm \cdot Hz^{1/2}/W$) at 800 Hz was obtained. The signal-to-noise ratio (SNR) and NEP are shown, as well the temperature dependence observed on the detectivity in figure 60. A diagram showing the performance of many commercial photodetectors is shown in Figure 61. The D* achieved in this work is not far from that of many fabricators of PbSe photodetectors.

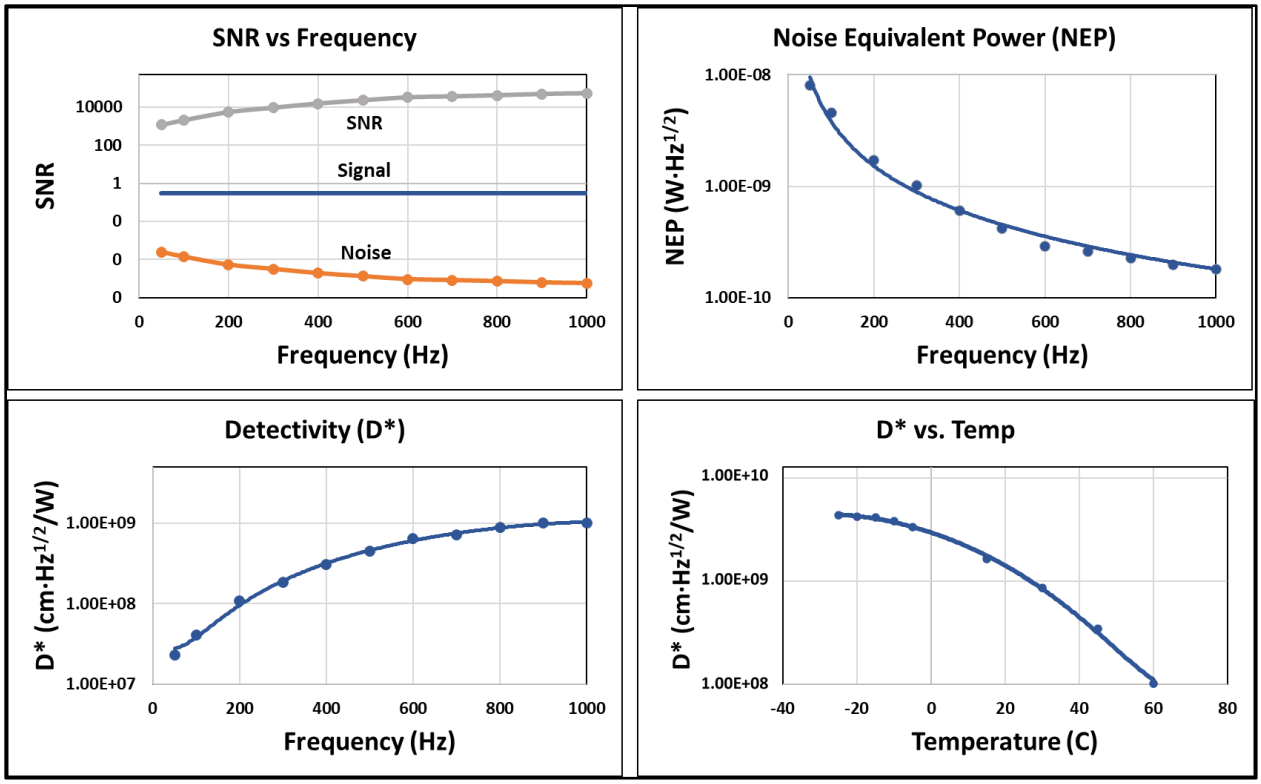

Figure 60: Figures of merit for small area device (SNR, Noise Equivalent Power, Detectivity vs. Frequency, and Detectivity vs. Temperature). A maximum D* value of 1.01 x 10^9 cm·$Hz^{1/2}$/W was achieved at room temperature. Also, shown are the signal-to-noise ratio (SNR), noise equivalent power (NEP), and D* versus temperature (upper left). The trends are all related to the 1/f noise response that is inherent to all electronics and this type of photodetector.

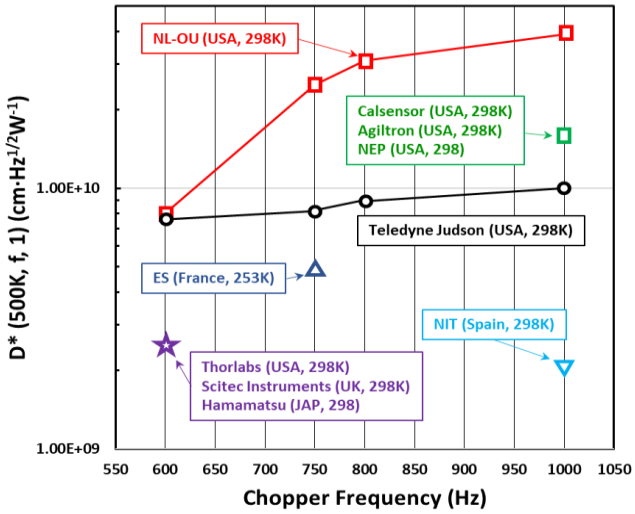

Figure 61: Diagram of room temperature D* performance for various commercial PbSe detector manufacturers. Our LSD fabricated prototype device D* value of 1.01 x 10^9 (cm·$Hz^{1/2}W^{-1}$) performance is shown in the red dot. This chart shows the large variations in performance across the commercial fabrication of PbSe photodetectors. This primary source of variation is related to the intended application, device size, and expense.[64]

Separate testing was performed on the comb structure to measure rise and fall times in response to the 2.7 μm modulated light source. The waveform is shown in Figure 62 and the rise and fall times are recorded as 360 μs and 440 μs, respectively.

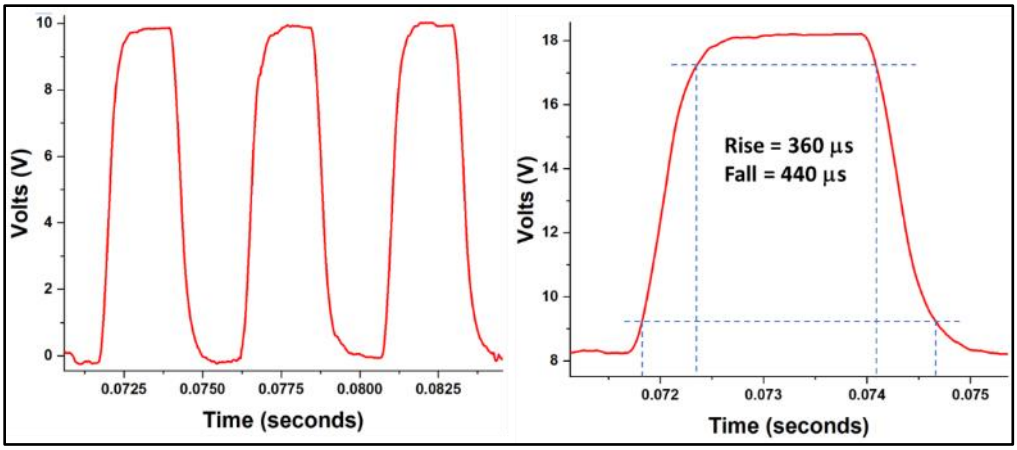

Figure 62: Example of timing (rise and fall times) of this PbSe detector showing a rise time of 360 µs and fall time of 440 µs.

8.3 Conclusion

This work shows that a laser fabricated PbSe photodetector device can be achieved. The performance of the laser fabricated PbSe-based photodetector has a comparable DelR response to other reported CBD films.[12,33,34] The detectivity (D*) of a 1.25 mm x 2.8 mm detector was measured to be 1.01 x 10^9 (cm·$Hz^{1/2}$/W) and is nearly the performance of some commercial devices of similar dimensions. While the Laser Sinter Deposition process is in its infancy, this shows a promising opportunity for continued research into PbSe and other thin film device fabrication. LSD is far from being mature enough for production device fabrication, the LSD process shows great promise as a tool for (1) experimentation with ultra-rapid annealing, (2) in-situ activation of dopants into thin films, and (3) spatially tailorable morphological control that is not achievable using traditional methods. The timing characteristics concerning rise and fall times are 360 µs and 440 µs, respectively. This will potentially allow a frame rate of 1 kHz.

It should be noted that the responsivity of LSD fabricated photodetectors is directly related to its thin film electrical characteristics; however, the D* and NEP are not as predictable and suffer from high variability in the film properties. Sample-to-sample variation ranged from as low as 3.0 x 10^6 (cm·$Hz^{1/2}$/W) to the maximum of 1.01 x 10^9 (cm·$Hz^{1/2}$/W). The source of the variation is believed to be localized variations in the microstructure and chemistry.

NOTE: A permanent reduction in the photoresponse of all samples exposed to the high-vacuum PEC system was noted after extended time in vacuum conditions of ~1 x 10^{-5} Torr. The dark current increased and the responsivity reduced by ~30%. This could be explained by iodine loss under high vacuum conditions. SEM-EDS did not show any measurable difference in atomic percent (Figure 63).

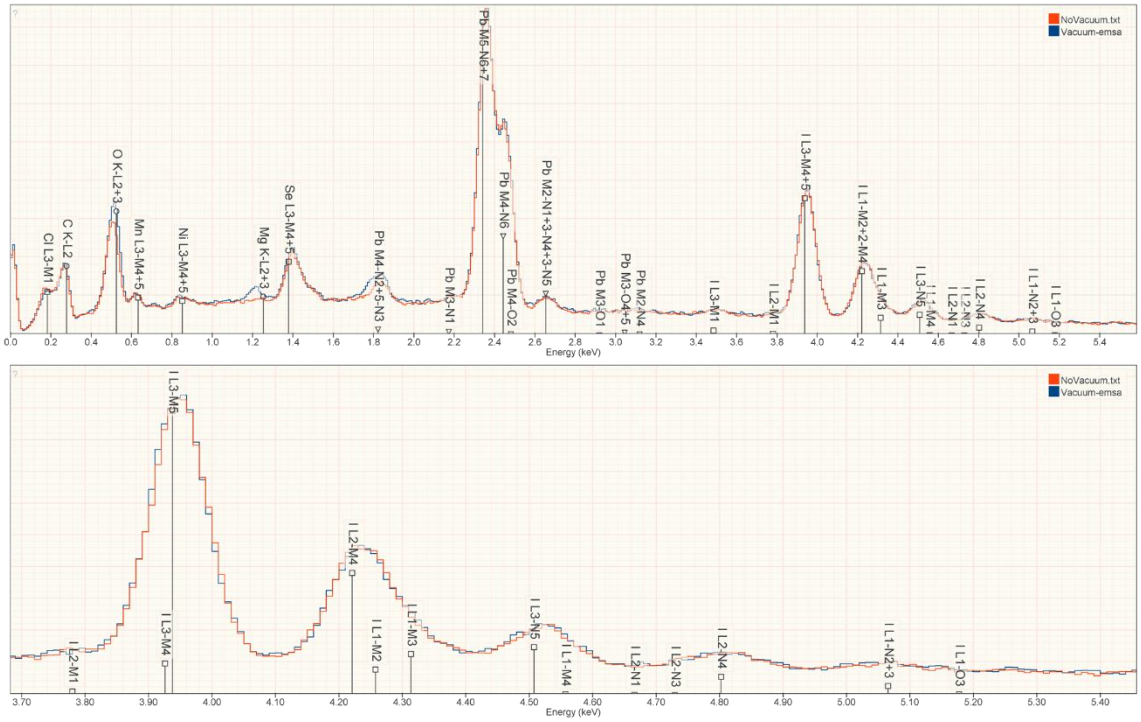

Figure 63: SEM-EDS spectra of a sample before and after extended exposure to high vacuum (1 x 10^{-6} Torr). No difference is seen in the iodine concentration

CHAPTER 9: Laser Patterned PbSe Focal Plane Arrays (FPA) Design, Fabrication, and Evaluation

9.1 Introduction

9.1.1 History of Focal Plane Array Fabrication

For decades infrared (IR) imaging devices are designed and fabricated as an array of photosensitive cells, also called pixels. These are referred to as focal plane arrays (FPA). FPA can be designed to be sensitive to a specific wavelength or range of wavelengths from ultraviolet (UV) to visible to infrared (IR). The wavelength of sensitivity is determined by the properties (bandgap) of the material(s) chosen. The concept of an FPA is simple in concept; an array of light-sensitive devices are fabricated and patterned on a substrate. Each cell (pixel) of the device has contacts for external sensing of an electrical response (usually a change in conductivity) driven by a photoresponse when illuminated with the wavelength of interest under external voltage bias conditions.

For fully integrated FPA that are assembled into camera systems, this is most often done with a second integrated chip for external connections (solder bumped, flip-chip, or stacked die). Camera systems for PbSe detectors require separate silicon-based complementary metal-oxide-semiconductor (CMOS) integrated chips (IC) along with optical lenses to ultimately be integrated into a complete imaging system. The stacked die design shown in Figure 64 is necessary for some FPA such as PbSe-based IR cameras because the CMOS process is incompatible with the PbSe process flow for depositing the thin film (chemical bath deposition). A hybrid process to make CMOS and PbSe-based FPA is a highly active area of research. Both the integration of the multi-chip, CMOS-based ROIC, as well as the hybrid CMOS-PbSe process is outside the scope of this work. This work focuses solely on the fabrication of the PbSe cells for the focal plane array using the previously described methods of fabrication of PbSe-based thin films and patterned into FPA using laser processing, without photolithography.

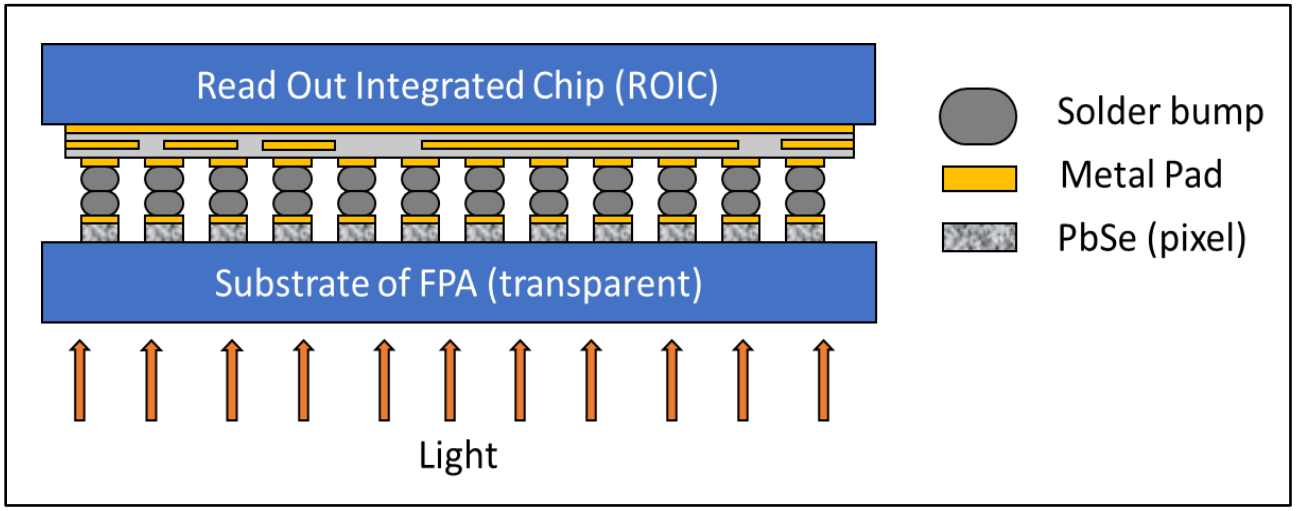

Figure 64: Schematic of a focal plane array (FPA) integrated with a read-out integrated circuit (ROIC) chip. Due to the incompatibility between the PbSe-FPA processing and the ROIC chip, these require a multi-chip stacked die design. The substrate beneath the PbSe FPA must be either optically transparent to the wavelength of light or polished away to expose the photocells to the illuminated light for photodetection.

The goal of this work is two-fold, (1) to introduce the new *flexible* and *tailorable* Laser Sinter Deposition (LSD) process and (2) to provide a solution for rapid and simple fabrication of *customized* PbSe-based MWIR focal plane array using only lasers to eliminate photolithography. This is achieved by using laser patterning to eliminate the need for the costly and time-consuming process of photolithography, currently necessary to make PbSe-based FPA. One of the drawbacks of

photolithography is the high equipment costs and materials investment in the design, fabrication, and revision process. Currently, photolithography requires photomasks that can be expensive, take time to fabricate, and require great care for maintenance and cleaning. Photolithography equipment is expensive and requires many separate pieces of equipment (spin coater, photolithography system, developer, chemical strip). Photolithography patterning usually requires entire wafers or batches of wafers to be patterned with the same design. This is only cost-effective for high volume commodity microelectronics chip fabrication due to economy of scale but is not cost-effective for lower volume production, particularly when custom designs are of interest.

Additionally, photolithography requires the deposition of photoresist and other sacrificial layers that are later chemically etched. These films and chemical processing contaminate the PbSe film and degrade the performance of the detectors.

9.1.2 Laser Patterning of Focal Plane Array

With laser patterning, the time between design and the final product is as fast as you can redraw or rescale your FPA drawing with software. The laser patterning takes only a few seconds per chip, depending on the design complexity. Last but not least, different designs can be fabricated adjacent to one another on the same wafer. Even device size (chip area cm^2) can be varied across the wafer. We have already shown that even the die-cutting (wafer wet-saw) can be integrated into the laser process to eliminate the wet saw process, eliminating additional process steps and the need for additional equipment.

A simple proof-of-concept prototype of FPA is fabricated in this work using laser processing to show the preliminary capabilities, as well as identify the limitations of laser patterning of FPA. Finally, the operation of a low-resolution (10 x 12 array of 150 μm square pixels) FPA prototype is demonstrated.

We show how laser pattering custom FPA without photolithography has the potential to enable a broader insertion into commercial and consumer products and inevitably improves the demand and technological advancement. This will also enable the ability for low volume, customized FPA, and fabrication of rapid prototype designs. While this work focuses on PbSe and MWIR FPA, this is applicable for other materials sets (HgCdTe, SiGeSn, or InSn), as well as beyond MWIR FPA applications.

9.2 Background

The types of FPA range from one-dimensional (1D) low resolution (linear) IR imagers to two-dimensional (2D) high-resolution IR cameras. All types are designed for use in quality and process control systems, IR spectroscopy, gas monitoring, imaging, thermography, and a multitude of military applications (e.g. muzzle flash sensors and missile seekers). The 1D linear imagers vary from an array of 40 μm x 40 μm square pixels to as large as 40 μm x 4,500 μm rectangular pixels in a 1 x 256 pixel array (Infrared Materials, inc.).

Similar to commercially available visible-light cameras, but designed for MWIR wavelengths, two dimensional (2D) MWIR cameras are fabricated across a large spectrum of pixel and array sizes, from as simple as 2 x 2 (with 2 mm x 2 mm pixels) to 80 x 80 (130 μm^2 pixels).[58] Due to the current PbSe deposition methods and material set, PbSe-based FPA suffers from incompatibility between the Si-CMOS fabrication process flow and the photodetector fabrication thin film deposition process. This has led to a lot of research into integrating or hybridizing the two fabrication types. It should be noted, that there are other higher performance MWIR FPA commercially available; however, they are not PbSe-based and outside the scope of this work. They are also extremely high in cost and complexity, comprised of multiple stacked material sets, and marketed for very small specialized and specific applications. A review article on these technologies is available as a reference.[4,59]

While visible light FPA (aka cameras) have enjoyed rapid technological advancements in the last 30+ years and have achieved a pixel density of tens of millions of megapixels, IR cameras do not yet have this demand, but the demand is growing rapidly thanks to automation. Visible light FPA are relatively low-cost and integrated into nearly everything in the commercial and consumer products markets, this is

driven by extremely high demand, the vast number of applications, and the compatibility of visible sensing materials with traditional silicon-based fabrication. These commercial FPA cameras have expanded to near-infrared (NIR) but cannot expand further into the mid-infrared regime. Unfortunately, a different material-set is required to detect wavelength deeper into the NIR and mid-wave infrared (MWIR) regime of 3 – 5 μm. MWIR detectors require materials such as lead selenide (PbSe) with an optical bandgap of ~0.28 eV, coinciding with a wavelength of ~4.2 μm. PbSe also allows tuning the bandgap (described previously) allowing it to be tailored from 4.5 μm down to near-infrared and below. This means it has the potential of bridging the gap between silicon (1.1 μm) and intrinsic PbSe (4.2 – 5.0 μm). This aligns perfectly with spanning the MWIR wavelengths; however, integrating PbSe thin films with Si-based CMOS technologies is a challenge. As mentioned above, PbSe focal plane array camera systems usually require interfacing separately with a read-out integrated circuit (ROIC). The integration costs and complexity of stacking and packaging multi-stacked chips are compounded with lower volume demand applications. This keeps new products and applications from expanding. High cost and low volume demand in commercial applications have delayed major technological advances in MWIR sensors.

The current cost of a simple one-dimensional linear array provided by Infrared Materials, Inc, is $6,100/unit. This price nearly doubles to include a read-out system for connecting for operation. Additionally, this company has only two options for cell size (40 μm x 40 μm and 40 μm x 4,050 μm pixels in a 256 x 1 array). The primary goal of this work is to introduce the flexibility and tailorability of the Laser Sinter Deposition (LSD) process, but also to provide a solution for fabricating custom PbSe-based MWIR focal plane array using laser patterning to eliminate photolithography and enable low-cost custom IR FPA. Figure 65 shows the progress of FPA technology in the assembly of FPA systems across all FPA types. The progress of integration technology and options for FPA systems is an indication of the rise in demand.

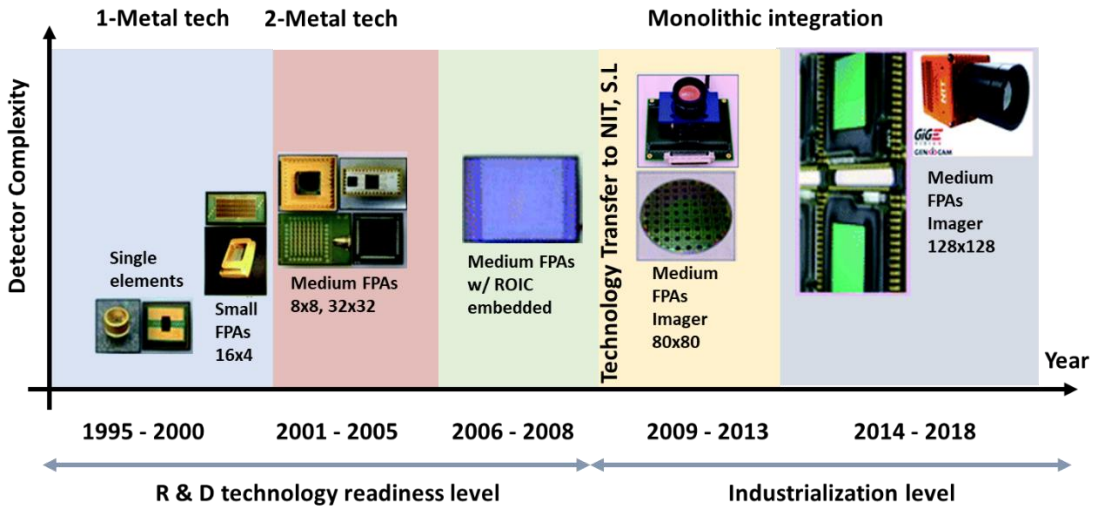

Figure 65: Timeline of commercially available PFA system integration and package designs as well as scaling. This is an indication that FPA demand and newer applications are advancing rapidly.[63]

9.2.1 Photolithography for Focal Plane Array Patterning

The traditional photolithography process for PbSe-based FPA primarily uses one of two methods both described in the liftoff method. Figure 66 shows a diagram of the two photolithography liftoff processes. Both require multiple steps of depositing resist on the substrate prior to the deposition of PbSe. They both expose the film to chemical contamination and both rely on a tapered side-wall profile of the photoresist to allow the chemical lift-off process to work. The two types are positive photoresist and negative

photoresist, which both use photomasks and differ only in how the light cures the photoresists. The two methods still require photomasks, photoresist, expensive photolithography equipment, and chemical to liftoff (undercut) the PbSe to form a pattern. The photoresist has to be compatible with the CBD or PVD process for subsequent PbSe deposition and rely on a very specific photoresist sidewall profile as well as a poorly conforming PbSe deposition process. The exposure of the sidewalls of the photoresist is critically necessary for the liftoff process to be successful; however, avoiding the contamination effects of the chemical resist strip step is the primary reason for using laser patterning.

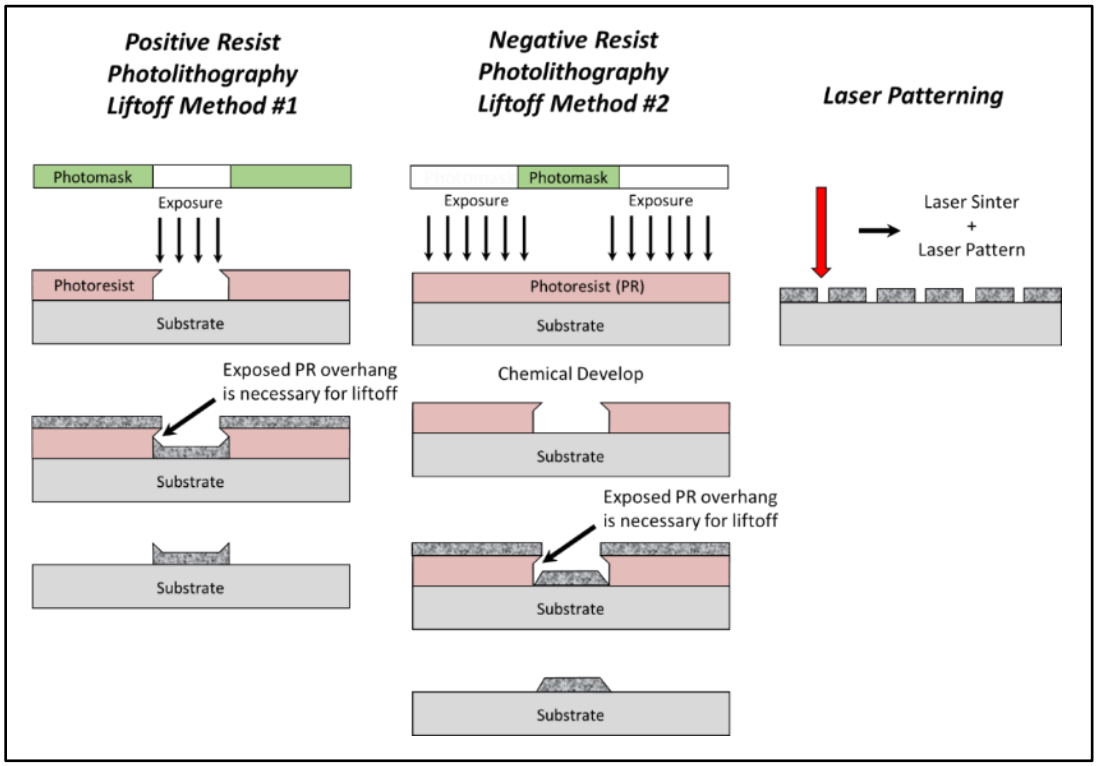

Figure 66: Schematic of two types of photolithography called liftoff. Positive resist (left) and negative resist (middle). Both require multiple steps that occur prior to the deposition of the PbSe (gray patterned material) and rely on the exposure of a sidewall of photoresist to allow the chemical lift to properly occur. Laser patterning (right) does not require any chemical processing to pattern and thus no chemical contamination. Even the deposition of the PbSe film itself is done without chemical exposure.

9.3 Fabrication Method for Focal Plane Array (FPA)

There is a significant amount of commercial and military interest in simple, low costs FPA fabrication methods. The following fabricated FPA prototype is meant to be a proof of concept to show the potential of laser patterning. The potential of scaling FPA array dimensions (pixel count, pixel size, and pitch) with laser patterning is evaluated but will be limited to the capabilities of the laser system that is available in our laboratory. The laser chosen for this work is a 355 nm wavelength (UV), diode-pumped solid-state (DPSS) short-pulse (25 ns) laser (Coherent MATRIX) and controlled by a galvo (Sino sg7210) using EZCAD software for pattern design and laser parameter controls.

There are three approaches to the fabrication of this focal plane array, as shown in Figure 67. The ***first*** is to use MWIR sensitized thin films of PbSe and show that laser patterning can be used to rapidly fabricate an array of individual, electrically isolated PbSe pixels without any need for photolithography. As described above, photolithography is both time-consuming and costly but also degrades the film with chemical reactions with photoresists and other chemicals. The ***second*** approach is more ambitious. The same PbSe thin film will be subsequently sputter-coated with a ~75-100 nm thick gold (Au) layer. In Chapter 7, we reported preliminary results of the selective laser patterning of surface metal coated on *unsensitized* PbSe. Here, we report the results of performing this selective metal patterning of Au on a

fully-sensitized PbSe film. This second approach is performed on sensitized PbSe to determine if the same film selectivity can be achieved. The ***third*** approach is to evaluate the ability of the fully sensitized PbSe and gold metal stack patterned for a vertical device, as described in Figure 68. This approach will be applicable for the through-substrate illumination configuration where one metal contact is on the top of the cell and the second contact is the conductive substrate (Figure 68 right).

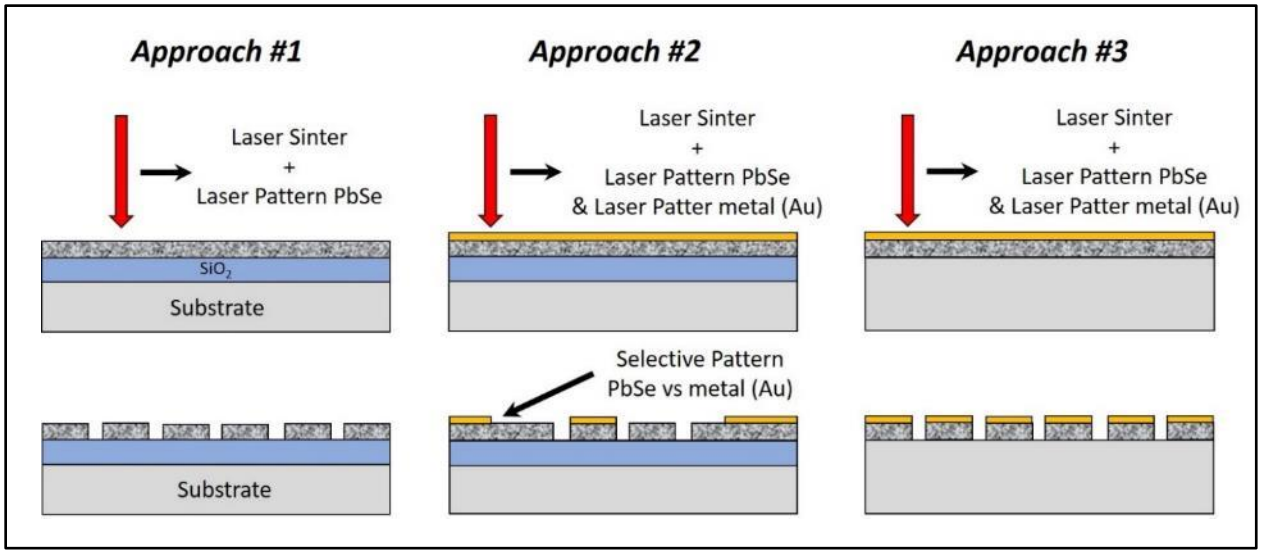

Figure 67: The three experimental approaches for laser patterning PbSe for focal plane array (FPA). Approach #1 is to simply pattern the PbSe using the 355 nm UV laser. Approach #2 is to deposit the PbSe and a thin layer of gold conductor and then patterns of the full stack followed by selectively patterning the gold. Approach #3 is to pattern a full stack of PbSe and gold for the application of fabricating a vertical pixel device described previously. One contact is on the surface of each cell and all the cells in the array share contact with the substrate (no SiO_2). The first two approaches are specifically for patterning an array of pixel cells with two contacts accessible from the surface (lateral device).

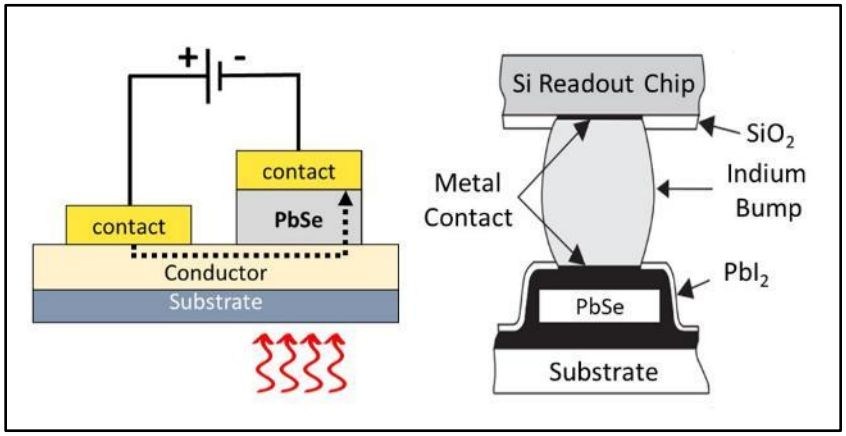

Figure 68: Approach 3 of laser patterning PbSe focal plane array (vertical device). There is also two contact devices; however, they are vertically oriented so a flip-chip (solder bumped) ROIC chip can be mounted directly on top and the silicon substrate is a shared ground contact for all photoconductive cells (pixels) in the array. One contact is on the top of each pixel and the second contact is direct to the substrate.

9.4 Fabrication Results

9.4.1 Patterning and Fabrication of PbSe Pixel Array (Approach #1):

The first approach is to simply laser-pattern the PbSe without damaging the SiO_2 of the substrate. This was accomplished to form small two-dimensional arrays of pixels. Figure 69 shows an example of a

simple array of 8 x 16 pixels, each with fanout trace patterning to allow probing from the periphery. These cells were sizable enough to easily probe individually.

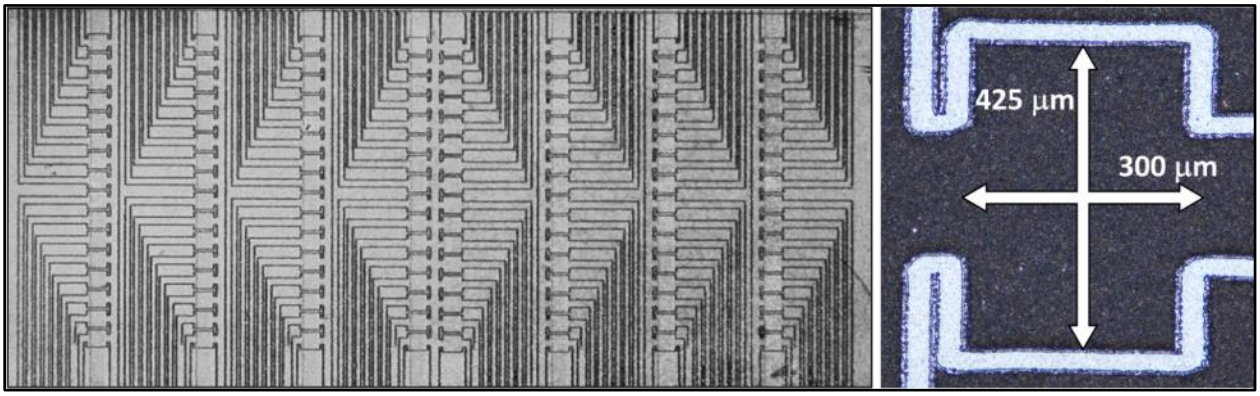

Figure 69: First attempt to pattern an array of cells. The routing lines were intended for allowing peripheral access for probing without impeding the illumination from the top. This shows 8 columns of 16 cells of 425 μm x 300 μm PbSe photocells (pixels). The eight columns are oriented vertically in the left image. The right image is an individual pixel device with dimensions.

9.4.2 Selectively Patterned FPA of a PbSe and Gold Metal Stack (Approach #2)

This approach was initially performed on unsensitized PbSe, and the results show extremely good selectivity between the PbSe and the thin sputtered gold (75 - 100 nm). While the process has two steps, they are performed back-to-back on the same system without any need for realignment or venting of the chamber, which is purged with argon and vacuum exhausted. This approach begins with a fully sensitized PbSe thin film which consists of (bottom-up): 400 nm of PbSe, 300 nm of a transition layer composed of $Pb_xSe_{(1-x)}O_yI_{(1-y)}$ compounds including $Pb_3Se_2O_6I_2$ and a top layer of ~100 - 200 nm of PbI_2. The melting point of PbSe is 1078° C, and the melting point of gold (Au) is 1064° C, therefore there is little margin for laser ablation selectivity. Fortunately, the absorbance in gold spikes at 355 nm, as seen in Figure 70. Again, we have already reported success in previous work in completely removing the gold without any significant removal or melting of the underlying PbSe (Section 8.2). Selectively ablating a fully *sensitized* PbSe thin film stack, as described here, presents a considerably larger challenge. The melting point of gold is only 14° C below PbSe, allowing a small margin for selective ablating with the pulsed UV laser. Unfortunately, the melting point of PbI_2 is only ~402° C, which is 662° C below the melting point of gold and the presence of lead selenite ($PbSeO_3$) which is also present in the transition layer between PbI_2 and PbSe has a melting point of only 500° C. Figure 71 shows a schematic of the previous success in selectively removing gold (Au) without disturbing the underlying PbSe (left) and the goal of approach #2 to repeat with a sensitized film (right).

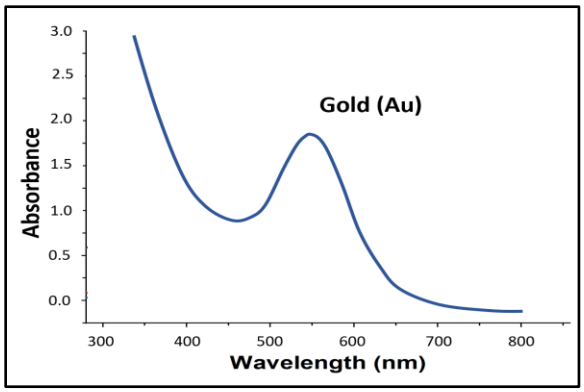

Figure 70: Absorbance of thin layers of gold and gold alloys. A peak occurs at the 355 nm wavelength which is the wavelength being used to selectively ablate the gold layer.

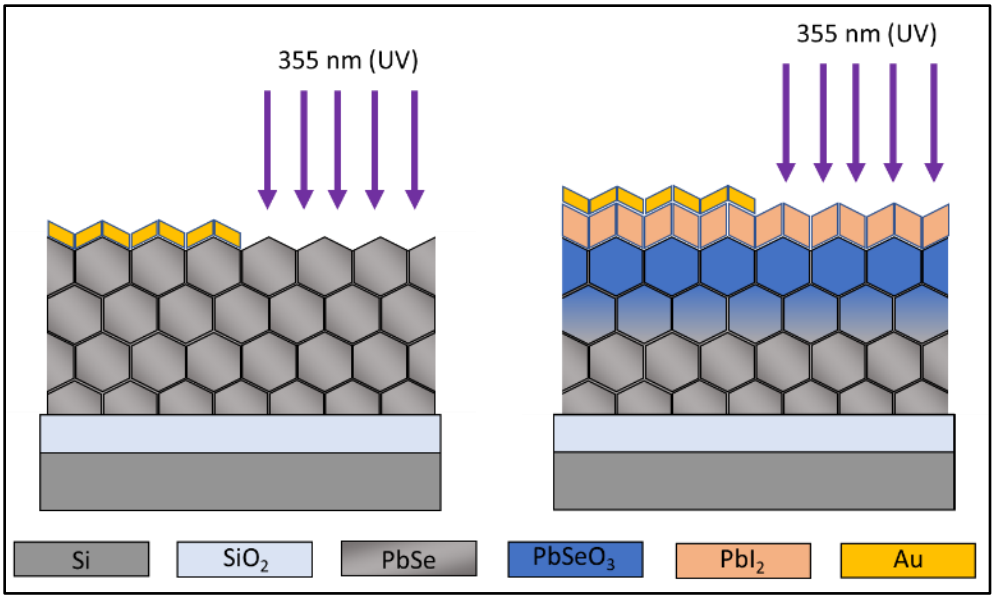

Figure 71: Schematic showing the goal of Approach #2. Selectively removing the gold (Au) was successful on the (pure) as-deposited PbSe (left). The goal now is to show the selectivity of gold (Au) to a fully sensitized film stack of PbI_2 and $PbSeO_3$ (right).

Despite these properties and the uncertainty of whether the sensitized film can afford to lose some amount of the PbI_2 surface layer, an attempt was made. Figure 72 shows the results of approach #2. The first step of removing both the sensitized PbSe and the Au was easily achieved. The second step of selectively removing the Au without degrading the photoresponse was unclear until we tested the DelR photoresponse and compared it to before and after values.

It was immediately clear upon optical inspection of the areas where the Au layer was removed, that the sensitized PbSe film had changed. The surface of the sensitized film is visibly matte gray with hints of yellow from the thin layer of PbI_2. The surface below the ablated areas (pixels) was not the color expected of sensitized PbSe as seen in Figure 72 (bottom). Exposure of the underlying PbSe (bright gray) and $PbSeO_3$ (vibrant blue) was evident in Figure 73 (right). Regardless of the laser parameters used, the Au removal using the 355 nm UV laser was removing the PbI_2 surface layer and degrading the photoresponse.

Measurements of the DelR photoresponse of each cell were 26% before the laser patterning and selective Au removal. After the Au was removed, samples exhibited only 12% DelR (~54% reduction in photoresponse). Regardless of the thickness of gold or laser power, pulse width, or scan speed, this approach is detrimental to the performance of the device. This proves the role of the PbI_2 layer is more than a passivation layer.

Using an insulative layer between the Au and PbI_2 for added margin could allow for a more selective metal patterning; however, this would require a contact open laser process to allow connectivity between metal and PbSe through the insulator. Secondly, the use of a lower melting point metal layer is a possibility and should be considered in future evaluations. Lead (T_m = 327° C), SnPb (T_m = 182° C) and Zinc (T_m = 460° C). Transparent conductive oxides (TCOs) are another option to consider. Figure 74 shows a schematic of the results of the full stack patterning and the selective gold removal from pure PbSe (left) versus the selective removal of gold on a sensitized PbSe film (right) without degrading the photoresponse. Another solution could be pursued in future work by using a picosecond pulse width laser where heat conduction beneath the layer will be minimal.

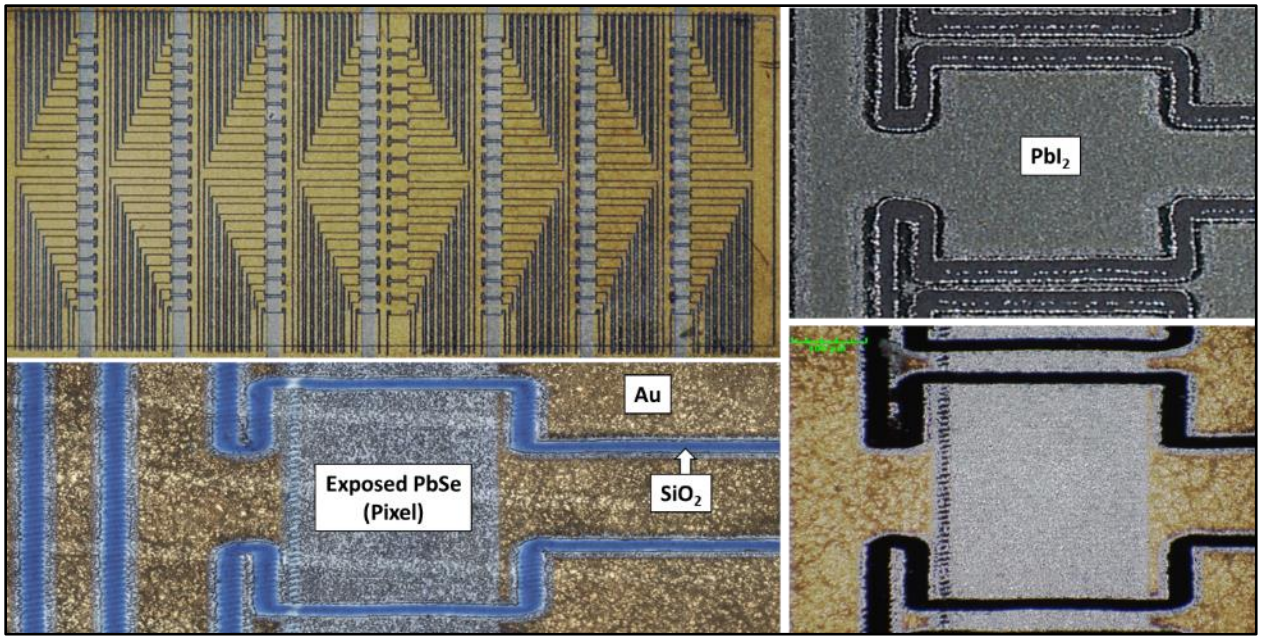

Figure 72: Optical image of the laser patterned FPA for approach #2. This is a fully sensitized PbSe thin film with a 100 nm metal (Au) coating layer. The first laser patterning of the full stack was successful (shown as bold black or blue lines). The second selective laser patterning for removing the Au to expose the individual FPA cells was very successful; however, the PbI_2 was also removed and negatively impact the photoresponse of the exposed PbSe pixel (bottom two images). NOTE: The purpose of the long metal traces is to allow for easy peripheral probing of each cell for topdown IR illumination and testing. This was not necessary for future design due to the back illumination method used from this point on.

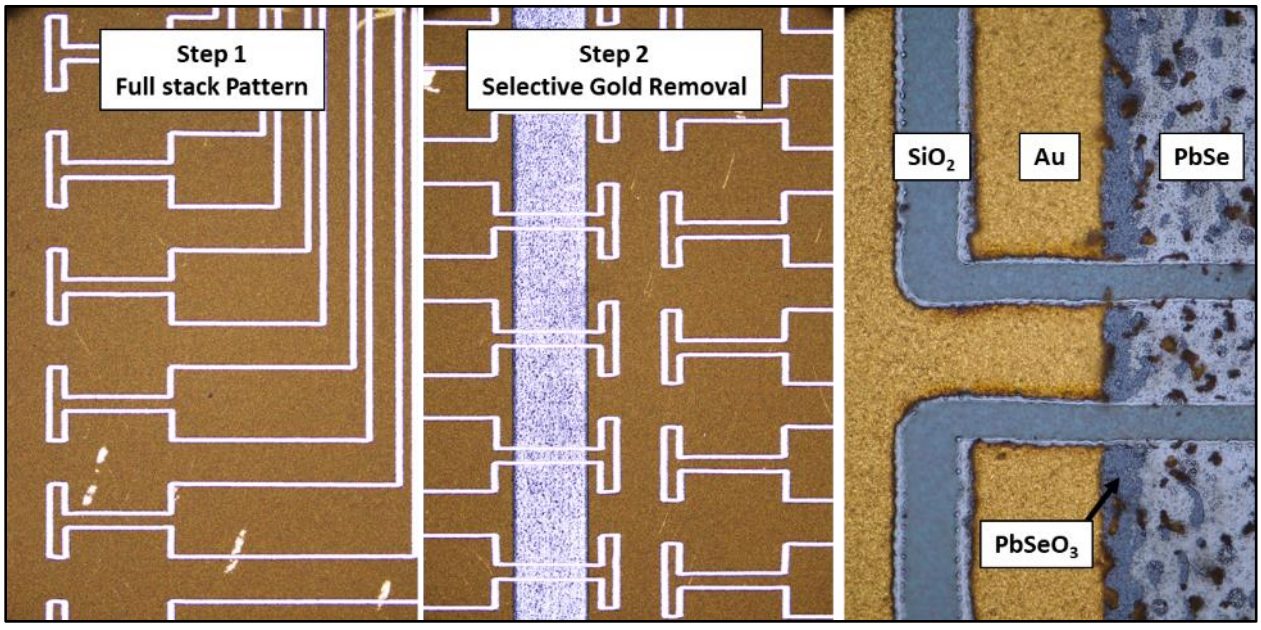

Figure 73: Optical image showing the full stack patterning (left), the selective metal removal (middle), and a closeup of the different areas exposed to laser (right). Notice the blue edge along the PbSe to Au which is the color of the $PbSeO_3$.

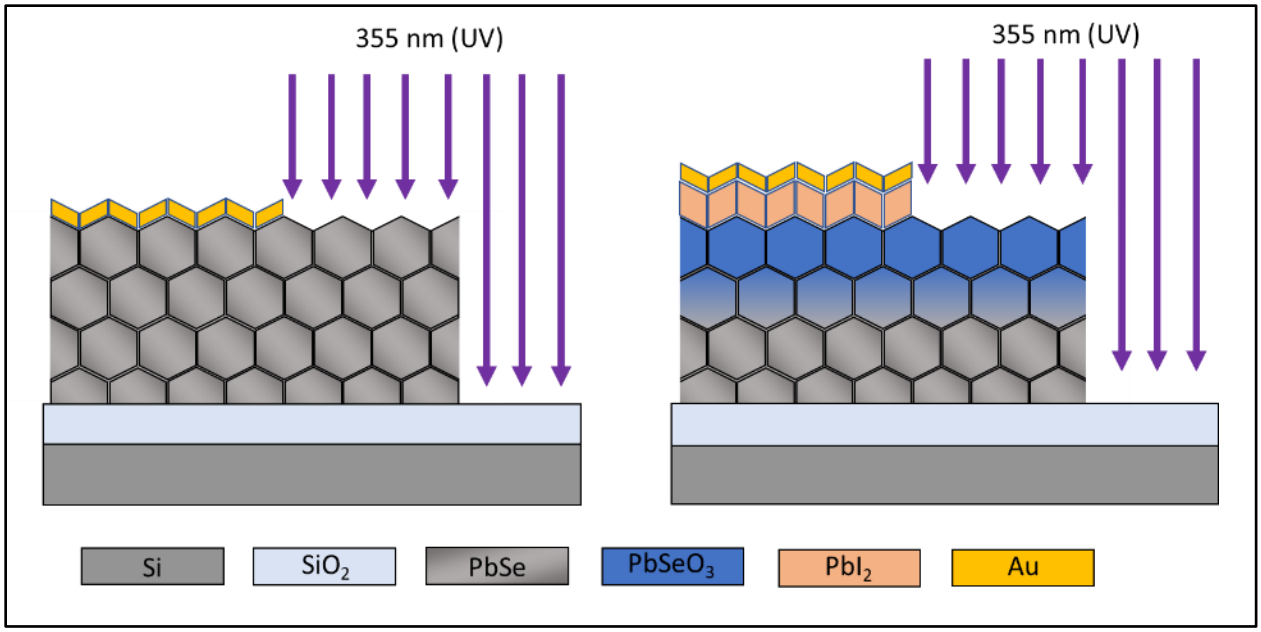

Figure 74: Schematic of the results of approach #2. The full stack was successfully patterned to expose the SiO_2 in both cases; however, the selectivity of the 355 nm laser was unable to ablate the gold layer without removing the PbI_2, exposing the underlying layers of $Pb_3Se_2O_6I_2$, $PbSeO_3$, and PbSe (right).

9.4.3 Pattern Array of a PbSe and Gold Metal Stack for Vertical Device Cells (Approach #3)

This process is achieved successfully by sensitizing a PbSe thin film and depositing a 100 nm coating of gold (Au). This approach will only be done as a proof of concept as the substrates are coated with 2 µm of SiO_2 and cannot act as a 2nd contact. For this approach, we will only report the ability to pattern the array and the minimum feature size cell achieved with the 355 nm UV laser. Figure 75 (left) shows the minimum size pixel achievable without significant degradation of the shape and top coating of metal. In this case, these were coated with gold-palladium (AuPd) due to the gold (Au) sputter target needed replacing. The minimum feature size achieved with the UV laser (minimum spot size of ~36 µm) was a 60 x70 µm pixel size with a 100 µm pitch. This would potentially allow an FPA with a pixel count of 37 x 68 cells array (2516-pixel FPA) on our standard 1 cm x 2 cm substrate. Figure 75 (right) shows the degradation that begins to occur when further scaling continues.

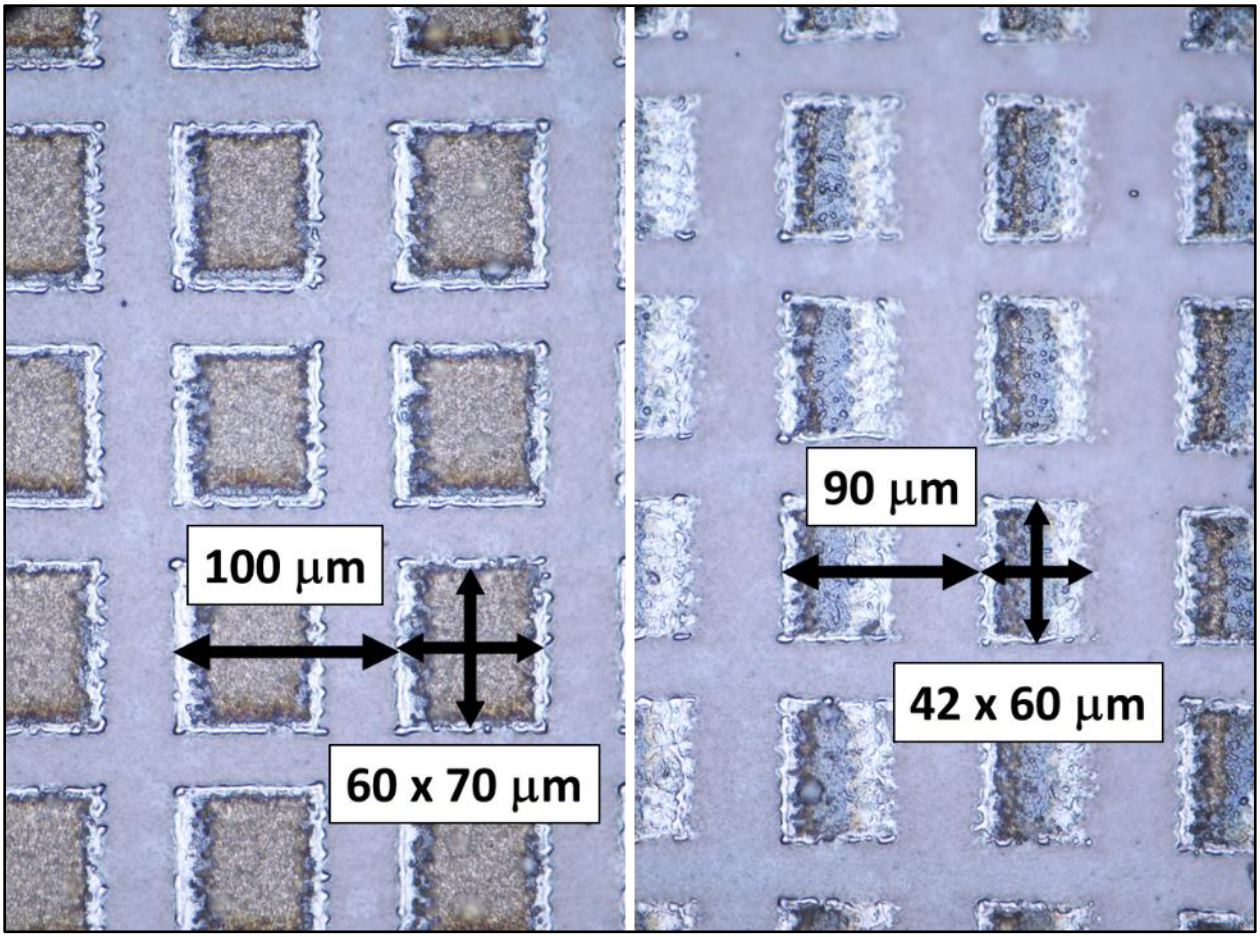

Figure 75: Optical images and measurements of minimum feature size and cell pitch for laser pattern PFA cells. The smallest cell achieved was a 60 x 70 μm cell with a 100 μm pitch (left). Anything smaller resulted in film degradation and cell malformation (right).

Upon discovery that backside illumination was very effective for electrically testing the individual FPA cells from the topside, a more traditional two-dimensional array of lateral photocells was patterned and tested. Figure 76 shows an example of a small section of cells patterned at 240 μm x 260 μm cells.

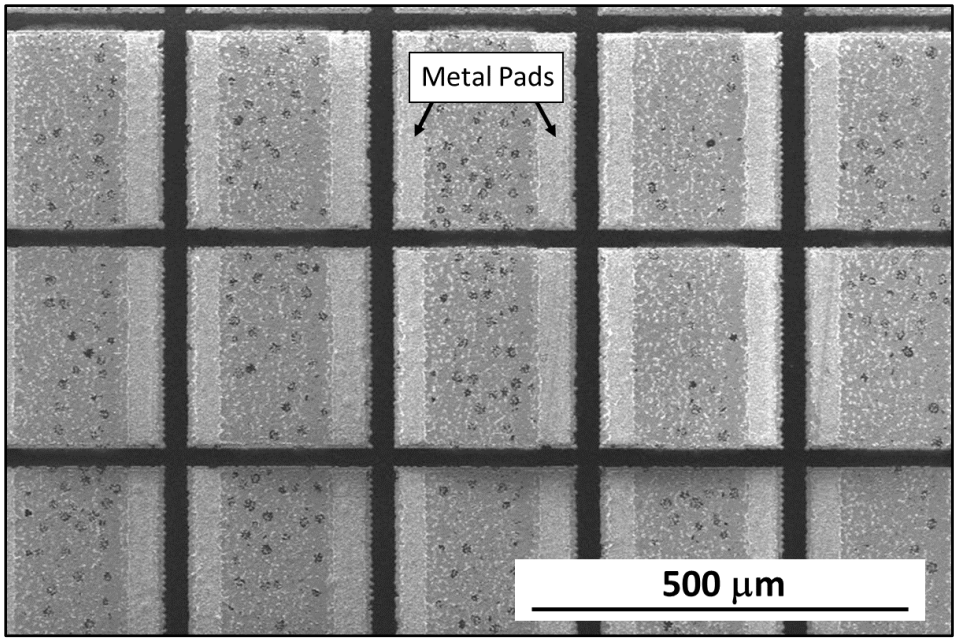

Figure 76: SEM image of an array of patterned cells using the two-step method of patterning the PbSe and Au stack followed by selective removal of the Au layer. The contacts are evident by contrast.

9.5 FPA Operational Setup

To demonstrate the operation of the prototype FPA, a backside illumination technique was used to project various IR patterns onto the array while probing individual array pixels from the topside contacts. The substrate is SiO_2 on silicon and is transparent to IR wavelength above ~1,110 nm (1.12 eV). A calibrated optical power-meter was used to determine the illumination intensity through the silicon to compensate for any absorption or reflection loss. The approach uses a probe station for topside probe access to each cell of the FPA and projects light through an opening in the probe table platform. This was modified for this operational test. Various laser-cut stencils and patterns were used to project patterned IR light onto and through the backside of the FPA. Each cell was then probed, and its DelR was collected to form an integrated MWIR image. Figure 77 shows a diagram of the approach.

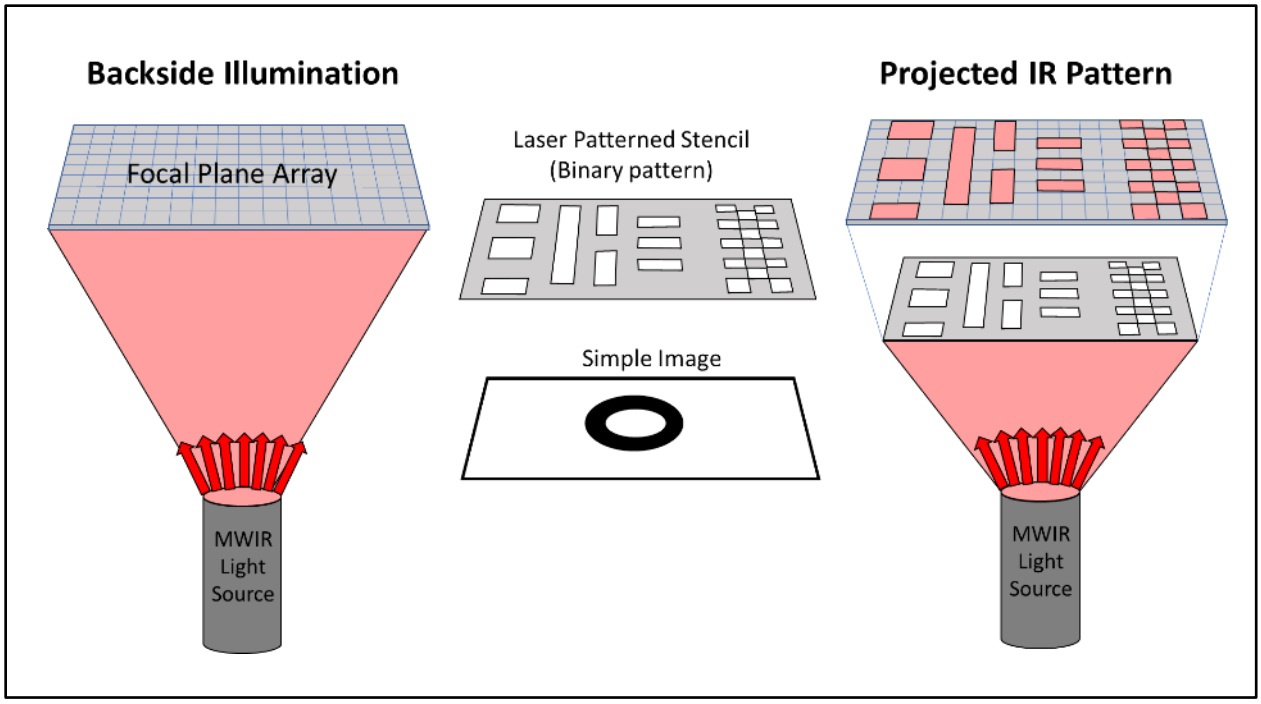

Figure 77: Setup for backside (through the substrate) operation and evaluation of FPA prototype. The stencil pattern confirms cell to cell isolation. The ring gradient pattern shows the range and ability to detect an analog gradient of light intensity.

The approach described above is further shown in Figure 78 and utilizes a 2.7 μm fiber laser fed into a collimator mounted on the underside of the probe table and fixed in place. The device under test (DUT) is then placed on a glass slide with the various masking patterns. The alignment of the FPA and the stencil/filter is achieved and maintained with laser alignment marks to assure cell to stencil alignment during the test. To assure the consistent illumination intensity is projected on each cell under test, the light source and probes were fixed in place while the FPA and the mounting patterns are adjusted in the x and y location.

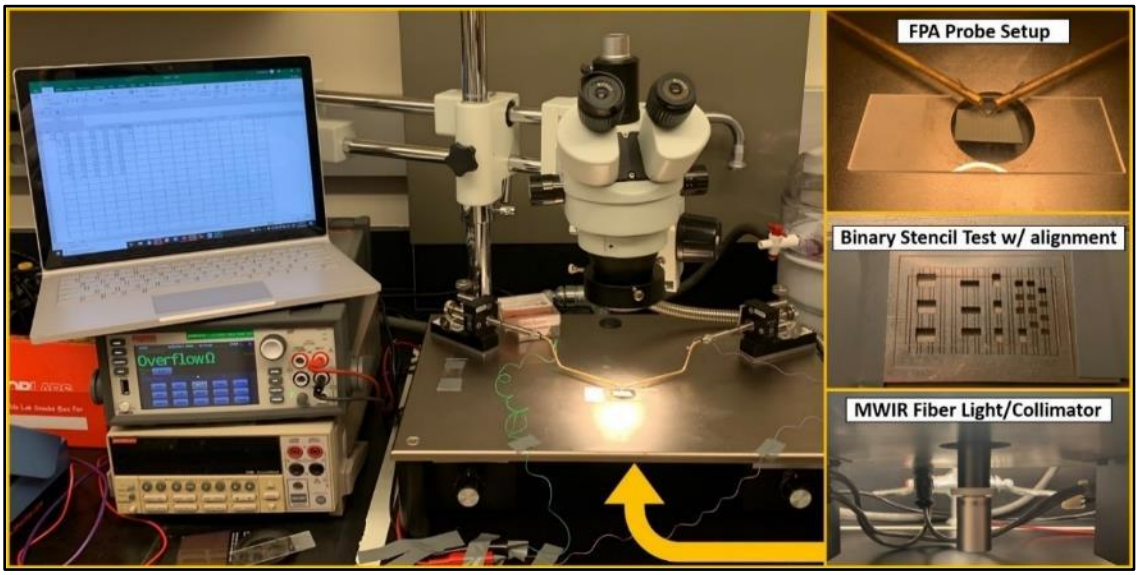

Figure 78: Modified probe station for operational testing of the FPA prototype by backside projected illumination.

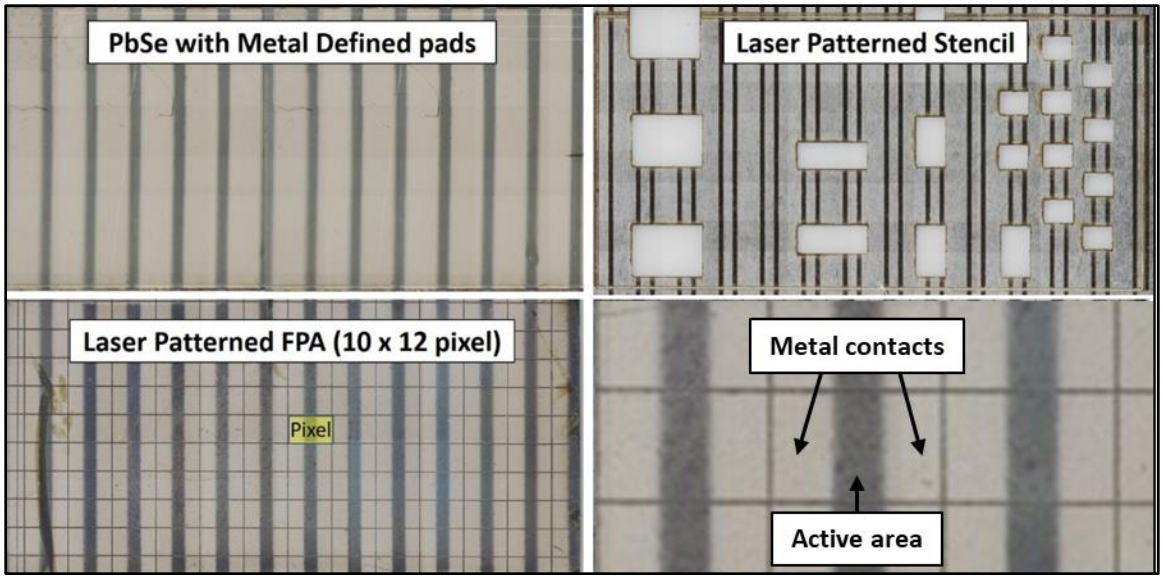

Figure 79: Topdown optical images of the fully sensitized FPA after metal pads deposition (upper left), post-laser patterning of the 10 x 20 FPA (lower left), the laser-drilled binary stencil (upper right), and a single pixel (bottom right). This approach determined the cell photoresponse of each cell. The DelR of all cells was measured and mapped to demonstrate the operation of the FPA. The fine vertical and horizontal dark lines are the laser-ablated cell-to-cell isolation lines (exposed SiO_2).

9.6 Results and Operation of Focal Plane Array

As described in the previous section, the 120-pixel PFA (10 pixel x 20 pixel) prototype was tested using the DelR figure of merit described in the early sections. Initially, a baseline map was produced to prove that this backside method was effective. First, the dark resistance (R_D) was measured for each cell, followed by the illuminated electrical resistance (R_L). The two values for each cell were then mapped and a 2-D image was formed for R_D, R_L, and DelR. Figure 80 and Figure 81 show the results of the baseline measurements. Notice that both the dark and illuminated maps show a similar center-to-edge gradient in resistance, respectively. Yet, the DelR in Figure 81 does not. This is a good indication that while the array (cell to cell) has varying resistant values, the percent difference between the two (DelR) is nearly unaffected. There is a small hot spot of cells near the middle bottom. The first row of cells around the periphery coincides with cells very close to the edge of the die and see an expected edge-effect from the heating gradient and laser raster dwell that occurs during laser sintering and sensitization. Note, that the bottom row was omitted from the maps due to severe degradation of those cells due to their proximity to the edge of the die.

162.00	66.00	39.50	38.50	44.20	33.20	28.40	26.20	32.00	36.10	44.60	105.00
167.00	77.20	39.10	35.10	27.20	22.70	20.50	22.30	23.20	31.70	37.20	87.00
184.00	77.20	42.10	33.50	25.20	21.80	18.80	20.00	21.10	29.90	33.90	97.00
179.00	68.90	40.10	29.70	24.10	20.10	19.20	20.80	25.30	34.20	57.00	105.00
192.00	72.50	48.00	31.00	22.60	29.70	18.60	21.20	24.70	36.90	68.10	112.00
158.00	66.30	50.40	33.60	24.30	20.80	16.20	18.20	21.80	32.40	61.60	121.00
165.00	71.10	55.20	39.20	27.20	22.10	21.30	19.70	20.50	29.10	68.90	117.00
171.00	79.00	59.20	41.60	38.10	34.90	37.00	33.10	39.80	39.10	84.00	171.00
192.00	199.00	201.00	210.00	221.00	233.00	250.00	197.00	190.00	187.00	172.00	168.00

142.00	54.90	33.10	32.50	36.00	27.00	22.70	21.50	26.70	30.40	36.90	88.80
140.00	64.00	32.60	29.30	22.90	19.20	17.50	18.80	19.60	26.70	31.70	74.90
152.00	64.60	35.10	28.00	21.00	18.20	16.10	17.10	18.00	25.50	29.10	82.00
149.00	57.80	33.40	24.50	20.00	16.80	16.40	17.80	21.60	28.90	48.10	89.00
160.00	61.00	40.00	24.90	18.60	24.90	16.00	18.20	21.30	31.20	57.00	96.00
133.00	55.90	41.99	27.40	20.10	17.30	13.90	15.50	18.70	27.40	51.70	103.00
137.00	59.60	46.20	32.30	22.60	18.50	18.30	16.80	17.70	24.70	57.90	100.00
145.00	66.40	49.90	34.90	31.80	29.30	30.80	27.70	33.90	32.50	70.00	145.00
167.00	171.00	174.00	176.00	174.00	170.00	175.00	149.00	153.00	152.00	139.00	143.00

Figure 80: An FPA map of dark resistance in MΩ (left) and illuminated resistance MΩ (right) of each pixel of the prototype focal plane array. The left is the dark resistance and the right is the resistance of each cell illuminated under 18 mW illumination of 2.7 μm light transmitted through the substrate and probed from the top as described in Figure 78.

0.12	0.17	0.16	0.16	0.19	0.19	0.20	0.18	0.17	0.16	0.17	0.15
0.16	0.17	0.17	0.17	0.16	0.15	0.15	0.16	0.16	0.16	0.15	0.14
0.17	0.16	0.17	0.16	0.17	0.17	0.14	0.15	0.15	0.15	0.14	0.15
0.17	0.16	0.17	0.18	0.17	0.16	0.15	0.14	0.15	0.15	0.16	0.15
0.17	0.16	0.17	0.20	0.18	0.16	0.14	0.14	0.14	0.15	0.16	0.14
0.16	0.16	0.17	0.18	0.17	0.17	0.14	0.15	0.14	0.15	0.16	0.15
0.17	0.16	0.16	0.18	0.17	0.16	0.14	0.15	0.14	0.15	0.16	0.15
0.15	0.16	0.16	0.16	0.17	0.16	0.17	0.16	0.15	0.17	0.17	0.15
0.13	0.14	0.13	0.16	0.21	0.27	0.30	0.24	0.19	0.19	0.19	0.15

Figure 81: PFA maps of DelR values (in %) under 18 mW illumination of 2.7 μm light transmitted through the substrate and probed from the top. Notice that while there is a center-to-edge pattern for the dark and illuminated resistance, the delR is minimally impacted.

Figure 82 shows the results of the binary stencil mask and ring mask used to test the operation of the FPA. The cells that aligned with the openings in the stencil mask showed a clear photoresponse as expected compared to the baseline Figure 82 (a,b,c). Some variation of all cells is expected due to probe contact variation. The dark cells neighboring illuminated cells did not indicate any noticeable pattern of bleeding or cell-to-cell coupling. This is a good indication of electrical isolation between cells and shows that this method of backside operation is successful in showing the simple operation of the FPA.

The right side of Figure 82 shows a simple ring pattern mask used to show the transition from sharp edges that cross pixels partially (gradient). Figure 82 (d,e,f) shows the result and further successful operation of the prototype PFA patterned with only laser processing without photolithography.

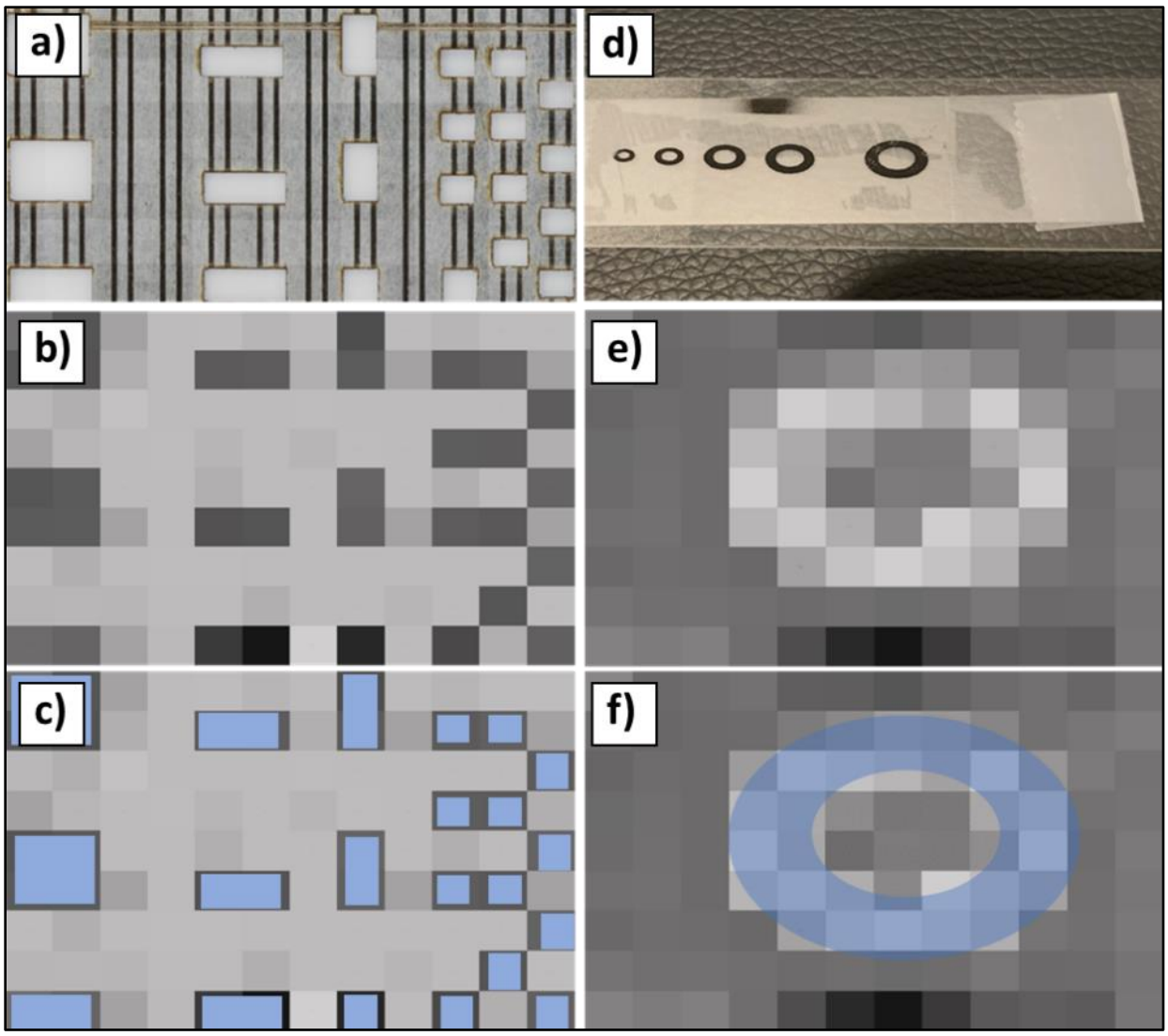

Figure 82: Operational mapping of the FPA prototype. (a) The metal stencil is used to mask light through the backside for each pixel measurement, (b) the results of the DelR measurement readout of each cell on a grayscale, (c) an overlay of the stencil showing correlation to the cell illumination. The right set of images is from a simple oval mask made with an inkjet printer on tape. Image (d) shows the mask on a glass slide, (e) shows the results of the DelR measurement readout of each cell, and (f) shows the overlay of the oval showing correlation to the cell illumination.

CHAPTER 10: Evaluation of Laser Sintering of Lead Telluride (PbTe)

10.1 Results on Laser Sinter Deposition of PbTe

To further prove the versatility of the laser sinter deposition process, a brief evaluation was performed on other lead chalcogenides to confirm the process is not limited to PbSe. This was limited to the thin LSD deposition process of () ball milling PbTe, (2) centrifuge deposition of nano/microcrystals, and (3) laser sintering of PbTe to form a continuous polycrystalline thin film. The three most common lead chalcogenides are lead sulfide (PbS), lead selenide (PbSe), and lead telluride (PbTe). All three are photosensitive to infrared light, and each has a different range of photosensitivity in the mid-wave infrared spectrum determined by their bandgap (E_g). Figure 83 shows the normalized spectral absorption versus energy (eV) versus temperature of PbS, PbSe and PbTe.

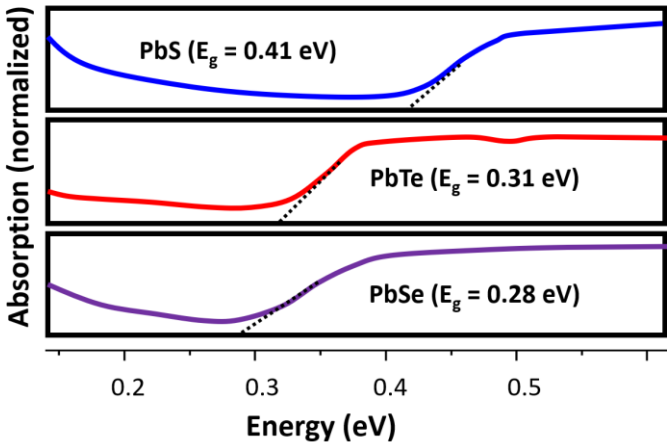

Figure 83: The normalized spectral absorption versus energy (eV) for lead chalcogenides (PbS, PbTe, and PbSe), indicating the difference in spectral response, determined by bandgap at room temperature.[62]

The identical LSD process recipes were used for PbTe and show very similar ball milling and centrifuge deposition characteristics. The same laser parameters were used on the lead telluride (PbTe) as those used for PbSe. Figure 84 shows topdown and cross-sectional SEM images of PbTe films laser sintered with and without potassium iodide (KI). Similar morphology to that of PbSe was observed after laser sintering PbTe for samples doped with and without potassium iodide (1.8 µMol). As with PbSe, the KI improved the densification of PbTe following laser sintering compared to samples without KI.

The film composition and stoichiometric balance were determined using SEM-EDS and electrical parameters were measured on the Ecopia Hall measurement system. The bottom right of Figure 84 shows the PbTe thin film stoichiometry for samples with and without KI treatment. Some loss in tellurium (Te) occurs following laser sintering, similar to that of selenium (Se) in PbSe films. The electrical parameters were reported only for the samples without KI since KI can contribute to ionic conduction if electrically tested prior to thermal sensitization. The sheet resistance of the laser sintered PbTe is similar to that of PbSe (without KI), however, the mobility for the PbTe is significantly higher than PbSe at 395 $cm^2/V{\cdot}s$ vs. 19.3 $cm^2/V{\cdot}s$, respectively. Hall measurements of PbSe following the standard LSD process indicate it to be p-type while the PbTe is n-type. The higher mobility of the PbTe is likely due to the slightly Pb-rich stoichiometry, the lower n-type carrier concentration (3.6×10^{16} cm^{-3}) versus, the higher p-type carrier concentration of PbSe (4.5×10^{17} to 5.8×10^{18} cm^{-3}) following laser sintering (without KI). Electron mobility is inherently higher than holes as well.

The melting point of PbTe is 924° C, compared to 1,078° C for PbSe which may explain the slightly different post-laser sintered electrical characteristics. The same laser sintering conditions combined with

the lower melting point of PbTe may have resulted in an increase in tellurium loss throughout the film. As in the case of PbSe, the Pb-rich form of PbTe is inherently n-type as well.

While PbSe is much more researched for MWIR photodetector research, PbTe is also a highly photoresponsive lead chalcogenide with a slightly large bandgap than PbSe (0.28 eV vs 0.31 eV, respectively). PbTe does have a 3x larger Bohr exciton radius than PbSe (46 nm vs. 150 nm) which may lend well to quantum dot or nanowire applications. Currently, PbTe is researched for both MWIR photodetectors and thermoelectrics in the form of polycrystalline thin films and nanowires.[8,60,61]

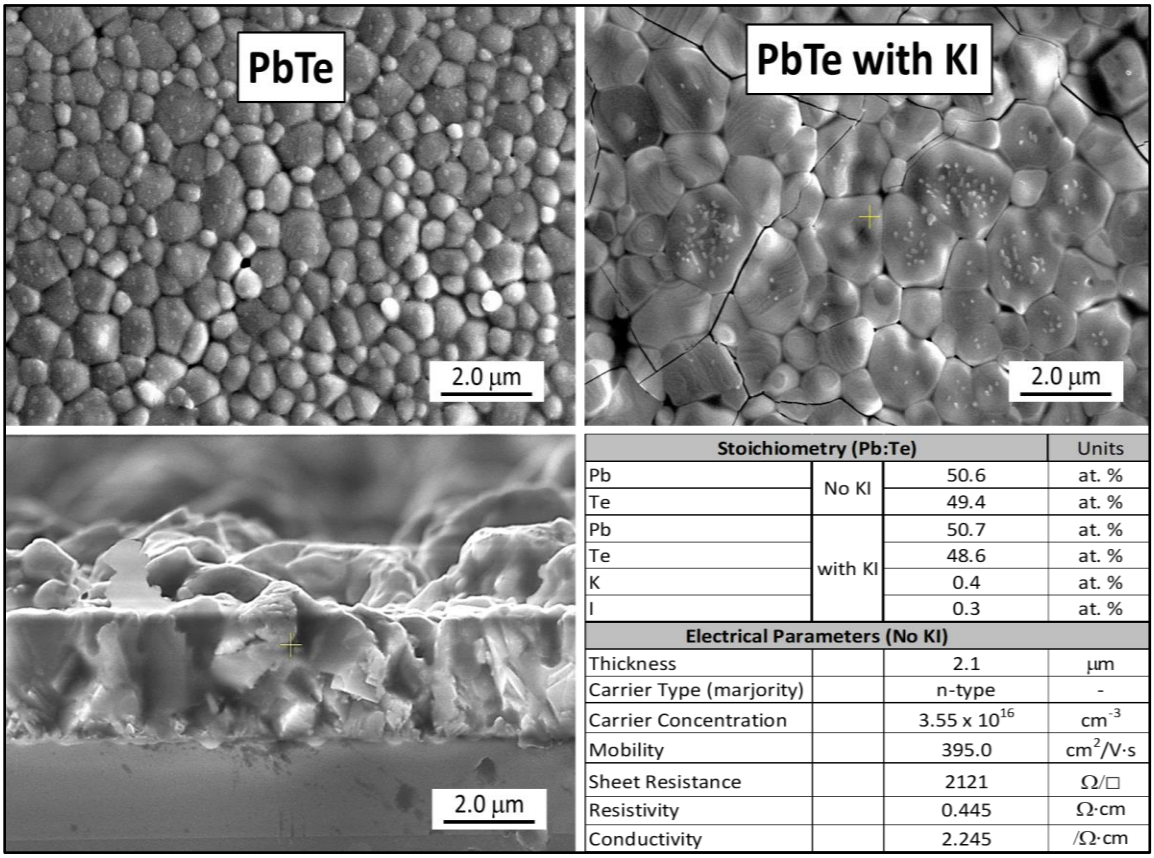

Stoichiometry (Pb:Te)			Units
Pb	No KI	50.6	at. %
Te		49.4	at. %
Pb	with KI	50.7	at. %
Te		48.6	at. %
K		0.4	at. %
I		0.3	at. %
Electrical Parameters (No KI)			
Thickness		2.1	µm
Carrier Type (marjority)		n-type	-
Carrier Concentration		3.55×10^{16}	cm^{-3}
Mobility		395.0	$cm^2/V{\cdot}s$
Sheet Resistance		2121	Ω/□
Resistivity		0.445	Ω·cm
Conductivity		2.245	/Ω·cm

Figure 84: Top-down of PbTe without KI (upper left), PbTe with KI (upper right), and cross-sectional scanning electron microscope (SEM) images of the LSD processed PbTe (bottom left) and energy dispersive spectroscopy (EDS) data for films with and without KI. A small amount of KI is detected. The carrier type and at. % stoichiometry agrees with literature in that n-type lead chalcogenides are Pb-rich and p-type are x-rich (x = Se, S, Te).

CHAPTER 11: Conclusions and Future Work

11.1 Summary of Work Completed

The three goals of this work are (1) to demonstrate a new method for PbSe thin film fabrication using laser sintering deposition (LSD) of micro/nanoparticles of PbSe (2) to improve the understanding of the photoconductive mechanism of PbSe thin films through optical, electrical, morphological, and structural characterization (3) to laser fabricate photodetectors and focal plane array devices using LSD combined with laser patterning to avoid the difficulties of photolithography liftoff. Each of these goals was accomplished throughout this body of work. In the process of advancing these goals some of the work described in this thesis was published as a review article entitled "photoconductive PbSe thin films for infrared imaging.[4] in the Royal Society of Chemistry.

One of the goals of this work is to develop a novel thin film deposition method for fabricating polycrystalline PbSe for MWIR photodetectors and improve on traditional methods. This was accomplished with the development of the Laser Sinter Deposition (LSD) method, and the results were reported and published.[33]. The *second* goal of using this novel laser sintering method is to improve the understanding behind the photoconduction mechanisms and it was accomplished by developing a model for optimizing the photoresponse of PbSe and the results were published in a scientific journal paper.[54] Additionally, the role of potassium iodide (KI) and its impact on improving the photoresponse of sensitized PbSe was discovered and results were published.[52] The *third* goal of this work was accomplished by successfully fabricating both PbSe-based photodetectors and laser patterning of a functional focal plane array (FPA), eliminating the necessity for photolithography. A manuscript for publishing these laser fabrication results is currently in draft form.

In summary, we have demonstrated that the films produced by the new laser deposition method are suitable for both photodetector and focal plane arrays (FPA) fabrication. In the process of demonstrating that laser patterning is possible for fabricating FPA, we have also identified many additional benefits of laser patterning PbSe thin films rather than using traditional photolithography liftoff methods. Photolithography is a major source of contamination for PbSe thin films from the organic photoresist residue and exposure to chemical etchants. Laser patterning solves this problem entirely. Laser patterning can be performed with a single laser system by first forming the initial PbSe thin film and then subsequently patterning the device. Changing laser parameters can occur quickly and allows custom patterns on an adjacent die of the same wafer.

In this study, we discovered that in addition to laser sintering of PbSe NCs to form thin films, various laser treatments could be utilized for surface smoothing/texturing, selective depth sintering, and even localized majority carrier type conversion (p-type to n-type).

We have also shown that laser processing is not limited to LSD deposited thin films, but can also be used to solve documented issues for other deposition methods, such as improving film adhesion to the substrate. We successfully show that laser treatments improve film adhesion of chemical bath deposited PbSe thin films. Laser treatment of chemical bath deposited (CBD) PbSe will no longer require pre-treating substrates to avoid film delamination. We also show how the laser parameters can be adjusted to eliminate wafer dicing.

The overall process flow and methodology for developing the LSD process and maturing it to produce functional PbSe photodetectors and functional focal plane array (FPA) are displayed in Figure 85. All aspects of this process flow and the above goals have been achieved and reported in this body of work.

In summary, we have successfully demonstrated a new method of thin-film deposition using laser sintering of nanoparticles, provided an enhanced understanding of the photoconductive mechanism in PbSe, and IR devices like photodetectors and focal plane arrays can be fabricated by direct laser patterning.

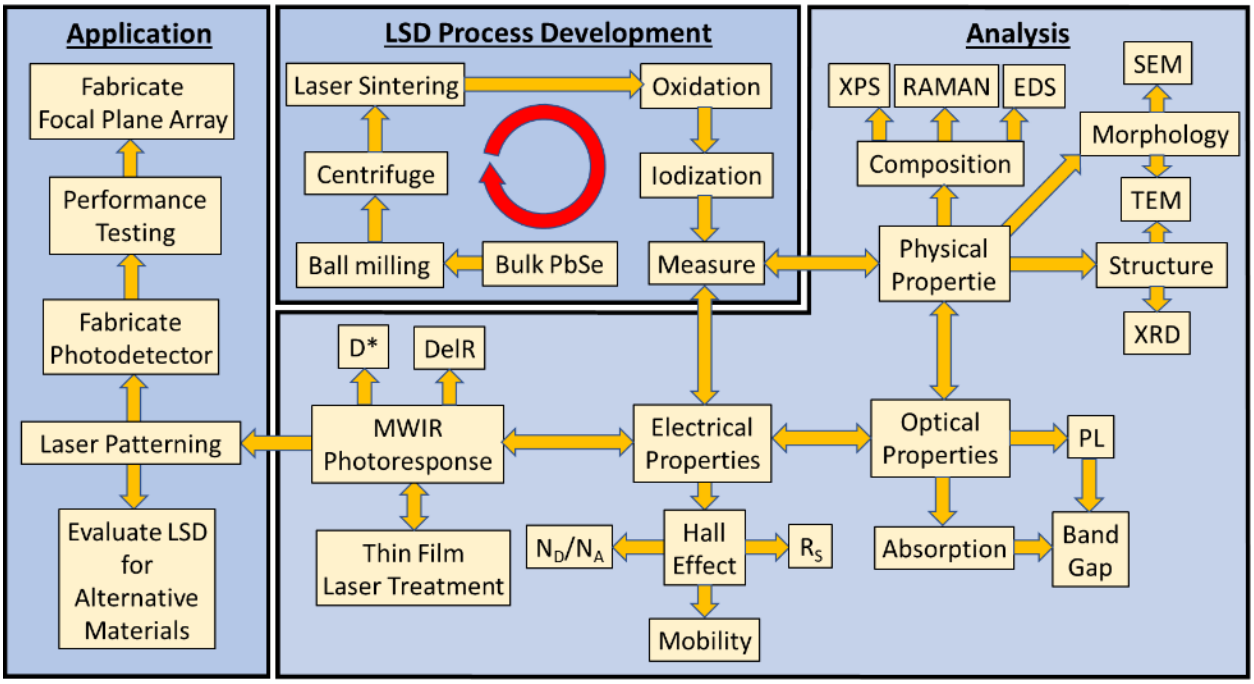

Figure 85: The first step was to develop the LSD process which required narrowing down the parameters necessary for laser sintering without melting or ablating the NCs to generate a few micron thick films suitable for device applications. Once this was achieved, the next step was analysis to characterize the physical properties, optical properties, and then electrical properties. Once this was determined to be repeatable and comparable to CBD, the process of photosensitizing the film was undertaken to determine the conditions for maximizing the photoresponse. The last step was to apply the LSD process and show that lasers can further be used for fabricating a device for applications like photodetectors and focal plane array (FPA).

11.2 Conclusions

By following the process flow and process characterization displayed in Figure 85, the laser sinter deposition (LSD) process was rigorously developed, and a successful demonstration of the viability of this method was proven. LSD and laser patterning are not limited to producing thin films of PbSe and patterning focal plane array. This work has proven laser processing to be a useful tool for improving and modifying traditionally deposited film, as well as an experimental tool for texturing, sintering, and activating dopants for other materials sets.

Within this work, it is concluded that the laser sinter deposition method is a repeatable and tailorable method for producing polycrystalline thin films of PbSe with the potential for other materials and applications. LSD offers many improvements and advantages over other traditional methods, including added process control, superior substrate adhesion, and rapid deposition rates (< 30 sec). The LSD deposition process also nearly eliminates hazardous waste. The flexibility, simplicity, and spatial tailoring of LSD are not possible using other thin film deposition methods. A suite of additional laser treatments is reported and summarized in Table 14.

The LSD process has provided an improved understanding of the mechanism behind the photosensitivity of PbSe. This work thoroughly investigated and developed a detailed, complex model of the symbiotic relationship between oxidation and iodization in the sensitization of PbSe thin films. This work led to the conclusion that a narrow process window exists in the oxidation step for achieving a high IR photoresponse. The optimum sensitization process (oxidation and iodization) leading to the highest IR photoresponse converts as-deposited PbSe thin films, of 1.2 μm thickness, into a multi-layered film with a 200 – 300 nm thick top layer of PbI_2, a transition layer containing $Pb_3Se_2O_6I_2$, and a bottom layer of PbSe of thickness 400-500 nm. Both oxygen and iodine were detected between the base layer PbSe grains. This

confirms some reports that both oxygen and iodine present at grain boundaries *may* influence the IR photoresponse by decreasing the dark current in the formation of a potential barrier for trapping minority carriers.

This work provides the first reported *optimized film stack model for the PbSe sensitization process* to maximize the IR photoresponse. The model concludes that a targeted $PbSeO_3$ layer thickness of 400 nm is needed to (1) restrict the PbI_2 surface layer thickness to less than 200 nm formed during iodization, (2) regulate the iodization process, allowing only trace amounts of iodine to diffuse along grain boundaries and recrystallize the PbSe base-layer, and (3) preserve the stoichiometric balance of the underlying PbSe layer. This work identified that $PbSeO_3$ iodizes to form PbI_2 at a rate of ~100 nm/minute. Pure PbSe as well as selenium-poor lead selenite $(PbO_3)_{(1-x)}$ $(Se)_x$ and $Pb_{(1-x)}O_x$ rapidly transform into PbI_2 at nearly 5x the rate of pure $PbSeO_3$. As such, it is concluded that $PbSeO_3$ *regulates* the diffusion of iodine into the film, and evidence supports that this allows the iodine to impact the morphology of the entire film, while simultaneously preventing the rapid conversion of PbSe into PbI_2. Through rigorous analysis, it is concluded that a narrow window exists in the oxidation process whereby too much, as well as too little oxidation, will both result in *rapid* conversion of the film stack to PbI_2. Both these scenarios lead to a thin PbSe base layer, resulting in an excessively high dark resistance (R_D > 500 MΩ) and a reduced MWIR photoresponse.

The findings of this work support the conclusion that low concentrations of iodine reaching the PbSe base-layer assist in recrystallizing the grains and increase inter-grain coupling by transforming the as-deposited PbSe morphology from an equiaxial round-grain to a highly planar faceted morphology throughout the entire film stack. While iodine concentrations vary with depth, the iodization process uniformly transforms morphology and increases grain size by 260% (242 -> 628 nm) for the entire film. For this to occur, it is concluded that the primary role of iodine is to diffuse along grain boundaries and improve inter-grain coupling by growing the inter-grain surfaces with planar faceting.

We discovered a new compound ($Pb_3Se_2O_6I_2$) formed between the PbI_2 surface and the PbSe base-layer, only present in samples with high MWIR photoresponse. The presence of this compound ($Pb_3Se_2O_6I_2$) supports the notion that iodine does play a *direct* role in the photoconduction mechanism. The presence of this compound may also be an indication that an equilibrium between oxidation and iodization has occurred. It is concluded that to maximize the MWIR photoresponse, the overall sensitization processing (oxidation & iodization) must include both oxidation and iodization but must also restrict PbI_2 to the surface while allowing trace amounts of oxygen and iodine to diffuse to PbSe base-layer grain boundaries. The trace levels of oxygen and iodine diffusion must be regulated to impact only the grain boundaries and maintain the stoichiometric balance of the underlying PbSe layer.

Concerning PbSe for MWIR sensitive films, this work has concluded that laser sinter deposition (LSD) is capable of producing thin films of PbSe with the same optical, electrical and physical properties as chemical bath deposition (CBD). The LSD process can produce films of p-type PbSe material with a carrier concentration of 4.5×10^{17} cm^{-3} compared to CBD of 7.1×10^{17} cm^{-3}. Throughout thermal sensitization, the stoichiometry, sheet resistance, and carrier concentration were compared between the two processes, and the results are shown in Table 16. The MWIR photoresponse between the LSD and CBD films is comparable with a DelR of 35.7% and 38%, respectively.

Table 16: Summary of electrical parameters of PbSe thin films through the MWIR sensitization process. Comparison between CBD and LSD deposition methods.

Sample	Carrier Type	Carrier Concentration (cm^{-3})	Mobility ($cm^2/V{\cdot}s$)	Sheet Resistance ($\Omega\square$)	Thickness (μm)	Stoichiometry (at. %)			
						Pb	Se	O	I
CBD (As-grown)	p-type	7.1×10^{17}	41.6	1,066	1.4	49.5	50.5	*	NA *
LSD (post-Sinter)	p-type	4.5×10^{17}	19.3	3,625	1.6	49.1	50.9	*	NA*
CBD (post-Ox)	p-type	6.6×10^{16}	9.2	51k	1.4	21.6	24.9	53.5	NA*
LSD (post-Ox)	p-type	1.1×10^{17}	9.8	79k	1.6	18.8	20.8	60.4	NA*
CBD (post-Iodization)	p-type	1.5×10^{14}	11.7	26.8M	1.4	29.2	18.8	26.6	25.4
LSD (post-Iodization)	p-type	6.2×10^{13}	16.4	76.5M	1.6	21.7	17.1	31	30.2

LSD also enabled a deeper understanding of the role of potassium iodide (KI) in sensitization by revealing how KI assists the iodization process by promoting recrystallization (flux) of the underlying PbSe without converting the PbSe grains to PbI_2, as can occur during thermal iodization. This work reveals that the laser sinter deposition process has the ability to in situ dope the PbSe thin film more precisely in multiple steps to selectively dope the PbSe with different concentrations of KI with film depth. This was reported as the two-step doping of KI and produced a film that was 3x more photoresponsive than a film with only single doping of KI.

The most impactful results of this work are reported regarding the performance, and photoresponse characterization of both discrete infrared detectors and laser patterned focal plane array (FPA) fabricated in full (or part) using laser processing and no need for photolithography. Considering the chemical bath deposition (CBD) method for PbSe thin films has been refined and improved for 70+ years, the LSD process is a promising method for fabricating highly photoresponsive, uncooled PbSe photodetectors (1.01×10^9 $cm{\cdot}Hz^{1/2}{\cdot}W^{-1}$) and focal plane array devices. LSD is not limited to photodetectors applications nor is laser processing limited to the PbSe material set. A huge opportunity now exists for expanding this laser process to other material sets and applications.

11.3 Future Work

11.3.1 Laser sintering

This work shows that laser sintering can produce polycrystalline thin films of PbSe and other lead chalcogenides, but the potential for laser sintering other materials should be pursued. This is the first report of successfully laser sintering thin films for photodetectors. Many other materials and applications like thermoelectric, piezo-electric, and other semiconductor compounds can now be laser sintered to identify unique properties, otherwise not achievable with traditional methods. The most potentially useful application of laser sintering is ultra-rapid sintering to activate dopants. One potentially useful application for laser sintering is ultra-rapid sintering to activate dopants in scenarios with little margin for thermal budget (isolated or localized anneal without diffusion of adjacent devices).

Additional work should focus on improvements in the LSD process to determine the full potential and mature the process to (1) improve sample-to-sample variability, (2) extend this process to larger size wafers, (3) fabricate better metal contacts, (4) reduction of surface reflection loss, and (5) improve the ablation selectivity between the metal conductive layer and the underlying photoconductive film.

11.3.2 Laser patterning

The laser patterning process is a promising option for customized focal plane array development and integrating multiple laser treatments into one system. This potential for rapid prototyping at low-cost is

now achievable. Notionally, a single 4” wafer could potentially have dozens of different devices patterned in real-time without the need for trial-and-error design concepts.

This work continues with a collaboration between Professor Gupta at the University of Virginia, and the Naval Surface Warfare Center, Dahlgren Division. These organizations have established a collaborative relationship now for 5+ years and continue to grow. An Educational Partnership Agreement (EPA) was established in 2018 between Dahlgren and UVA and a joint patent application was submitted in 2021 for the LSD process. A CRADA (Cooperative Research and Development Agreements) is now being established between the University of Virginia, the U. S. Navy, and Johns Hopkins University. The author of this thesis is the Co-PI (Principal Investigator).

References

1. Vergara, G. *et al.* Polycrystalline lead selenide: The resurgence of an old infrared detector. *Opto-electronics Review* **15**, 110–117 (2007).

2. Sanchez, F. J. *et al.* Progress on monolithic integration of cheap IR FPAs of polycrystalline PbSe. in *Infrared Technology and Applications XXXI* vol. 5783 441 (SPIE, 2005).

3. Shandalov, M. & Golan, Y. Microstructure and morphology evolution in chemical solution deposited semiconductor films: 2. PbSe on as face of GaAs(111). *EPJ Applied Physics* **28**, 51–57 (2004).

4. Gupta, M., Harrison, J. & Islam, M. T. Photoconductive PbSe Thin Films for Infrared Imaging,. *Royal Society of Chemistry, Materials Advances* **2,** 3133-3160 (2021) doi: Materials Advances, 2021, DOI: 10.1039/D0MA00965B.

5. Schluter, M., Martinez, G & Cohen, M. L. *Pressure and temperature dependence of electronic energy levels in PbSe and PbTe*. *Physical Review B* vol. **12**, #2 (1975).

6. Wei, S. H. & Zunger, A. *Electronic and structural anomalies in lead chalcogenides*, *Physical Review B* vol. **55**, #20 (1997).

7. A. Svane, N. E. Christensen, M. Cardona, A. N. Chantis, M. van Schilfgaarde, and T. Kotani, Quasiparticle self-consistent GW calculations for PbS, PbSe, and PbTe: Band structure and pressure coefficients. *Physical Review B - Condensed Matter and Materials Physics* **81**, (2010).

8. Ekuma, C. E., Singh, D. J., Moreno, J. & Jarrell, M. Optical properties of PbTe and PbSe. *Physical Review B - Condensed Matter and Materials Physics* **85**, (2012).

9. Streltsov, S. v., Manakov, A. Y., Vokhmyanin, A. P., Ovsyannikov, S. v. & Shchennikov, V. v. Crystal lattice and band structure of the intermediate high-pressure phase of PbSe. *Journal of Physics Condensed Matter* **21**, (2009).

10. Jang, M. H. *et al.* Mid-wavelength infrared photo response and band alignment for sensitized PbSe thin films. *Journal of Applied Physics* **126**, (2019).

11. Jang, M. H., Yoo, S. S., Kramer, M. T., Dhar, N. K. & Gupta, M. C. Properties of chemical bath deposited and sensitized PbSe thin films for IR detection. *Semiconductor Science and Technology* **34**, (2019).

12. Jang, M.-H. *et al.* Photoconductive mechanism of IR-sensitive iodized PbSe thin films via strong hole–phonon interaction and minority carrier diffusion. *Applied Optics* **59**, 10228 (2020).

13. Suh, Y. & Suh, S.-H. Effect of iodine doping in the deposition solution and iodine vapor pressure in the sensitization treatment on the properties of PbSe films. *Optical Engineering* **56**, 091607 (2017).

14. Gorer, S., Albu-Yaron, A. & Hodes, G. Chemical Solution Deposition of Lead Selenide Films: A Mechanistic and Structural Study. *Chemistry of Materials* **7**, 1243–1256 (1995).

15. Grozdanov, I., Najdoski, M. & Dey, S. K. A simple solution growth technique for PbSe thin films. *Materials Letters* **38**, 28–32 (1999).

16. Hankare, P. P. *et al.* Synthesis and characterization of chemically deposited lead selenide thin films. *Materials Chemistry and Physics* **82**, 505–508 (2003).

17. Sarkar, S. K., Kababya, S, Vega, S., Cohen, H., Woicik, J., Frenkel, A., Hodes, G., Effects of solution pH and surface chemistry on the postdeposition growth of chemical bath deposited PbSe nanocrystalline films. *Chemistry of Materials* **19**, 879–888 (2007).

18. Kassim, A., Ho, S. M., Abdullah, A. H. & Nagalingam, S. XRD, AFM and UV-Vis optical studies of PbSe thin films produced by chemical bath deposition method. *Scientia Iranica* **17**, 139–143 (2010).

19. Templeman, T. *et al.* Chemically deposited PbSe thin films: Factors deterring reproducibility in the early stages of growth. *CrystEngComm* **16**, 10553–10559 (2014).

20. Jang, M. H. *et al.* Mid-wavelength infrared photo response and band alignment for sensitized PbSe thin films. *Journal of Applied Physics* **126**, (2019).

21. Jang, M. *et al.* Photoconductive Mechanism of IR Sensitive Iodized PbSe Thin Films via Strong Hole-Phonon Interaction and Minority Carrier Diffusion. *Applied Optics* **59**, 10228–10235 (2020).

22. Jang, M. H., Yoo, S. S., Kramer, M. T., Dhar, N. K. & Gupta, M. C. Properties of chemical bath deposited and sensitized PbSe thin films for IR detection. *Semiconductor Science and Technology* **34**, (2019).

23. Smirnova, Z. I., Bakanov, V. M., Maskaeva, L. N., Markov, V. F. & Voronin, V. I. Effect of an iodine-containing additive on the composition, structure, and morphology of chemically deposited lead selenide films. *Physics of the Solid State* **56**, 2561–2567 (2014).

24. Yurk, V. M., Maskaeva, L. N., Markov, V. F. & Bamburov, V. G. Effect of Antioxidants on Stability of Aqueous Solutions of Selenurea and on Properties of Lead Selenide Films Obtained with These Antioxidants. *Russian Journal of Applied Chemistry* **92**, 394–403 (2019).

25. Maskaeva, L. N. *et al.* Composition, structure and functional properties of nanostructured PbSe films deposited using different antioxidants. *Materials Science in Semiconductor Processing* **108**, (2020).

26. Shandalov, M. & Golan, Y. Microstructure and morphology evolution in chemical solution deposited semiconductor films: 2. PbSe on as face of GaAs(111). *EPJ Applied Physics* **28**, 51–57 (2004).

27. Jang, M. H., Yoo, S. S., Kramer, M. T., Dhar, N. K. & Gupta, M. C. Electrical transport properties of sensitized PbSe thin films for IR imaging sensors. *Semiconductor Science and Technology* **34**, (2019).

28. Suh, Y., Suh, S. H., Lee, S. Y. & Kim, G. H. Morphological and microstructural evolution of PbSe films grown on thermally oxidized Si (111) substrates by chemical bath deposition. *Thin Solid Films* **628**, 148–157 (2017).

29. Kumar, P. *et al.* PbSe mid-IR photoconductive thin films (part I): Phase analysis of the functional layer. *Journal of Alloys and Compounds* **724**, 316–326 (2017).

30. Kumar, P., Pfeffer, M., Berthold, C. & Eibl, O. PbSe mid-IR photoconductive thin films (part-II): Structural analysis of the functional layer. *Journal of Alloys and Compounds* **735**, 1654–1661 (2018).

31. Qiu, J., Weng, B., McDowell, L. L. & Shi, Z. Low-cost uncooled MWIR PbSe quantum dots photodiodes. *RSC Advances* **9**, 42516–42523 (2019).

32. Templeman, T. *et al.* Oriented Attachment: A Path to Columnar Morphology in Chemical Bath Deposited PbSe Thin Films. *Crystal Growth and Design* **18**, 1227–1235 (2018).

33. Harrison, J. T., Pantoja, E., Jang, M. H. & Gupta, M. C. Laser sintered PbSe semiconductor thin films for Mid-IR applications using nanocrystals. *Journal of Alloys and Compounds* **849**, (2020).

34. Jang, M.-H., Kramer, M. T., Yoo, S.-S. & Gupta, M. C. Laser annealing to improve PbSe thin film photosensitivity and specific detectivity. *Applied Optics* **59**, 9409 (2020).

35. Wang, H., Liu, Q., Wang, X., Yan, J. & Tang, H. MgxZn1−xO films synthesized by laser sintering method and UV detectors. *Journal of Alloys and Compounds* **847**, (2020).

36. Yan, J. *et al.* Al0.3Zn0.7O film UV detector and its laser sintering synthetic process. *Applied Surface Science* **504**, (2020).

37. Hechster, E. & Sarusi, G. Design and measurements of the absorption section of an up-conversion device based on PbSe quantum-dots. *Opt Mater (Amst)* **50**, 188–192 (2015).

38. Brown, M. S. & Arnold, C. B. Fundamentals of Laser-Material Interaction and Application to Multiscale Surface Modification. Springer Series in Materials Science **135**, 91-120 (2010). doi:10.1007/978-3-642-10523-4__4.

39. Harrison, J. T., Pantoja, E., Jang, M. H. & Gupta, M. C. Laser sintered PbSe semiconductor thin films for Mid-IR applications using nanocrystals. *Journal of Alloys and Compounds* **849**, (2020).

40. Malamatari, M., Taylor, K. M. G., Malamataris, S., Douroumis, D. & Kachrimanis, K. Pharmaceutical nanocrystals: production by wet milling and applications. *Drug Discovery Today* **vol. 23** 534–547 (2018).

41. Khorsand Zak, A., Abd. Majid, W. H., Abrishami, M. E. & Yousefi, R. X-ray analysis of ZnO nanoparticles by Williamson-Hall and size-strain plot methods. *Solid State Sciences* **13**, 251–256 (2011).

42. Kidero Unuma. Sintering of Chemically Synthesized Lead(II) Selenide Fine Powders. *j. Am. Ceram. Soc* **81** [2] 444-46 (1998).

43. Wang, Z. *et al.* Understanding phonon scattering by nanoprecipitates in potassium-doped lead chalcogenides. *ACS Applied Materials and Interfaces* **9**, 3686–3693 (2017).

44. Golubchenko, N. v., Moshnikov, V. A. & Chesnokova, D. B. Investigation into the microstructure and phase composition of polycrystalline lead selenide films in the course of thermal oxidation. *Glass Physics and Chemistry* **32**, 337–345 (2006).

45. Golubchenko, N. v., Moshnikov, V. A. & Chesnokova, D. B. Doping effect on the kinetics and mechanism of thermal oxidation of polycrystalline PbSe layers. *Inorganic Materials* **42**, 942–950 (2006).

46. Yang, H., Chen, L., Li, X. & Zheng, J. Intrinsic stoichiometry optimization of polycrystalline lead selenide film in the sensitization process by iodine concentration regulation. *Materials Letters* **169**, 273–277 (2016).

47. Yang, H., Li, X., Wang, G. & Zheng, J. The electrical properties of carrier transport between lead selenide polycrystallites manipulated by iodine concentration. *AIP Advances* **8**, (2018).

48. Romano-Trujillo, R. *et al.* Synthesis and characterization of PbSe nanoparticles obtained by a colloidal route using Extran as a surfactant at low temperature. *Nanotechnology* **23**, (2012).

49. Kuzivanov, M. O., Zimin, S. P., Fedorov, A. v. & Baranov, A. v. Raman scattering in lead selenide films at a low excitation level. *Optics and Spectroscopy (English translation of Optika i Spektroskopiya)* **119**, 938–942 (2015).

50. PbSeO3 (RRUFF ID: R140388). RAMAN Spectroscopy Standard. https://rruff.info/molybdomenite.

51. PbO (RRUFF ID: R060454 & R060959). RAMAN Spectroscopy Standard. https://rruff.info/

52. Harrison, J. T. & Gupta, M. C. Photoconductive PbSe Thin Films and the Role of Potassium Iodide. *Journal of Alloys and Compounds* **905**, 164155 (2022) doi:10.1016/j.jallcom.2022.164155.

53. Shkir, M. *et al.* A facile synthesis of Au-nanoparticles decorated PbI2 single crystalline nanosheets for optoelectronic device applications. *Scientific Reports* **8**, (2018).

54. Harrison, J. T. & Gupta, M. C. Mechanistic studies of oxidation and iodization of PbSe thin film sensitization for mid-infrared detection. *Journal of Applied Physics* **131**, 025308 (2022).

55. Makuła, P., Pacia, M. & Macyk, W. How To Correctly Determine the Band Gap Energy of Modified Semiconductor Photocatalysts Based on UV-Vis Spectra. *Journal of Physical Chemistry Letters* vol. **9** 6814–6817 (2018).

56. Hamamatsu. *Characteristics and use of infrared detectors 2*. (Technical Whitepaper)

57. Yang, H., Li, X., Mei, T. & Zheng, J. The lead selenide photoconductive sensitization via oxygen ion implantation with enhanced optical absorption and carrier mobility. *Journal of Materials Science* **52**, 10779–10786 (2017).

58. Vergara, G. *et al.* 80×80 VPD PbSe: the first uncooled MWIR FPA monolithically integrated with a Si-CMOS ROIC. in *Infrared Technology and Applications XXXIX* vol. **8704** 87041M (SPIE, 2013).

59. Rogalski, A., Martyniuk, P. & Kopytko, M. Challenges of small-pixel infrared detectors: A review. *Reports on Progress in Physics* vol. **79** (2016).

60. Gradauskas, J., Dzundza, B., Chernyak, L. & Dashevsky, Z. Two-color infrared sensor on the pbte: In P-N junction. *Sensors (Switzerland)* **21**, 1–9 (2021).

61. Hao, X. *et al.* Performance Optimization for PbTe-Based Thermoelectric Materials. *Frontiers in Energy Research* vol. **9** (2021).

62. Gibbs, Z. M. Kim, H., Wang, H., White, R., Drymiotis, F., Kaviany, M., Snyder, J,. Temperature dependent band gap in PbX (X = S, Se, Te). Applied Physics Letters **103**, 262109 (2013).

63. Qiu, J. *et al.* Modified vapor phase deposition technology for high-performance uncooled MIR PbSe detectors. *RSC Advances* **11**, 34908–34914 (2021).

64. Weng, B. *et al.* Recent development on the uncooled mid-infrared PbSe detectors with high detectivity. in *Quantum Sensing and Nanophotonic Devices XI* vol. 8993 899311 (SPIE, 2013).

65. Brown, M.S., Arnold, C.B. Fundamentals of Laser-Material Interaction and Application to Multiscale Surface Modification. In: Sugioka, K., Meunier, M., Piqué, A. (eds) Laser Precision Microfabrication. Springer Series in Materials Science, vol **135**. Springer, Berlin, Heidelberg (2010). https://doi.org/10.1007/978-3-642-10523-4_4

List of Publications

1. Harrison, J. T. & Gupta, M. C. Photoconductive PbSe Thin Films and the Role of Potassium Iodide. *Journal of Alloys and Compounds* **905**, 164155 (2022) doi:10.1016/j.jallcom.2022.164155.

2. Harrison, J. T. & Gupta, M. C., Mechanistic Studies of Oxidation and Iodization of PbSe Thin Film Sensitization for Mid-infrared Detection. *Journal of Applied Physics* **131**, 025308 (2022).

3. Gupta, M., Harrison, J. & Islam, M. T. Photoconductive PbSe Thin Films for Infrared Imaging, Feb. 24, 2021. *Royal Society of Chemistry*, *Materials Advances* **2** 3133-3160 (2021) doi:Materials Advances, 2021, DOI: 10.1039/D0MA00965B.

4. Harrison, J. T., Pantoja, E., Jang, M. H. & Gupta, M. C. Laser sintered PbSe semiconductor thin films for Mid-IR applications using nanocrystals. *Journal of Alloys and Compounds* **849**, (2020).

Expected Publication:

1. Laser Fabrication of Lead Selenide thin-films and Focal Plane Array, Summer 2022

2. Optical and Electrical Properties of Laser Sinter Deposited PbSe Thin Films, Fall 2022

Professional Experience

Motorola Semiconductor Products Sector, Device Engineering and Process Engineering (2000-2004)

Infineon Technology, Failure Analysis Engineer (2004-2009)

Department of Navy, NSWCDD, Microelectronics Subject Matter Expert (SME) Engineer (2009-present)

List of Awards, Funding, and Other Notable Activities

- 2017 Patent Award: (US10403595B1): “Wiresaw removal of microelectronics from printed circuit board”
- 2021 Prevision Patent filing (TBD): “Laser Sinter Deposition Method for Thin Film Processing”
- 2017-2019 Naval Surface Warfare Center, Dahlgren Division Academic Fellowship recipient
- 2020 Naval Surface Warfare Center, Dahlgren Division Naval Innovation Science and Engineering (NISE) Fellowship recipient
- 2020-2022 In-House Laboratory Research (ILIR) Award for Laser Sinter Deposition
- STEM Outreach at local middle schools (Richmond Area)
- Recognized by Naval Research Labs (NRL) 2021 end-of-year Review Naval Surface Warfare Center, Dahlgren Division (NSWCDD)

List Acronyms

AFP	Academic Fellowship Program
ALD	Atomic Layer Deposition
CBD	Chemical Bath Deposition
CMOS	Complementary Metal Oxide Semiconductor
CRADA	Cooperative Research and Development Agreement
CVD	Chemical Vapor Deposition
CW	Continuous Wave
DelR	Delta Resistance
DOE	Design of Experiment
DUT	Device Under Test
ECE	Electrical and Computer Engineering
EDS	Energy Dispersive Spectroscopy
EM	Electromagnetic
ENBW	Equivalent Noise Bandwidth
EPA	Educational Partnership Agreement
eV	Electron Volt
FIB	Focused Ion Beam
FPA	Focal Plane Array
FTIR	Fourier Transform Infrared
FWHM	Full Width Half Maximum
Gpa	Gigapascal
HRTEM	High Resolution Transmission Electron Microscope
IC	Integrated Chip
ILIR	In-House Laboratory Research
INSTEC	INSTECT Corporation
IR	Infrared
KI	Potassium Iodide
LPCVD	Low Pressure Chemical Vapor Deposition
LSD	Laser Sinter Deposition
MBE	Molecular Beam Epitaxy
MCT	Mercury Cadmium Telluride
MSE	Material Science Engineering
mW	milliwatt
MWIR	Midwave Infrared
N_A	Acceptor Carrier (hole)
NC	Nanocrystals
N_D	Donor Carrier (electron)
NEP	Noise Equivalent Power
NIR	Near Infrared
NISE	Naval Innovation in Science and Engineering
nm	nanometer (10^{-9} meter)
NMCF	Nanomaterials Characterization Lab
NRL	Navy Research Lab
NSWCDD	Naval Surface Warfare Center, Dahlgren Division

PbS	Lead Sulfide
PbSe	Lead Selenide
PbTe	Lead Telluride
PEC	Process Evaluation Chip
PECVD	Plasma Enhanced Chemical Vapor Deposition
PL	Photoluminescence
PVD	Physical Vapor Deposition
QCW	Quasi Continuous Wave
QD	Quantum Dot
QE	Quantum Efficiency
R_D	Dark Resistance
R_L	Illuminated Resistance
ROIC	Read-out Integrated Circuit
RT	Room Temperature
RTA	Rapid Thermal Anneal
SAED	Selective Area Electron Diffraction
SDS	Selective Depth Sintering
SEM	Scanning Electron Microscope
SNR	Signal to Noise Ratio
STEM(1)	Science, Technology, Engineering, and Math
STEM(2)	Scanning Transmission Electron Microscope
TBD	To Be Determined
TCO	Transparent Conductive Oxide
TEM	Transmission Electron Microscope
UV	Ultraviolet
UV-VIS-NIR	Ultraviolet-Visible-Near infrared
XPS	X-ray Photoelectron Spectroscopy
XRD	X-ray Diffraction